INVESTIGATION OF THE COMBINED METHODS OF FILTRATION, COPPER OXIDE NANOPARTICLES AND MICROALGAE ON PALM OIL MILL EFFLUENT (POME) TREATMENT

By

PHANG YOU KANG

A thesis/dissertation submitted to,

Faculty of Science,

Universiti Tunku Abdul Rahman,

in partial fulfilment of the requirements for the degree of

Master of Science

December 2022

ABSTRACT

INVESTIGATION OF THE COMBINED METHODS OF FILTRATION, COPPER OXIDE NANOPARTICLES AND MICROALGAE ON PALM OIL MILL EFFLUENT (POME) TREATMENT

Phang You Kang

In the developing country like Malaysia, the demand of freshwater and water pollutions has become the issues concerned by the society. The water pollution caused by the agroindustry especially the palm oil industry requires a long duration to recover. The research on palm oil mill effluent (POME) is to discover the alternative treatment method that can reduce current treatment time, at the same time improve the water quality effectively. In this research, the POME was undergone pre-treatment by passing through a conventional filtration system set up using coarse sand, fine sand and activated carbon. Then, the filtered POME was treated with heterogeneous photocatalytic degradation. The copper oxide nanoparticles (CuO NPs) photocatalyst used for degrading the POME was greenly synthesized using papaya peel extract and copper (II) nitrate trihydrate salt. The green-synthesized CuO NPs were characterized with different analytical methods such as ultraviolet-visible (UV-vis) spectroscopy,

Raman spectroscopy, transmission electron microscopy (TEM), field emission scanning electron microscopy (FE-SEM) and other instrumentations. The analysis revealed that the CuO NPs were able to degrade 66 % of POME under ultraviolet light irradiation. After photodegradation, the treated POME was polished with two different microalgae which were *Chlorella vulgaris* and *Chlamydomonas reinhardtii*, respectively. The growth of both microalgal were observed without dilution of the pre-treated POME. As a result, the combination of these physical, chemical and biological treatment able to remove more than 90 % of colour, phosphate and ammoniacal nitrogen and remove more than 80 % of chemical oxygen demand (COD) and biochemical oxygen demand (BOD). The phytotoxicity of the treated POME was studied by monitoring the growth of mung bean seeds. The phytotoxicity of the treated POME was reduced 95 % after undergone the combination treatments.

ACKNOWLEDGEMENT

Firstly, I would like to thank my main supervisor, Dr. Tey Lai Hock and my co-supervisor, Dr. Mohammod Aminuzzaman from the bottom of my heart for their guidance, dedication, encouragement, patience and helpful suggestions throughout the research period. Their valuable knowledge and experience helped me a lot whenever I faced difficulties during the research period.

Next, I would like to express my gratitude to my university, Universiti Tunku Abdul Rahman (UTAR) for providing the opportunity, funding and necessary facilities and instruments in this research. Besides, I would like to thank all the lab officers from the Department of Chemical Science, Faculty of Science for their kindly assistance, technical support and guidance on handling some of the instruments in the laboratories.

Lastly, I appreciate sincerely all the moral and physical support from my lovely family and friends. I am pleased with their considerations, motivations and understanding throughout my research.

APPROVAL SHEET

This thesis entitled **"INVESTIGATION OF THE COMBINED METHODS OF FILTRATION, COPPER OXIDE NANOPARTICLES AND MICROALGAE ON PALM OIL MILL EFFLUENT (POME) TREATMENT"** was prepared by PHANG YOU KANG and submitted as partial fulfilment of the requirements for the degree of Master of Science at Universiti Tunku Abdul Rahman.

Approved by:

Tey Lai Hock

_____

(Dr. TEY LAI HOCK) Date: …20 DECEMBER 2022…
Assistant Professor/Supervisor
Department of Chemical Science
Faculty of Science
Universiti Tunku Abdul Rahman

A. Zaman

_____

(Dr. MOHAMMOD AMINUZZAMAN) Date: …20 DECEMBER 2022...
Assistant Professor/Co-supervisor
Department of Chemical Science
Faculty of Science
Universiti Tunku Abdul Rahman

FACULTY OF SCIENCE

UNIVERSITI TUNKU ABDUL RAHMAN

Date: 20 DECEMBER 2022

SUBMISSION OF THESIS

It is hereby certified that **PHANG YOU KANG** (ID No: **19ADM04144**) has completed this thesis entitled **"INVESTIGATION OF THE COMBINED METHODS OF FILTRATION, COPPER OXIDE NANOPARTICLES AND MICROALGAE ON PALM OIL MILL EFFLUENT (POME) TREATMENT"** under the supervision of Dr. Tey Lai Hock (Supervisor) from the Department of Chemical Science, Faculty of Science, and Dr. Mohammod Aminuzzaman (Co-supervisor) from the Department of Chemical Science, Faculty of Science.

I understand that the University will upload softcopy of my thesis in pdf format into UTAR Institutional Repository, which may be made accessible to UTAR community and public.

Yours truly,

(PHANG YOU KANG)

DECLARATION

I Phang You Kang hereby declare that the thesis is based on my original work except for quotations and citations which have been duly acknowledged. I also declare that it has not been previously or concurrently submitted for any other degree at UTAR or other institutions.

_____

(PHANG YOU KANG)

Date: 20 DECEMBER 2022

TABLE OF CONTENTS

LIST OF TABLES

LIST OF FIGURES

LIST OF ABBREVIATIONS

ADMI	American Dye Manufacturer's Institute
Å	Armstrong
A	Absorbance
APHA	American Public Health Association
BBM	Bold's basal medium
BOD	Biochemical oxygen demand
COD	Chemical oxygen demand
cm	Centimetre
cm^{-1}	Inverse centimetre
cm^{3}	Cubic centimetre
Cu	Copper
Cu^{2+}	Copper(II) ions
CuO NPs	Copper oxide nanoparticles
^{o}	Degree
^{o}C	Degree Celsius
$^{o}s^{-1}$	Degree per second
eV	Electronvolt

Fe_2O_3	Iron(III) oxide
g	Gram
g/g	Weight by weight in grams
g/L	Grams per litre
h	hours
kHz	kilohertz
L	Litre
m^3	Cubic metre
mg/L	Milligram per litre
mL	Millimetre
mL/s	Millimetre per second
mm	Millimetre
M	Molarity
NaOCl	Sodium hypochlorite
NH_4-N	Ammonniacal nitrogen
nm	Nanometre
N	Normality
OP	Orthophosphate
P	Phosphorus

PO_4^{3-}	Phosphate
POME	Palm oil mill effluent
ppm	Parts per million
Pt/TiO_2	Platinum doped titanium dioxide
rpm	Revolutions per minute
θ	Theta
TiO_2	Titanium dioxide
TN	Total nitrogen
TP	Total phosphate
UV	Ultra-violet
UV-vis	Ultra-violet visible
µm	Micrometre
W	Watts
WO_3	Tungsten oxide
wt%	Weight percent
% (w/v)	Percent of weight of solution in the total volume of solution
ZnO	Zinc oxide

CHAPTER 1

INTRODUCTION

1.1 Background of Study

In agricultural sector, palm oil industry is one of the main contributors to Malaysia's economy. The oil palm trees in Malaysia are *Elaeis guineensis* which are native to West Africa. The oil palm trees were introduced by British to Malaysia at first as ornamental plants then as commercial agricultural crop. Oil palm plantation occupies the largest surface area of land in agriculture activities of Malaysia to about 4.49 million hectares of land (MPOC, 2020a). The palm oil industry in Malaysia was accelerated in the 1960s under the agricultural diversification programme launched by the Malaysian government (MPOC, 2020a).

The palm oil industry is one of the booming industries in the world owing to the high demand for economical, nutritional and edible plant oil. Malaysia is one of the largest palm oil exporters in the world account for 11 % of world's oils and fats production and export trade of 27 % (MPOC, 2020b). Malaysia ranks the second palm oil producer in the world after Indonesia since 2006 (Phang et al., 2021). As industrial activities and urbanization increases the wastewater generation increases proportionally. According to the report of (Goi, 2020), the number of rivers categorized as clean in Malaysia were decreasing from the year 2008 to 2017. For example, water was divided into three

categories which were clean water, greywater and blackwater. Clean water was the water from the groundwaters, purified water and rainwater. Greywater and blackwater were usually referred to the domestic wastewater. The wastewater come from the kitchen, showers, and laundry were known as greywater while wastewater generated from the toilets including urine and faeces were classified as blackwater (Maurya et al., 2020). The major roots of pollution of the rivers were industrial activities and discharge of sewage. In Malaysia, the water pollution is mainly due to no strict jurisdiction, lack of public and industries participation in water resources management, and insufficient emphasis on non-structural measures such as social learning and application of science policy (Ahmed et al., 2020: Pahl-Wostl, 2002).

The treatment process for industrial wastewater is very tedious because the wastewater contains a huge amount of organic and inorganic pollutants which some of them may not be biodegradable. In order to preserve and maintain the sustainability of the environment, the palm oil industry in Malaysia have to comply with local laws and regulations such as Environmental Quality Act 1974 and Environmental Quality (Clean Air Regulations) 1978 (MPOC, 2020c). The common wastewater treatment used in palm oil industry are aerobic and anaerobic treatment. The wastewater of this industry is mainly generated at the stage of palm oil milling process. The brownish viscous colloidal liquid generated at this process is called palm oil mill effluent (POME).

1.2 Problem Statement

Oil palm industry in Malaysia has been developed since decades ago. However, the pollutions caused by this industry are still happening and needed further concerned. The amount of POME generated for every tonnes of fresh fruit brunch processed is approximately 0.5–0.75 tonnes (Yacob et al., 2006). The brownish acidic (pH 4.5–5) POME mostly consist of water (95–96 %) followed by 4–5 % of total solids made up of 2–4 % of suspended solids and trace amount of oil and grease (0.6–0.7 %) (Dashti et al., 2020). Another characteristic of POME is the very high amount of organic matters which gives rise to high chemical oxygen demand (COD) (> 40,000 mg/L) and biochemical oxygen demand (BOD) (> 25,000 mg/L) (Alhaji et al., 2016). Some of the examples of organic pollutants that contribute to COD and BOD are lignin (~ 4700 mg/L), phenolics (~ 5800 mg/L), pectin (~ 3400 mg/L) and amino acids (Charles and Cheng, 2019).

The most common method used in POME treatment is ponding system which more than 91 % of palm oil mills in Malaysia are practicing this way. However, the outcome of this treatment is either barely achieve or unable to meet the permissible discharge limit set by the local authorities. According to the Malaysian Department of Environment (DOE), parameters such as three-day biochemical oxygen demand (BOD_3) was set to be lower than 20 ppm and the content of total nitrogen must be less than 150 ppm (Zainal et al., 2017). In addition, ponding system not only consume an enormous space but also

generating greenhouse gases during the long retention time (> 60 days) of the POME degradation (Cheng et al., 2017).

The two typical processes used in the industrial wastewater treatment are primary treatment which mainly removes the solids and particles in wastewater and secondary treatment that employs microorganisms to clean-up the organic pollutants and nutrients remained in the water (Udaiyappan et al., 2017). Either the physical, chemical or biological treatment alone is not sufficient to purify the polluted water. The physical treatment such as filtration can remove the insoluble particles effectively but not the soluble substances like nutrients (phosphate and ammonia). Chemical treatment such as coagulation-flocculation with coagulants (aluminium sulphate, iron salts and etc.) are usually coupled with physical treatment. The coagulants will aggregate the small particles and neutralize the ions in the wastewater to form a larger clump that can be easily removed by filtration. In some cases, the overdose of chemicals may result in secondary pollution and increase the treatment cost.

Besides, ponding system of POME treatment employs microorganisms, for examples, bacteria, fungi and algae to degrade the organic pollutants. The application of biological treatment is usually slow and need a longer time (Cheng et al., 2017). In order to increase the efficiency of POME treatment, pre-treatment must have been done to remove any solid particles present in the effluent that may block light penetration which is essential for autotrophic organisms. The greenhouse gases produced during the anaerobic degradation of

POME can also be reduced and oxygen content in the water system will be increased due to activities of autotroph. Advanced oxidation process (AOP) applying Fenton process and photocatalysis is not a new method in wastewater treatment but it has attracted researcher's attention in degrading POME and it is still new to be discovered (Kanakaraju et al., 2017). The study of POME degradation with photocatalyst are very limited with only few metal oxide nanoparticles (e.g. WO_3, TiO_2, ZnO) had been tried in the POME treatment (Alhaji et al., 2017; Cheng et al., 2017; Zainuri et al., 2018).

1.3 Objectives

The objectives of this project are to develop a wastewater treatment system for POME treatment using combination of filtration, copper oxide nanoparticles and microalgae. To be more specific, the objectives will be as followings:

1. To synthesize copper oxide nanoparticles using papaya peel biowaste and their characterizations using various analytical tools.

2. To investigate the effect of the POME after undergone filtration and photocatalytic degradation, as a nutrient on the microalgae growth (e.g. *Chlorella vulgaris* and *Chlamydomonas reinhardtii*).

3. To study the effectiveness of the combined treatment methods on POME wastewater by determining the physico-chemical analysis (e.g. pH,

ammoniacal nitrogen and phosphorus content) and water quality (e.g. COD and BOD) of the treated POME.

4. To evaluate the impact of the treated POME on the growth of mung bean seeds (*Vigna radiata*).

1.4 Novelty of Study

A lot of studies have been done on POME degradation and utilization of POME as nutrients source for various microalgae. Application of photocatalyst to degrade POME is still rarely revealed. The most common catalyst studied in POME degradation is titanium dioxide (TiO_2) due to its well-known photocatalytic performance. Other possible catalysts or alternative methods are needed to be discovered to broaden the knowledge in POME degradation. Copper oxide nanoparticles are a type of semiconductor that had been reported in other wastewater treatment such as textile industry and dye degradation but there is no publication in POME degradation (Das et al., 2018; Sreeju et al., 2017). Physical treatment like membrane technology was also used in the POME treatment since it can effectively remove the pollutants in POME (Jasney et al., 2014). However, a conventional filtration system is proposed in this study as membrane technology costs highly. Previously, a combination of physical, chemical and biological treatment had been done on leachate sample (Kamala et al., 2018). The combination treatment showed an excellent result (>94 %) in removing COD, BOD, total organic carbon and heavy metals. Up to date, there is no other research using the integration of trio methods in POME

treatment. Besides, the established treatment is expected to be applicable to POME, hence, investigation was carried out in this research to study the efficiency of pollutants removal.

CHAPTER 2

LITERATURE REVIEW

2.1 POME and Its Impacts to Environment and Health

Malaysia is one of the largest palm oil producers in the world. The oil palm tree in Malaysia also known as African oil palm. In the lifespan of the oil palms, they can contribute to palm oil production for 20–25 years. In this period, they can generate about 10–35 tonnes of fresh fruits every year from every hectare of plantations (Lin et al., 2016). In 2015, an average of 62 million tonnes of POME had been generated from the production of about 20 million tonnes of crude palm oil (Ding et al., 2020). The palm oil industry is still growing, the agricultural wastes especially the POME will be increasing annually.

POME is mainly produced from clarifier, sterilisation, hydrocyclone wastewater and separator sludge (Lin et al., 2016; Poh et al., 2010). Basically, POME including palm press fibres, empty fruit brunches, palm kernel shells, oil palm fronds and trunks are the examples of agro-wastes generated from this industry (Lin et al., 2016; Hazman et al.,2018). Among the wastes generated, POME occupied the largest portion. As a result, the high organic content in the POME contributed to elevated COD (> 50000 mg/L), BOD (> 25000 mg/L), total solids (> 40000 mg/L), residual oil (~ 6000 mg/L), total nitrogen content (~ 750 mg/L) and colour (ADMI) (> 500) (Bello and Raman, 2017). The organic

pollutants in the POME also extensively reduce the light penetration of the water if directly discharged to the water bodies. Lignin, carotene, humic acids are parts of the degraded by-products of lignocellulosic matters that darkened the colour of POME (Bello and Raman, 2017).

Moreover, the high nutrient loads (phosphorus, nitrogen and trace metals) in the POME may cause eutrophication which can increase the rate of oxygen depletion and suffocate the aquatic lives if the POME is disposed to the environment without any further treatment (Alhaji et al., 2016; Halim et al., 2016; Lin et al. 2016; Ding et al., 2020). Eventually, this situation may interrupt the aquatic food chain and clean water source (Soleimanianadegani and Manshad, 2014). In wastewater, the nutrients will promote the growth of bacteria. The wastewater must be treated and disinfected to prevent these harmful microorganisms being released to the surroundings. Bacteria that can cause harmful diseases like diarrhoea, cystitis, peritonitis and etc. will be a high threat to public health. *Escherichia coli* (*E. coli*) is the most common pathogenic microorganisms found in municipal and industrial wastewater and usually targeted in wastewater treatment (Wong et al., 2019).

The degradation of POME will liberate greenhouse gases that may give rise to global warming (Putri et al., 2011). According to Ding et al. (2020), for one tonne of POME, about 28 m^3 biogas will be generated. In the biogas, more than half of it is methane gas (CH_4) and the remaining will be carbon dioxide (CO_2) and hydrogen sulphide (H_2S). In addition, the utilization of the methane

gas as the fuel for energy generation for the factory will further release additional CO_2 gas to the environment. Other than greenhouse gases emission, the smoke and airborne particulates released from the palm oil mills will risk public health if the milling factory is too close to the residential area (Alhaji et al., 2016). The air pollutants will also have an unpleasant odour (Kanakaraju et al., 2017).

Industrial wastewater must be monitored and treated before discharged to the environment inclusive of POME. Although POME is non-toxic effluent, the high organic loads and nutrients content will induce other severe environmental problems. Since palm oil industry has high economic remunerable value, it is the industry's responsibility to preserve the environment in order to ensure the sustainability development and economic growth (Azmi and Yunos, 2014). Local authorities such as Environmental Protection Agency (EPA), Malaysia's Department of Environment (DoE) and the Malaysian Environmental Quality Regulations have implemented proper waste management to reduce the pollution caused by POME disposal (Halim et al., 2016; Ng and Cheng, 2016; Hazman et al., 2018). As stated in Environmental Quality (Prescribed Premises) (Crude Palm Oil) Regulations 1977, the permissible standard discharge limits for the POME to be dumped into environment are as following.

Table 2.1: Standard discharge limits for POME

Parameters	Standard discharge limits (Year 1984 onwards)
Biochemical oxygen demand (BOD), 3 days (mg/L)	100
Chemical oxygen demand (COD) (mg/L)	-
Total solids (mg/L)	-
Suspended solids (mg/L)	400
Oil and grease (mg/L)	50
Ammoniacal Nitrogen (mg/L)	150*
Total Nitrogen (mg/L)	200*
pH	5.0–9.0
Temperature (^{o}C)	45

* Referring filtered sample.

There were several POME treatment methods that have been practiced to diminish the environmental pollutions. Demand of freshwater will become a growing issue when clean water sources decrease due to uncontrollable disposal of industrial effluent and the competition of freshwater between industrial and domestic.

2.2 Current POME Treatment Methods

2.2.1 Anaerobic Ponding System

As reported in literature, more than 85 % of local palm oil mills were practicing anaerobic digestion and facultative pond system (Ding et al., 2016; Kanakaraju et al., 2017; Putri et al., 2017). In wastewater treatment especially POME treatment, anaerobic digestion was the most applied method for primary treatment (Poh et al.., 2010). The main reason for this treatment to be chosen as primary treatment was low cost in term of labour investment. However, the wastewater discharged from this treatment method was barely meet the standard discharge limit set by local authorities (Sayuti, and Azoddein, 2015). Not only that, there were many drawbacks in aerobic digestion method.

One of the main disadvantages of this method was a long retention time (>2 months) needed (Azmi and Yunos, 2014; Ding et al., 2016; Kanakaraju et al., 2017). Besides, in order to set up the ponding system, a large area of space was needed (Azmi, and Yunos, 2014; Kanakaraju et al., 2017). Bacteria were involved in the process since it was an anaerobic reaction. Greenhouse gases such as methane, carbon dioxide and hydrogen sulphide were some of the potential by-products released during the reaction. Consequently, they will cause pollution issues (Azmi and Yunos, 2014; Ding et al., 2016). In addition, the biogases generated can be odorous and dangerous as it may catch fire easily (Azmi and Yunos, 2014; Kanakaraju et al., 2017).

This POME treatment method can be improved even there were a lot of negative impacts. There was a group of researchers developed high-rate anaerobic bioreactor to overcome its drawbacks (Poh et al., 2010). The high-

rate anaerobic bioreactor required smaller space and sorter retention time compared to the conventional ponding system. Moreover, the biogases produced from the degradation process can be collected and used for other purpose, for instance, electricity generation (Poh et al., 2010; Ding et al., 2016). It was reported that high-rate anaerobic bioreactors like upflow anaerobic sludge blanket, upflow anaerobic sludge fixed film, anaerobic contact digester, expanded granular sludge bed and anaerobic filler were able to reduce chemical oxygen demand (COD) in POME to 90 % (Poh et al., 2010).

2.2.2 Filtering Technique

Other than chemical and biological method, physical treatment is another common method applied in wastewater treatment. Filtration is one of the common physical method that can almost be applied to all kind of wastewater.

2.2.2.1 Membrane Separation Technology

Membrane separation technology is an advanced filtration method which demonstrates the same mechanism that wastewater is passing through a certain pore size to remove the undesirable particle. Membrane separation technology had been applied in variety field of industry due to its high applicability in wastewater treatment. According to Azmi and Yunos (2014), the outgoing water after membrane separation technology had more consistent water quality regardless the influent variations. The membrane separation wastewater treatment plant does not require high skilled operator as the systems are fully automated. The water treated from the system can be reclaimed and reused

concurrently reducing water supply cost. The application of membrane separation technology is effective to industrial wastewater as well as POME, in terms of water quality and time.

Despite the benefits of using membrane separation technique, there is still one main drawback of it. The installation and maintenance fee of the system is relatively high at starting stage. The maintenance cost of the treatment system can be lowered by pretreatment of the POME to reduce suspended solids before passing through the ultrafiltration membrane, in addition, increase the lifespan of the membrane. Besides, the treatment time of the technology is shorter than conventional treatment and high spatial consumption will increase the cost of treatment compared to separation technique (Azmi and Yunos, 2014).

Moreover, Azmi and Yunos (2014) reported pretreatment of POME using adsorption treatment with activated carbon fabricated from palm kernel shell. After adsorption, the particles will settle down to the bottom and improve an average of 60 % of the water quality. Then, the resultant water will be treated with ultrafiltration method. Ultrafiltration is a very effective treatment that can remove more than 99 % of pollutants in POME which can be observed trough the parameters of total solids, dissolved solids, suspended solids, BOD_5, COD and turbidity.

2.2.2.2 Sand Filtration System

Sand filtration system consists of sands in different grain size to meet the purpose of application in different types of water and wastewater treatment. There are two common types of sand filtration system which are slow sand filtration (SSF) and rapid sand filtration (RSF).

Slow sand filtration (SSF) system is a low cost, low energy demand, simple and sustainable technology that utilizes the combination process of physical, chemical and biological treatment in removing the contaminants in wastewater (Verma et al., 2017). The filter columns are usually composed of fine sand and coarse sand as the media and supported by pebbles and gravels at the bottom of the column. The efficiency of the filtration system is mainly affected by the depth of the sand bed and particle size of the sand (Verma et al., 2017). In the SSF, the particle size of the sand is relatively small which is in the range of 0.15–0.3 mm (Maurya et al., 2020). The flow rate of the SSF is reduced due to the smaller gap between particles but the surface area of contact with wastewater is increased because of the smaller particle size (Maurya et al., 2020).

In slow sand filtration process, a slimy matrix might be formed on top layer of the filter medium. This biological active layer is known as *schmutzdecke* layer composed of bacteria, fungi, protozoa and basically the green algal (Verma et al., 2017; Maurya et al., 2020). The narrow gap and closely compact filter media reduces the flow rate of the wastewater. Therefore,

the long retention time of the water gradually allows the microorganisms to develop the *schmutdecke* layer on the granular media (Maurya et al., 2020). The biological active layer of the SSF plays a more significant role in this water purification process (Brandt et al., 2017). According to Brandt et al. (2017), the filter can be differentiated into three functioning zones which are the *shmutzdecke* (top layer), 'autotrophic' zone and the 'heterotrophic' zone. The top layer functions to absorb colloidal organic material in the wastewater while the autotrophic layer plays the role to oxidize the filtrate in this layer. The plant life grows in this region will decompose the organic materials, uptake the nutrients (phosphorus and nitrogen), and also release oxygen for the oxidation process (Brandt et al., 2017). In the third layer of the SSF, bacteria will be the dominating organism. At this stage, the bacteria grow rapidly, hence, increase the rate of decomposition of organic matter leaving the leftover of inorganic substances and salts (Brandt et al., 2017).

Another type of sand filtration is rapid sand filtration (RSF). This filtration system is not as effective as SSF since the particle size used to construct this system is larger (0.4–1.5 mm) (Brandt et al., 2017). The RSF system does not contain the microorganisms layer on top of the filter media, hence, the filtration only involves single treatment process which is physical treatment (Maurya et al., 2020). The flow rate of RSF is higher than SSF since the larger particle size gives a larger void between particles. Besides, RSF is able to remove suspended solids and biological particles such as algal (5–20 µm), protozoan cysts (3–10 µm), bacteria (0.2–2 µm), and viruses (0.01–0.1 µm) (Maurya et al., 2020). Both SSF and RSF are proved capable to remove

microorganisms like *Giardia* cysts, *Cryptosporidium* oocysts, fecal coliform, *Salmonella*, *Pseudomonas aeruginasa*, *Escherichia coli*, total coliform, *Entamoeba histolytica* cysts and etc. (Verma et al., 2017).

2.2.3 Advanced Oxidation Process (AOP)

Degradation of POME by oxidation process is rather a new trend compared to the conventional methods mentioned above. There is still limited research on treating POME using advanced oxidation process up to date. Advanced oxidation process is a treatment method by generating reactive oxidative species or highly reactive radicals such as hydroxyl radicals ($OH^{\bullet}$) and superoxide anions ($O_2^{-\bullet}$) to decompose organic pollutants (Kanakaraju et al., 2017). There are several reactions that can be applied to generate the powerful oxidizing agents, for instance, photocatalysis, ozonation, wet ozonation and Fenton reaction (Kanakaraju et al., 2017).

In order to initiate the radical chain reaction, an activator is needed. The common activating agents used in the reaction are ultra-violet (UV) irradiation, metals, heat and hydrogen peroxide (Lin et al., 2016). Kanakaraju and co-workers (2017) reported treatment of POME by Fenton reaction initiated by UV from sunlight. A Fenton reaction is a reaction carried out in acidic condition by oxidation of ferrous ions (Fe^{2+}) to ferric ions (Fe^{3+}). The oxidation reaction of the photo-Fenton reaction is shown below.

$$Fe^{2+} + H_2O \rightarrow Fe^{3+} + OH^- + OH^{\bullet} \quad \text{(Eq. 2.1)}$$

As reported by Kanakaraju's team (2017), photon is essential for the activation of Fenton reagents. This statement can be supported by their research which the catalytic performance under solar irradiation is better than the indoor reaction. At optimum condition, the maximum efficiency of COD removal for solar photo-Fenton reaction is 89 % while for indoor photo-Fenton reaction is 78 %, after 3 hours of irradiation.

Other than Fenton process, there is another oxidation process named persulphate oxidation utilizing persulphate anions ($S_2O_8^{2-}$) as an oxidizing agent (Lin et al., 2016). Hydrogen peroxide can be used coupled with persulphate anions as an oxidizing agent and activator of the reaction. The radicals released from the persulphate oxidation are sulphate radical ions ($SO_4^{\bullet-}$) and hydroxyl radicals ($OH^{\bullet}$). The predominant radical released in acidic and alkaline environment are different. The predominant radical generated in acidic condition is $SO_4^{\bullet-}$ while in alkaline condition is $OH^{\bullet}$. The equations below are the radical formation in acidic and alkaline conditions (Lin et al., 2016).

Acidic: $$S_2O_8^{2-} + H^+ \rightarrow HS_2O_8^- \quad \text{(Eq. 2.2)}$$

$$HS_2O_8^- \rightarrow H^+ + SO_4^{\bullet-} + SO_4^{2-} \quad \text{(Eq. 2.3)}$$

Alkaline: $$SO_4^{\bullet-} + OH^- \rightarrow SO_4^{2-} + OH^{\bullet} \quad \text{(Eq. 2.4)}$$

$$SO_4^{\bullet-} + H_2O \rightarrow SO_4^{2-} + OH^{\bullet} + H^+ \qquad \text{(Eq. 2.5)}$$

The weight ratio of persulphate and hydrogen peroxide, $S_2O_8^{2-}/H_2O_2$ (g/g) is identified and the degradation of POME is carried out at the optimum condition. Lin et al. (2016) reported a dosage ratio of $S_2O_8^{2-}$:H_2O_2 at 1.0:1.5 had the highest COD removal of 56.9 % within 20 minutes of reaction time.

The most common oxidative degradation applied in wastewater treatment is by using heterogeneous photocatalyst. Solar spectrum consists of light with different energy and wavelength, specifically about 46 % of visible light and 5 % of UV light (Cheng et al., 2017). Photocatalytic degradation has become a new green alternative to treat POME due to its promising advantages. The main advantages of using catalyst are low cost, high chemical stability, non-toxicity, well absorption to solar spectrum and robust to photo-corrosion (Alhaji et al., 2017; Cheng et al., 2017).

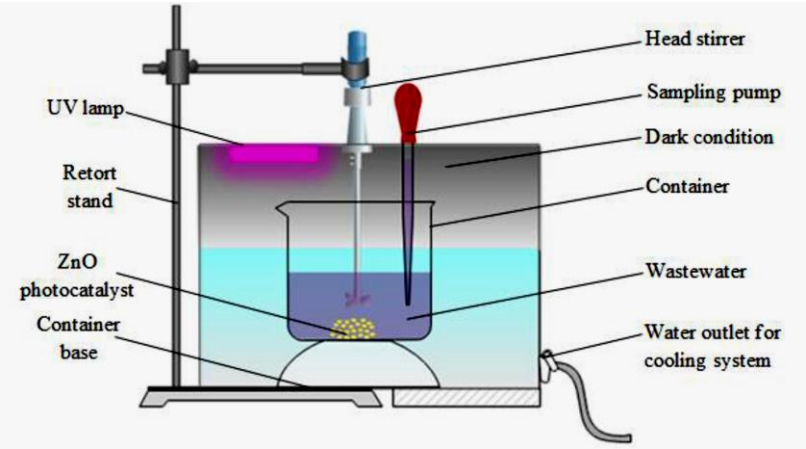

Figure 2.1: Laboratory scale degradation of POME by UV illumination (Zainuri et al., 2018)

Since the catalyst need photon energy to be activated, they are usually semiconductor or materials doped with semiconductor. The photon irradiated on the surface of catalyst will excite the semiconductor materials to generate electron-hole pairs which react with oxygen and water to form reactive oxidative species likely $O_2^{-\bullet}$ and $OH^{\bullet}$ (Alhaji et al., 2017). Different photocatalysts, for example, TiO_2, WO_3, Fe_2O_3, ZnO, etc. have been applied to POME degradation but TiO_2 has the best photocatalytic performance among the others. Kanakaraju and co-workers (2017) compared the efficiency of COD removal in POME by using TiO_2 and ZnO under solar irradiation. In their study, the former was better as it can remove 88.5 % of COD with lesser catalyst loading (0.1 g/L). The COD removal efficiency by using ZnO was much lower (60.5 %) even though the catalyst loading was 20 times higher than TiO_2. Besides, they also found that ZnO exhibit photo-corrosion in acidic environment.

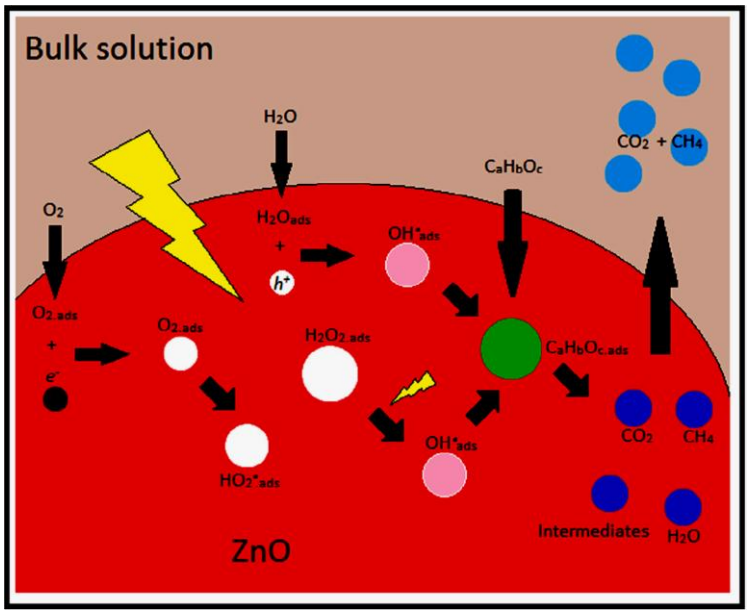

Figure 2.2: Mechanisms of photodegradation of POME using zinc oxide nanoparticles and UV light proposed by Ng and Cheng (2016).

There was another group of researchers also studied the effectiveness of TiO_2 in POME degradation. Cheng and co-workers (2015) have increased the properties of TiO_2 by doping with Platinum (Pt). TiO_2 has a wide band gap nearly 3.3 eV which is effective in UV absorption. The band gap of the semiconductor can be narrowed by depositing Pt on TiO_2 to broaden the absorption of light spectrum (Cheng et al., 2015). In their research, Pt/TiO_2 had a higher ability to remove organic pollutants in the pre-treated POME as compared to pure TiO_2, under the irradiation of both UV and visible light. The Pt/TiO_2 was capable of removing 90 % of organic compounds in 300 mL of pre-treated POME with a concentration of 0.5 wt% catalyst loading after 8 hours of reaction time.

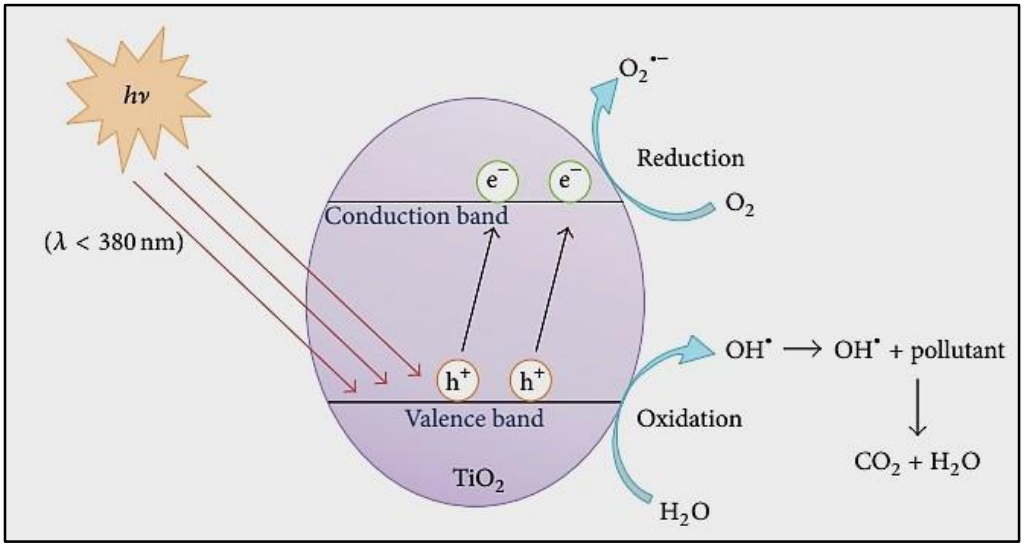

Figure 2.3: General photocatalytic degradation of organic pollutants by TiO_2 (Feng et al., 2014).

The amount of visible light occupied nearly half section of the solar spectrum hence research should be focusing on harvesting visible light spectrum

to activate a photocatalyst (Cheng et al., 2017). Other than TiO_2 and ZnO, tungsten oxide (WO_3) was studied to evaluate its photocatalytic activity towards POME degradation (Cheng et al., 2017). The optimum amount of WO_3 to be used in POME degradation had been investigated at a duration of 4 hours using UV light irradiation. Colour and COD were the targeted pollutants in the study. The catalyst loading ranging from 0.2 g/L to 3.0 g/L were investigated. A higher dosage of catalyst does not always promise a higher catalytic rate as when the organic pollutants are bound to the catalyst, the exceeding catalyst will have no effect and be gone to waste. It was found that 0.5 g/L of WO_3 had the highest efficiency in removing COD and colour (Cheng et al., 2017). The COD removal efficiency at 0.5, 1.0, 2.0, 3.0 and 0.2 g/L in descending order were 51.15 %, 50.45 %, 50.00 %, 48.31 % and 32.71 %, respectively. While decolouring using WO_3 at 0.5, 1.0, 2.0, 3.0 and 0.2 g/L were 96.21 %, 96.07 %, 95.87 %, 95.81 % and 95.23 %, respectively.

2.2.4 Microalgae Treatment

POME is the wastewater discharged after the palm oil fruits milling process. It contains a very huge amount of bioavailable compounds like nitrogenous compounds, sugars, lipids, and other nutrients needed for microorganisms' growth (Ibrahim et al., 2015). Among the treatment methods applied to POME, biological treatment is the most widely used in local due to cost saving and environmentally friendly (Selmani et al., 2013). However, methods such as anaerobic digester and aerated lagoons are not effective as they can barely meet the permissible limit set by local authorities (Kamyab et al., 2015).

Although these biological treatment methods are not effective, microalgae can be employed as a new potential alternative in treating POME. Kamyab et al. (2015) reported that microalgae have been involved in wastewater treatment since 1950. Microalgae are prokaryotic or eukaryotic photosynthetic microorganism that utilize solar energy and nutrients in water to grow (Selmani et al., 2013; Ibrahim et al., 2015).

Microalgae have attracted a lot of attention in wastewater treatment. Microalgae are capable to grow and reproduce rapidly as their photosynthetic efficiency are forty-two times higher than terrestrial plants thus, high yield of biomass can be processed for value-added products (Ding et al., 2016). Besides, microalgae are persistent in extreme environment and even utilize the organic and inorganic pollutants in wastewater as their nutrients to survive (Kamyab et al., 2015; Ding et al., 2016). Application of microalgae in wastewater treatment is a promising green technology with low demand of freshwater. In addition, it is a renewable source that can be cultivated continuously if the condition is remained suitable for its growth.

Various species of microalgae have been studied and applied in municipal, agriculture and industrial wastewater. POME is wastewater with high chemical oxygen demand (COD) and biochemical oxygen demand (BOD) which can be 100 times higher than municipal sewage (Kamyab et al., 2015). The high nitrogen and phosphorus content in POME will promote the growth of microalgae and increase the efficiency in removing the pollutants.

Application of microalgae in wastewater remediation requires a shorter retention time compared to the conventional ponding system. The application of different species of microalgae in wastewater treatment and their efficiency in removing pollutants are summarized in the table below.

Table 2.2: Summary of various microalgae in different industrial wastewater treatment

Microalgae species	Wastewater	Pollutants	Efficiency (%)	References
Spirulina platensis	POME	NH_4-N	93.8	Kamyab et al., 2015
		TN	91	
		P	96.8	
		COD	84.9	
		BOD	78.3	
Scencedesmus dimorphus	POME	NH_4-N	88.5	Kamyab et al., 2015
		TN	87.5	
		P	92.5	
		COD	79	
		BOD	71.5	
Botryococcus Braunii	POME	NH_4-N	92.85	Ibrahim et al., 2015
		OP	56.5	
Chlamydomonas sp.	Pre-treated POME	TP	38.15-68.53	Ding et al., 2016
		COD	8.59-29.13	
		TN	43.5-72.97	
		NH_4-N	58.58-100	
Chlamydomonas incerta	POME	COD	67.35	

Characium sp.	Anaerobic POME	COD	45.4	
		TN	90.35	
		NH_4-N	90.35	
		Phosphate	99.5	
Chlorella pyroidosa	Soybean processing wastewater	COD	~77.8	
		TN	~88.8	
		NH_4-N	~89.1	
		TP	~70.3	
Chlorella sp.	POME	TN	~59	Elystia et al., 2019
		COD	34.4-63.1	

2.2.5 *Chlorella vulgaris* and its application in POME treatment

Chlorella vulgaris is a type of common microalgae that can be easily found in nature such as freshwater, ocean and also terrestrial environment (Ru et al., 2020). *C. vulgaris* is a green microalga which can undergo photosynthesis as it has the green pigments, chloroplasts similar to that of higher plants (Coronado-Reyes et al., 2020). The characteristics of the *C. vulgaris* can be identified by the relatively spherical shape of the single microalgae cell in microscopic size ranging from 2 – 10 µm (Coronado-Reyes et al., 2020). Besides, *C. vulgaris* does not have any feature such as flagella that can aid in mobility. These microalgae exist in the environment either in individual or in a cluster of colonies up to 64 cells. According to Coronado-Reyes et al. (2020), *C. vulgaris* can grow better in mixotrophic condition as higher yield of biomass was reported in literature. In a medium rich with organic carbon source, it can carry out heterotrophic growth with the absence of light energy. Moreover, *C. vulgaris* can survive in extreme environment where there is limited nutrient source and high stress (Wirth et al., 2020).

Since microalgae is not a new technology in wastewater treatment, application of *C. vulgaris* in different types of wastewater have been explored. The cultivation of *C. vulgaris* can be found in municipal wastewater and agricultural wastewater such as poultry industries and palm oil mill effluent (Lee et al., 2016; Khalid et al., 2019; Wirth et al., 2020). Liquid waste was always the quintessential source of nutrients for the growth of microalgae due to the higher bioavailability of soluble nutrients to the microalgae even the

insoluble nutrients can be available through natural conversion process (Khalid et al., 2019). Previous research found that POME possessed a high potential as the feedstock for the cultivation of *Chlorella* sp. for lipid and biodiesel productions (Cheah et al., 2018; Cheah et al., 2019). To be more specific, *Chlorella* sp. was well known for its rapid growth, ability to accumulate lipid, capable of assimilating organic and inorganic pollutants definitely enhanced its application in the pre- and post-treatment of POME (Hazman et al., 2018; Tan et al., 2018).

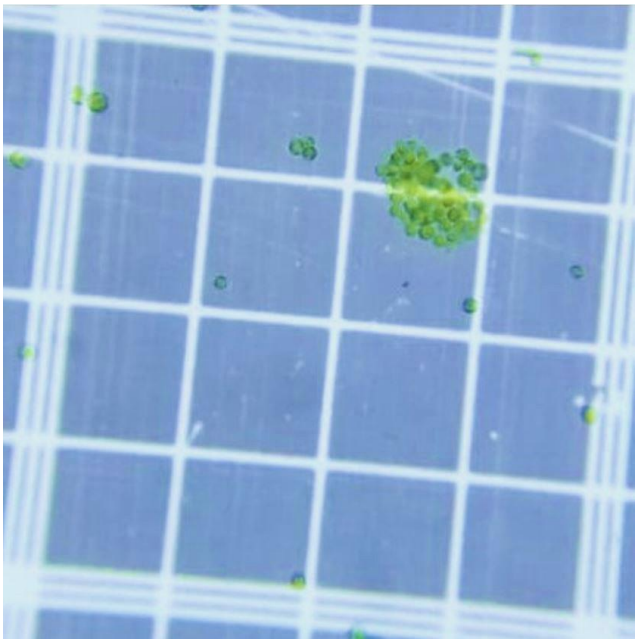

Figure 2.4: Microscopic view of *C. vulgaris* under microscope (Coronado-Reyes et al., 2020)

2.2.6 *Chlamydomonas reinhardtii*

Chlamydomonas reinhardtii is a typical green algae used widely in the research of metabolic pathways and in numerous experiments (Zhang et al., 2017).

According to Pascoal et al. (2021), the *Chlamydomonas* genus is oval in shape with two antenna-like flagella in the head. *C. reinhardtii* is a mobile microalga in the freshwater using flagella. Ahmadi et al. (2021) introduced *Chlamydomonas* as the ancestor of the green algae. Mixotrophy is the best cultivation mode for *Chlamydomonas*. *Chlamydomonas incerta* showed the highest yield of biomass, highest specific growth rate and best pollutants' removal efficiency when cultivated in mixotrophic mode (Alqadi et al., 2017). A study conducted by Moon et al. (2013) using *C. reinhardtii* also proved that *Chlamydomonas* can grow better in mixotrophic cultivation because higher amount of biomass and lipid production can be obtained.

2.3 Factors Affecting Photocatalysis

As discussed in the previous section, photocatalysis is one of the advanced oxidation processes (AOPs). The generation of reactive oxidative species such as hydroxyl radicals ($OH^{\bullet}$) and superoxide anions ($O_2^{-\bullet}$) are the main role in AOPs. Application of photocatalysis in wastewater treatment using metal oxides have been extensively studied since recent decades due to easier generation of $OH^{\bullet}$, small amount of catalyst loading and rapid reaction time (Bello and Raman, 2017). Bokare and Choi (2014) suggested that AOPs can be applied alone or worked together with biological treatment. AOPs can be used as the pre-treatment of wastewater, however, the high organic pollutants in wastewater might nullify the function of $OH^{\bullet}$. They also claimed that application of AOPs as post-treatment after biological treatment would have a better efficiency and reduce the oxidative radicals' competitive scavenging by

the biodegradable pollutants. In fact, there are many factors that may affect the effectiveness of photocatalysis in wastewater treatment.

2.3.1 pH

The pH of the sample will affect the efficiency of removal of specific pollutants and the performance of semiconductor metal oxides. A nitrite and ammonia removal study by Ye and co-workers (2019) showed that efficiency of nitrite removal by using Zinc ferrite/Activated carbon hybrid catalyst under UV-Vis illumination was increased when the pH was increased from 8.5 to 9.5. At pH 8.5, the removal of nitrite was 54.7%. The efficiency of removal was increased approximately two folds to 92.7 % when the pH value was increased to 9.5. When above the optimum pH, the efficiency started to drop from pH 10.0 onwards. The same situation applied to removal of ammonia where highest efficiency of 64.0 % was achieved at pH 9.5 and started to reduce until 36.5 % at pH 10.5. Hydrogen ions (H^+) will be released during the oxidation of ammonia while reduction of nitrite involved H^+ ions. Equilibrium was achieved at pH 9.5 which was the optimum pH of the simultaneous removal of both pollutants. The equations for removal of nitrite and ammonia are as following (Ye at al., 2019).

$$2\ NH_3 + 6\ h^+\ (\text{valence band}) \rightarrow N_2 + 6\ H^+ \qquad \text{(Eq. 2.1)}$$

$$2\ NO_2^- + 8\ H^+ + 6\ e^-\ (\text{conduction band}) \rightarrow N_2 + H_2O \qquad \text{(Eq. 2.2)}$$

There was another research investigated that changing in pH of POME sample would affect the degradation efficiency or not. Cheng et al. (2017) had altered the POME sample to acidic and basic using sulphuric acid and sodium hydroxide solution. In their findings, basic POME sample (pH 9 and 12) become foggy, hence, it was not suitable to be used for photocatalytic treatment with tungsten oxide (WO_3). On the other hand, the acidic POME sample (pH 3 and 5) had photodegradation efficiency similar to un altered POME sample (pH 7). The COD removal by pH 3, 5 and 7 were 50.32 %, 51.84 % and 51.15 %, respectively. At the end of the experiment, it was found that the initial pH alteration did not affect the pH of the POME samples after photocatalytic treatment.

Besides, pH value will affect the properties of the catalyst. Surface charge of the catalyst will be altered under acidic or alkaline condition. The protonated surface will attract anionic pollutants while deprotonated will easily attract cationic pollutants. In the report of Alhaji et al. (2016), in the pH range of 4.5–7.0, the surface charge of TiO_2 will be zero where there is no electrostatic force of attraction towards any pollutants. The change in electrostatic force will affect the location of conductance and valence bands and the size of the aggregated particles. The surface properties of TiO_2 in acidic and basic condition were illustrated by Gaya and Abdullah (2008) as shown below.

Acidic: $TiOH + H^+ \rightarrow TiOH^+$ (Eq. 2.3)

Basic: $TiOH + OH^- \rightarrow TiO^- + H_2O$ (Eq. 2.4)

2.3.2 Amount of catalyst

Since photocatalyst is an important agent used in photocatalytic treatment of wastewater, the amount of catalyst used is very essential in enhancing the efficiency of photodegradation. In the photodegradation of humic acid using TiO_2, Andayani and Bagyo (2011) reported that increase in the amount of TiO_2 constantly increase the effectiveness of degradation. The reason was the increase in total surface area of photocatalyst generatess more reactive oxidative species.

Another study conducted by Neena et al. (2018) using Fe-Cd co-doped ZnO in mineralizing Rhodamine B and methylene blue dye solutions showed the increase in the amount of catalyst will increase the rate of degradation. In fixed concentration of dye solutions (20 mg/L), they increased the concentration of photocatalyst from 50 mg/L to 150 mg/L to photodegrade the dyes for 140 minutes under visible light irradiation. As reported by Andayani and Bagyo (2011), the increase in catalyst's dosage increase the total surface area of catalyst for the generation of radicals. However, when the amount of catalyst above 150 mg/L, the efficiency of degradation was found to be decreasing. When the catalyst above the optimum dosage, the excess catalyst will increase the cloudiness of the solution and interrupt the light penetration and absorption (Neena et al., 2018).

Furthermore, ZnO photocatalyst was used by Ng and Cheng (2016) to degrade POME under UV irradiation. They investigated the relationship of the

amount of ZnO ranging from 0 to 1.5 g/L and efficiency of degradation. The degradation efficiency of POME was increased from 0.1 g/L to 1.0 g/L of ZnO. The percentage of COD removal was from more than 20 % until it achieved 50 % at the optimum ZnO dosage at 1.0 g/L. Again, when the amount of catalyst above optimum dosage, the removal of COD was reduced to 48.3 %. A similar research had been done by Cheng et al. (2017) to treat POME with WO_3 catalyst. They also found that when the catalyst loading over the optimum amount, the efficiency of photodegradation dropped. The excess catalyst in the POME samples will aggregate and cause light scattering effect.

2.3.3 Amount of substrate

The amount of photocatalyst used will definitely affect the rate of degradation of pollutants. Other factor such as the concentration of pollutants in the solution will be affecting the effectiveness of the photocatalytic performance of catalyst. In the photodegradation of rhodamine B and methylene blue using Fe-Cd co-doped ZnO, the rate of degradation of the dyes decreased as the concentration of the dyes increased (Neena et al., 2018). The generation of reactive oxidative species (ROS) is the important step to initial the degradation reaction. When the concentration of dyes increased, the active site on the surface of catalyst will be occupied by the pollutants, as a result, the generation of ROS will be inhibited. Besides, the high concentration of pollutants will affect the amount of light absorption by the photocatalyst. The excess pollutants will absorb the light before it reached the surface of the photocatalyst. Without sufficient light

energy, the production of ROS will be reduced, hence, affecting the photocatalytic performance (Neena et al., 2018).

2.3.4 Duration of reaction

The amount of pollutants and photocatalyst should be balance in order to have the optimum photocatalytic performance. When the condition is ideal for photocatalytic degradation, the contact time of the photocatalyst with the pollutants will become the factor affecting the efficiency of degradation. Cheng and co-workers (2017) demonstrated the importance of the contact time between POME samples and WO_3 photocatalyst. In the study, they had irradiated POME samples with WO_3 photocatalyst under UV irradiation for one day (24 hours). The rate of COD removal was very high within the first 12 hours of the reaction that may be caused by the higher amount of substrate at the beginning of the experiment. The degradation rate was 84.7 % at 16 h and become consistent at the subsequent hours. Meanwhile, the decolourization of the POME samples was also investigated. The WO_3 photocatalyst was able to remove 98.3 % of the colour intensity within 8 h of reaction. After that, there was no further reaction occurred after 8 h.

Moreover, similar trend of photocaalytic performance was obtained by Ng and Cheng (2016) using ZnO photocatalyst. The photodegradation of POME using ZnO and UV irradiation was very fast at the first four hours. Then, the rate of degradation was slowed down. Ng and Cheng (2016) suggested that this might due to the reduction of concentration of organic pollutants and deposition

of carbon on the surface of photocatalyst, thus, reduced the photocatalytic performance after 4 hours of reaction. The intermediate species generated during the photomineralization also might accumulate on the catalyst and reduce the generation of ROS which were essential in degrading organic molecules (Gong et al., 2015).

2.4 Metal oxide nanoparticles

Metal oxide nanoparticles are semiconductors that showed high potential and ability as photocatalysts in degrading various organic pollutants including dyes, surfactants, solvents, pesticide, phenolic compounds, etc. into less harmful products under the irradiation of light energy (Phang et al., 2021). Due to their well-known semiconductor properties, intense research had been done to diversify the synthesis method and their application in wastewater treatment, in recent decades.

The common metals that were studied for this purpose including titanium dioxide (TiO_2), zinc oxide (ZnO), nickel oxide (NiO) and copper oxide (CuO). Some of the examples of the application of metal oxide nanoparticles in industrial wastewater treatment inclusive of landfill leachate (TiO_2), palm oil mill effluent (ZnO) and dye industry (NiO and CuO) (Das et al., 2018; Chai et al., 2019; Aminuzzaman et al., 2020; Azadi et al., 2020).

Zinc oxide (ZnO) nanoparticles was a famous photocatalyst which has a wide band gap energy (3.37 eV) making it excellent in degrading pollutants present in the water. Besides, it was one of the best choices as photocatalyst because of its abundance in environment, low toxicity and cost (Naseem and Durrani, 2021). Another metal oxide from the essential metals family, iron oxide, also showed its potential in wastewater treatment. The high porosity, large surface area to volume and magnetic properties of iron oxide nanoparticles made it a desire adsorbent of pollutants in wastewater especially in heavy metals removal and it can be easily separated from the water system using a magnet (Naseem and Durrani, 2021). He and co-workers (2017) reported the synthesis of iron oxide-biochar nanocomposite adhered with photosynthetic bacteria (PSB/Fe_3O_4/Biochar) as the material exhibited sorbent and/or catalytic properties. The report claimed that 83 % of COD, 86 % of NH_4^+ and 94 % of PO_4^{3-} were successfully removed by the PSB/Fe_3O_4/Biochar synthesized. The main mechanism for the nanocomposite to remove the pollutants was adsorption. The pollutants will adsorb on the porous nanocomposite followed by catalytic reaction under light irradiation. The bacteria adsorbed on the PSB/Fe_3O_4/Biochar will take up the carbon-containing substrate and nutrients in the wastewater.

Titanium dioxide (TiO_2) was the most concerned nanomaterials in photocatalytic studies. The extensive application of TiO_2 was due to its low toxicity, chemical stability, excellent photocatalytic performance and also antimicrobial activities (Naseem and Durrani, 2021). The high photocatalytic activities of TiO_2 has been highly applied in the degradation of pollutants in

wastewater such as dyes, palm oil mill effluent, landfill leachate and other industrial applications.

Other than photocatalyst and adsorbent, disinfectant used in wastewater treatment also plays a vital role to guarantee the safety and health of public and environment. Silver nanoparticles (Ag NPs) were reported to be an antimicrobial agent in sanitizing water. The Ag NPs can interact with the sulphur and phosphorus elements in the cells and enzymes which will cause disruption and deactivating enzymatic activities within the cell, eventually causing cell's death (Abdelbasir and Shalan, 2019). Moreover, silver oxide nanoparticles (Ag_2O NPs) were synthesized for the same purpose. Ag_2O NPs also showed excellent abilities as antimicrobial agent and photocatalyst. Jiang et al., (2015) studied the photocatalytic mechanism of Ag_2O NPs in degradation of methyl orange dye under the illumination of sunlight, ultra-violet light and visible light. The Ag_2O NPs showed superb results in degrading the dye. Similar to Ag NPs, Ag_2O NPs also capable to function as antimicrobial agent in inhibiting *Escherichia coli*, *Pseudomonas aeruginosa*, *Proteus mirabilis*, *Enterococcus faecalis*, *Staphylococcus aures* and etc. (Naseem and Durrani, 2021).

Various synthetic approaches have been reported for both chemically and biologically methods. The examples of chemical synthetic methods were sol-gel, chemical precipitation, γ-irradiation, solid-state interaction and other methods (Aminuzzaman et al., 2017). However, biologically approach was

gradually dominating in nanoparticles synthesis owing to this approach utilizing various parts of plants (leaves, root, flowers, fruits and seeds) and microorganisms (bacteria, fungus and algae) as one of the precursors in the synthesis process (Singh et al., 2018).

2.5 Synthesis of metal or metallic oxide nanoparticles

2.5.1 Chemical synthesis

The extensive studies of metal and metallic oxide nanoparticles by researchers for many years had diversified the synthesis methods. Among the synthesis pathways, chemical approaches were the common methods applied in industry. In this section, a few common chemical synthesis methods were discussed.

Co-precipitation or chemical precipitation of nanomaterials by chemicals were considered the simple and rapid method. In this method, sodium hydroxide (NaOH) was always used as the reductant to reduce the metal salt precursors. The desired metals salts can be in any forms (sulphate, nitrate, acetate, etc.) as long as they were soluble in water to become their respective ions form. The completion of the reduction of metal ions by the chemicals can be related to the colour change of the solutions. The synthesis of CuO nanomaterials from its metal salt solution can be observed from the decolourization of the Cu^{2+} blue colour. A final product of black precipitate (CuO) was usually observed at the end of reaction which can be separated by filtration or centrifuge (Suleiman et al., 2015; Hassan and Mahdi, 2016; Aboud et al., 2020). Surfactant such as tetraoctylammonium bromide (TOAB) had been

studied to be able to alter the size of the CuO nanomaterials to smaller particles and with more regular shape (Suleiman et al., 2015). Precipitation by using chemical reducing agents not only applicable to CuO but also other metals such as iron and zinc oxide (Hassan and Mahdi, 2016; Aboud et al., 2020). Other than NaOH, reducing agents such as ammonium hydroxide (NH_4OH), oxalic acid dehydrate solution were also utilized to reduce the metal salts (Mokhtari et al., 2013; Zainuri et al., 2018). The formation of ZnO can be identified as the formation white precipitate (Aboud et al., 2020). For the calcium ferrite ($CaFe_2O_4$) catalyst synthesized by Charles and Cheng (2019) using ethylene glycol and NaOH, the completion of the reaction was observed by the formation of reddish-brown precipitate that can be easily separated by centrifugation.

There was another method to synthesis metallic nanoparticles in smaller size and stable form. A high purity of metallic nanoparticles can be synthesized using electrochemical method. In the study conducted by Singaravalen and Alwar (2015), the only chemical needed for the synthesis of silver nanoparticles was the silver nitrate solution, acting as the electrolyte. The silver nanomaterials synthesized by this method was found to be highly crystalline and pure that was proven by the high intensity and sharp peaks of the XRD spectrum. Other than pure metal nanoparticles, metal oxide nanoparticles can also be synthesized by electrochemical method with the aid of reducing and capping agents. The stable, high purity and small size of CuO nanocrystals were synthesized in this way (Momin et al., 2010). In their set up, the Cu anode that was dissociated in to Cu ions will be oxidized and capped by tetra-trimethylammonium-bromide

(TTAB). The synthesis pathway was claimed to be simple, fast and high yield of quantum dots of CuO can be obtained.

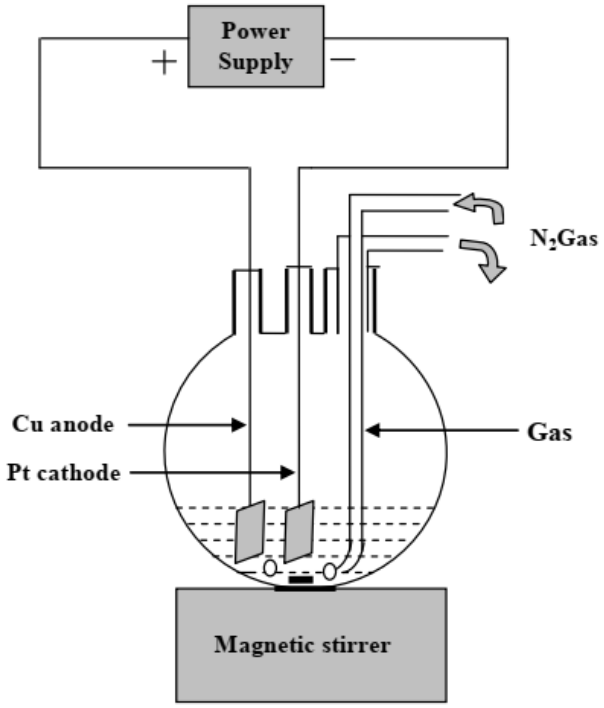

Figure 2.5: Electrochemical synthesis method set up by Momin et al. (2010)

Regarding CuO nanoparticles synthesis, Singh et al. (2016) synthesized flower-like CuO nanoparticles using NaOH and potassium hydroxide (KOH) as the reducing agents and electrolytes in the electrochemical synthesis. The CuO nanoparticles obtained by NaOH and OH were 15–20 nm and 13–18 nm, respectively.

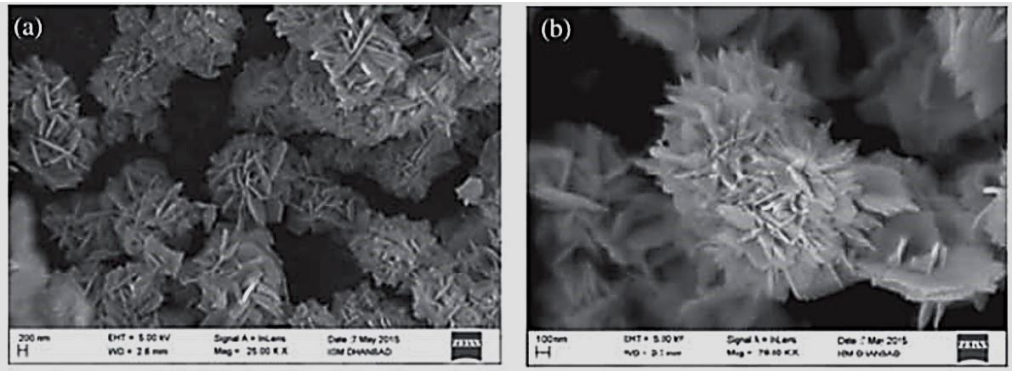

Figure 2.6: Flower-like CuO nanoparticles synthesized by using electrochemical method with (a) KOH and (b) NaOH (Singh et al., 2016)

Besides, synthesis of nanoparticles can be achieved by hydrothermal method. Hydrothermal synthesis of nanomaterials is a synthesis method utilizing a wide range of temperature from room temperature to high temperature in a solution based reaction mixture (Gan et al., 2020). Khedr and co-workers (2019) had applied this method to synthesize titanium dioxide (TiO_2) photocatalyst to degrade microcystin-LR produced by cyanobacteria. The synthesis of TiO_2 photocatalyst was carried out by heating the reaction mixture of sodium nitrate ($NaNO_3$), titanium (III) sulphate [$Ti_2(SO_4)_3$], aqueous glycine solution and NaOH under 200 ^oC for 20 hours. Then, the washed and dried samples were subjected for calcination at 300–500 ^oC to study the morphologies, properties and photocatalytic performance of the TiO_2 prepared. The synthesis method of CuO nanomaterials proposed by Qiu et al. (2012) was microwave assisted hydrothermal method. This synthesis pathway required a shorter reaction time from 5–30 minutes. An urchin-like and flower-like CuO nanomaterials were synthesized in their research. In addition, Hasanpoor et al. (2015) found that adjusting the power and time of microwave irradiation could

result in various morphologies of ZnO nanoparticles. According to their findings, the ZnO nanoparticles synthesized at lower power (510 W) were in needle-like shape while the higher power (680 W) were in flower-like shape. A report by Zou et al. (2015) stated that Cu_2O/ZnO nanorod arrays for application in photovoltaic devices can be synthesized through hydrothermal method followed by chemical bath deposition on the indium-doped tin oxide (ITO) glass substrates. The ZnO seed layer was prepared by zinc acetate dehydrate and monoethanolamine in ethanol before coating on the glass substrate. The ZnO seed layer was later immersed in mixture solution of zinc nitrate and examethylenetatramine to be heated at 148 ^oC for 3 hours. Then, the Cu_2O was deposited on the ZnO through chemical bath deposition process in solutions of $CuSO_4$, $Na_2S_2O_3$ and NaOH to complete the synthesis process.

Furthermore, sol-gel method was another common method reported in previous researches. Metal oxide such as TiO_2 nanoparticles can also be prepared using sol-gel method (Alhaji et al., 2016). In their research, titanium isopropoxide was used as the metal precursor for the synthesis. The isopropanol and acetic acid used in the synthesis were fully removed at the end of the reaction which can be proven by absence of C–H stretching band in the FTIR spectrum. CuO nanoparticles with antimicrobial properties were synthesized through gel-combustion method (Azam et al., 2012). The only chemicals used for this synthesis were copper nitrate trihydrate [$Cu(NO_3)_2.3H_2O$] and citric acid. The mixture solution was heated at 100 ^oC with constant stirring to allow gel formation. The gel was then heated at 200 ^oC before calcined at different temperatures ranging from 400–700 ^oC which yielded CuO nanoparticles with

crystalline size of 20–27 nm. The CuO nanoparticles annealed at 400 ℃ had the smallest particle size (20 nm) and highest antimicrobial properties against *Escherichia coli*, *Pseudomonas aeruginasa*, *Bacillus subtilis* and *Staphylococcus aures* observed from the zone of inhibition caused by the CuO nanoparticles (Azam et al., 2012). Another study by Muthuvel et al. (2020) also prepared CuO nanoparticles in a simple sol-gel method. They prepared copper nitrate and NaOH in the molar ratio of 1:2 and heated the mixture solution at 80 ^{o}C for 2 hours under ultrasonic and constant stirring. After filtration and washing process, the black precipitate was dried at 400 ^{o}C for 4 hours.

There were many synthesis methods for metal oxide nanoparticles reported to date. Radio frequency (RF) sputtering was a less reported method for the synthesis of nanoparticles. According to Ooi et al. (2013), the benefits of this method were uniform thickness of film on the substrate, better stoichiometric control and low substrate heating during film formation. Moreover, a low cost and simple sonochemical approach can be used to synthesize metal oxide nanoparticles. Dhineshbabu et al. (2016) reported a direct synthesis of CuO nanoparticles using NaOH and $Cu(NO_3)_2.2H_2O$. The reaction mixture was well mixed before subjected to sonication at the frequency of 25 kHz for 60 minutes, at the constant interval of 60 seconds. The blackish brown precipitate collected was washed to remove impurities followed by calcination at 400 ^{o}C to obtain the final product of CuO nanoparticles. Based on their findings, the CuO nanoparticles were in spherical shape with an average size of 57 nm.

2.5.2 Green synthesis

Among the green synthesis methods, synthesis of metal/metallic oxide nanoparticles by using plant materials had gained a lot of attention from the researchers. The bioactive compounds naturally occurred in the plant extracts were the main attraction to the scientists. The involvement of natural products in plants can assist in fabricating metal oxide into various morphologies and size (Muthuvel et al., 2020). Most of the natural phytochemicals in plants had strong antioxidant properties that can reduce the radicals due to the presence of various polyphenolic groups in the chemical structure (Nasrollahzadeh et al., 2015a).

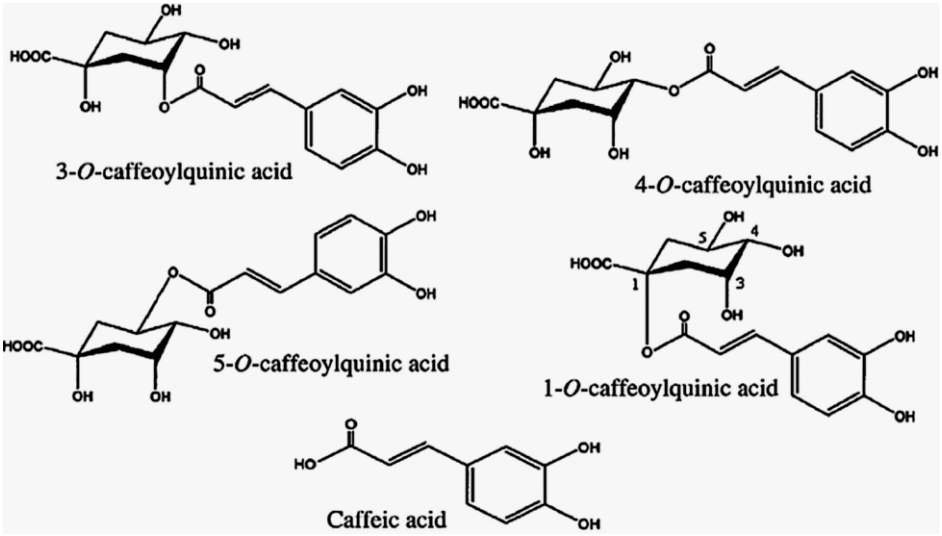

Figure 2.7: Natural components found in *Gundelia tournefortii* with phenolic groups (Nasrollahzadeh et al., 2015a)

In the application of green synthesis method, there will be no hazardous chemicals being used in the metal oxide nanoparticles synthesis pathway. Metal nitrates were the common oxidizing agents used in nanoparticles synthesis

because of their solubility and their ability to form a homogeneous solution (Udayabhanu et al., 2015). The utilization of plant wastes as one of the starting materials for the synthesis of metal oxide nanoparticles also required lower cost compared to chemical and physical synthesis pathways (Sreeju et al., 2017). Usage of plant based materials in synthesizing nanoparticles is not only environmental friendly but also faster in rate of production. Nanoparticles synthesized in this way had lower toxicity, various in size and shapes and more stable (Padil and Černík, 2013). In the synthesis of metal oxide nanoparticles, for instance, copper oxide nanoparticles, the bioactive compounds in the plant extracts reduced the Cu^{2+} into Cu^{0}. The lone pair of electrons from the polar groups of phenolic compounds will involve in the redox reaction making the bioactive compound a bio-reducing and capping agent (Sutradhar et al., 2014).

In general, plants can be known as the factories of the natural phytochemicals. An eco-friendly synthesis method of CuO NPs was studied by Nasrollahzadeh et al. (2015b) by using the flower extracts of medicinal herbs known as *Anthemis nabilis*. The application of the bioactive compounds

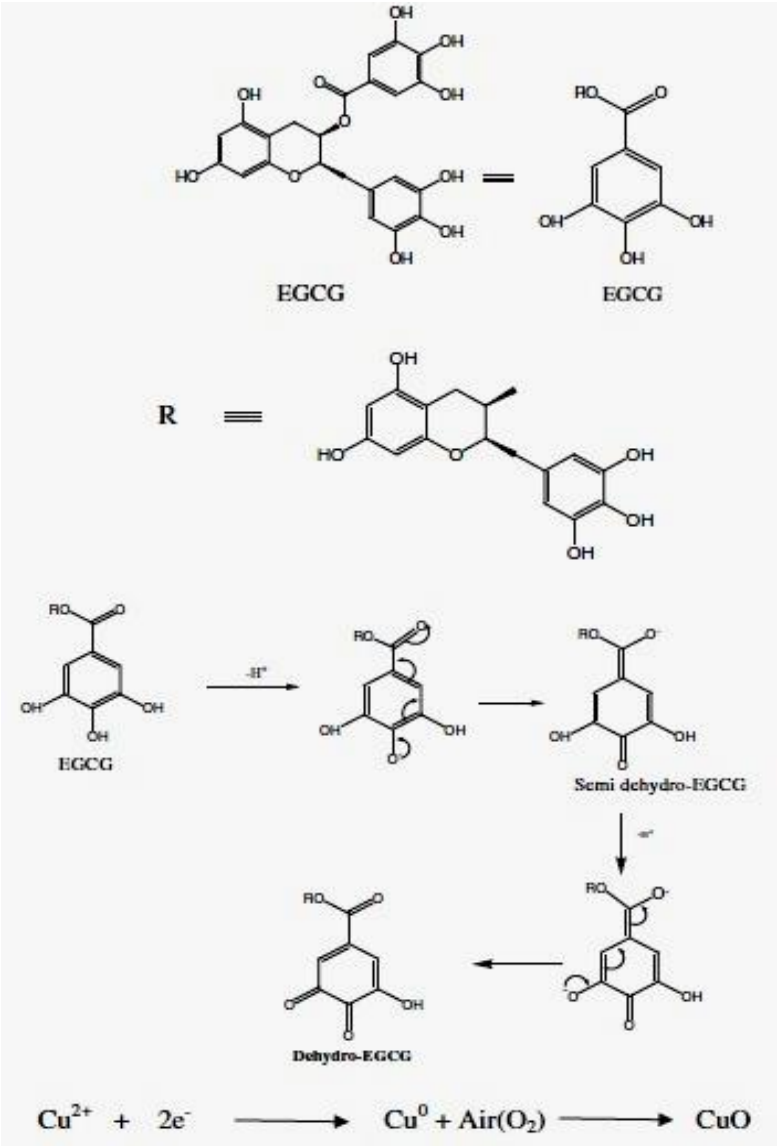

Figure 2.8: Mechanism of CuO naoparticles synthesis using coffee and tea extracts proposed by Sutradhar et al. (2014)

in the plant extract for the synthesis of nanoparticles was confirmed by the disappearance of phenolics signals in the UV-vis spectrum and the appearance of maximum absorbance at 250 nm due to the surface plasmon absorption of CuO NPs.

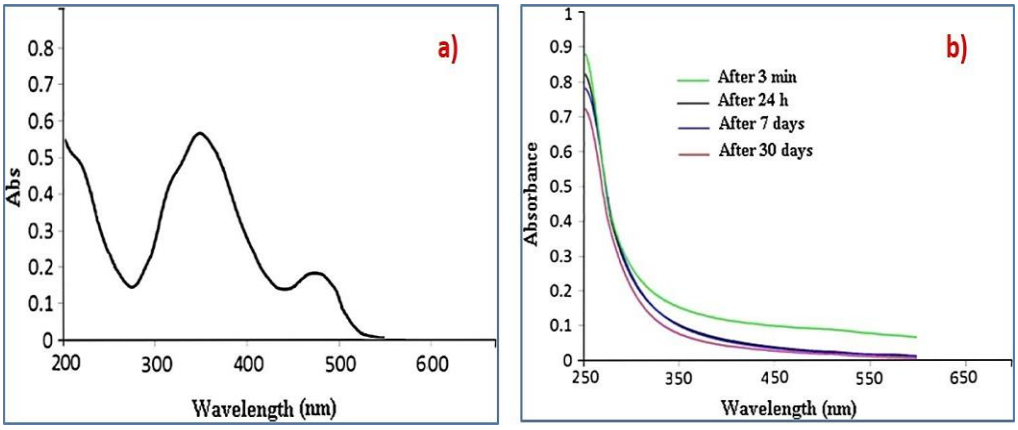

Figure 2.9: Comparison of the UV-vis spectra of a) flower extract of *Anthemis nobilis* and b) CuO NPs (Nasrollahzadeh et al. (2015b)

The aqueous extract of *Cordia sebestena* flower contained a rich amount of secondary metabolites which possessed pharmacological properties. These phytochemicals were revealed to be a potent reducing and stabilizing agent in green synthesis of CuO NPs (Prakash et al., 2018). The CuO NPs synthesized from *C. sebestena* flower was an effective photocatalyst for the photodegradation of bromothymol blue (BTB) dye and a potential inhibitor for bacteria due to its smaller particle size ranging from 20–35 nm (Prakash et al., 2018). Das et al. (2018) studied the synthesis of CuO NPs by using the water extract of a traditional medicinal plant, *Madhuca longifolia* flowers. In this case, the CuO NPs synthesized by *M. longifolia* flowers (~100 nm) were larger than the CuO NPs synthesized from *C. sebestena* flowers (20–35 nm) (Das et al., 2018; Prakash et al., 2018).

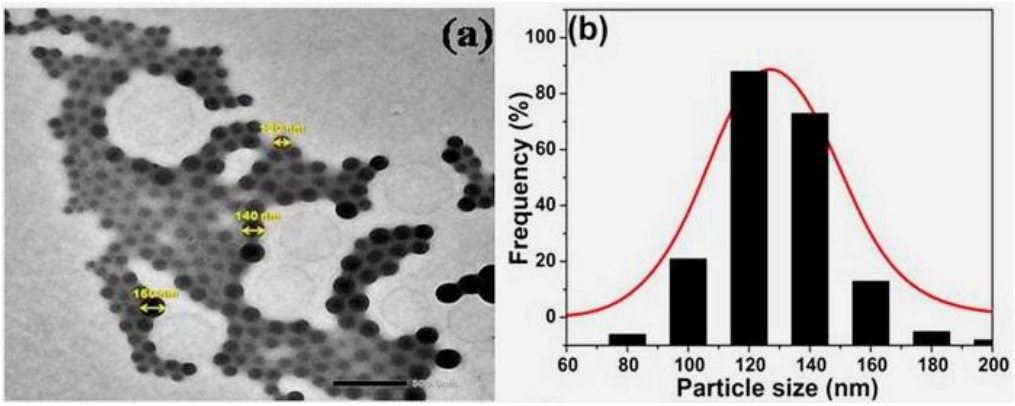

Figure 2.10: The (a) TEM image and (b) particle size distribution graph of CuO NPs synthesized from *Madhuca longifolia* flower extract (Das et al., 2018)

Besides, CuO NPs derived from the seed extract of *M. longifolia* plant were also found to be smaller (~30 nm) than CuO NPs synthesized from the flower extract (Das et al., 2018).

Microorganisms were one of the biological precursors used in the biosynthesis of metal oxide nanoparticles. Microbes such as fungi and bacteria were potential materials used in green synthesis of nanoparticles because of their abilities to synthesize variety of bioactive metabolites. The reason of bacteria chosen in the synthesis of nanoparticles was the ease of controlling the bacteria (Singh et al. 2018). A wide range of bacterial strains had been studied for the purpose of biosynthesis of nanoparticles. For instance, *Escherichia coli*, *Bacillus sp.*, *Pseudomonas proteolytica*, *Enterobacter cloacae*, *Shewanella alga* and many others (Singh et al. 2018). Rahman et al. (2009) reported the synthesis of CuO NPs extracellularly using *Phormidium cyanobacterium*. After 42 h of reaction

between *Phormidium cyanobacterium* and $CuSO_4$ solution, the pure CuO NPs with particle size of 10–40 nm were formed. The completion of reaction was indicated by the colour change of the solution from light blue to green followed by appearance of brown and finally black colour was observed. The proteins secreted by bacteria would be the reducing agent involved in the CuO NPs synthesis (Rahman et al., 2009). Green synthesis of metallic nanoparticles using fungi was also able to form monodispersed and nanoparticles with well-defined morphologies (Singh et al., 2018). In a report by Saravanakumar et al. (2019), the formation of CuO NPs by *Trichoderma asperellum* cell-free extract was due to the presence of secondary metabolites acting as the catalyst, encapsulating or reducing agents. The formation of the CuO NPs was identified by the colour change of the solution from yellow to brown colour. In order to inspect further, the UV-vis scanning was applied to identify the surface plasmon resonance peak in CuO NPs which was not observed in the cell-free extract (Saravanakumar et al., 2019). This phenomenon was similar to the research done by Nasrollahzadeh et al. (2015b) using *Anthemis nobilis* flower extract that was discussed in the previous paragraph. Fungi can be the more decent organism used for synthesis of nanoparticles as more enzymes, proteins and reducing compounds can be found on the cell surfaces, in addition, a larger yield of nanoparticles can be obtained compared to bacteria (Singh et al., 2018).

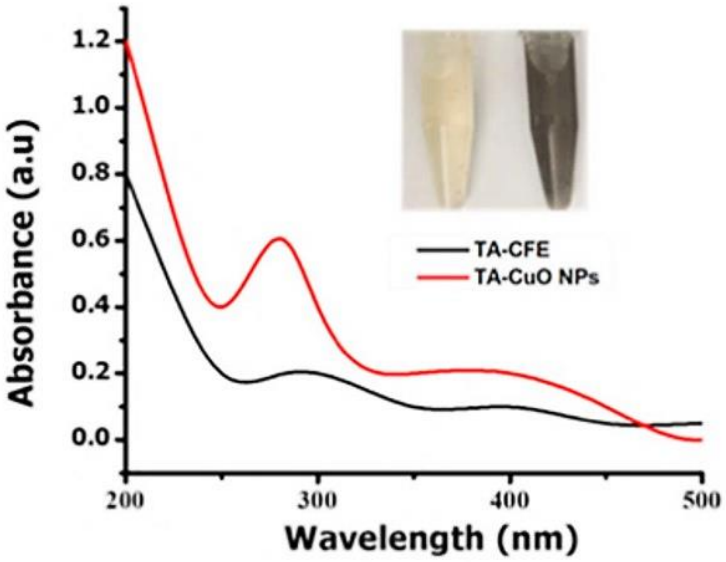

Figure 2.11: The appearance of the surface plasmon resonance peak was observed in the CuO NPs when compared to the spectrum of *Trichoderma asperellum* cell-free extract (TA-CFE) (Saravanakumar et al., 2019)

The green synthesis of nanomaterials emphasized on using environmentally friendly materials especially plant based materials. The biowaste of plants such as the peels would be the feasible choice. Various types of fruit peels had been studied comprehensively in synthesizing numerous nanoparticles for the different applications in industries. The utilization of fruit peels in the synthesis of metallic nanoparticles had been successfully conducted by researchers from different regions. Metal or metal oxide nanoparticles such as copper, silver and nickel oxide nanoparticles with antimicrobial, antifungal and photocatalytic properties were synthesized using different peels like *Carica papaya*, *Citrus reticulate* and *Annona muricata* L. (Kokila et al., 2016; Trang et al., 2018; Aminuzzaman et al., 2020). The synthesis of CuO NPs as a catalyst using

two different types of banana peels showed that the particles size was in the range of 10–40 nm. The banana peel synthesized CuO NPs were used to speed up the oxidation of aldehyde and photocatalytic degradation of Congo red dye (Tamuly et al., 2014; Aminuzzaman et al, 2017).

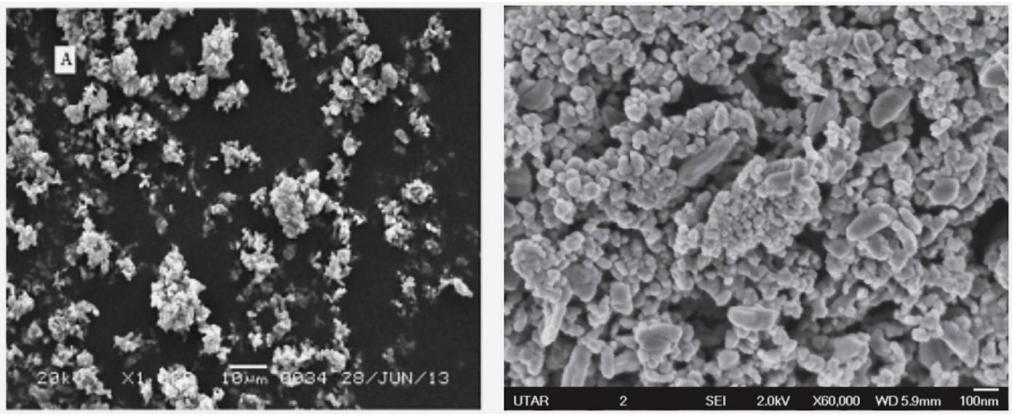

Figure 2.12: SEM images of CuO NPs synthesized from peels of *Musa balbisiana* (left) and Cavendish bananas (right) (Tamuly et al., 2014; Aminuzzaman et al, 2017)

Relatively spherical shape of CuO NPs synthesized using pomegranate (*Punica granatum*) peel extract were around 35.8 nm in size and showed an efficient ability as a non-toxic antibacterial agent to inhibit growth of microorganisms (Siddiqui et al., 2021).

Last but not least, leaves would be the most selected choice for the synthesis of nanoparticles as leaves were the major part of most of the plants. For instance, *Carica papaya* leaves had been studied to synthesize silver and zinc oxide nanoparticles for antibacterial, photocatalytic and

photovoltaic applications (Banala et al., 2015; Rathnasamy et al., 2017). The zinc oxide nanoparticles synthesized by Rathnasamy et al. (2017) and Kwabena and Aquisman (2019) using *Carica papaya* leaves extract shown the nanoparticles were agglomerated in nature.

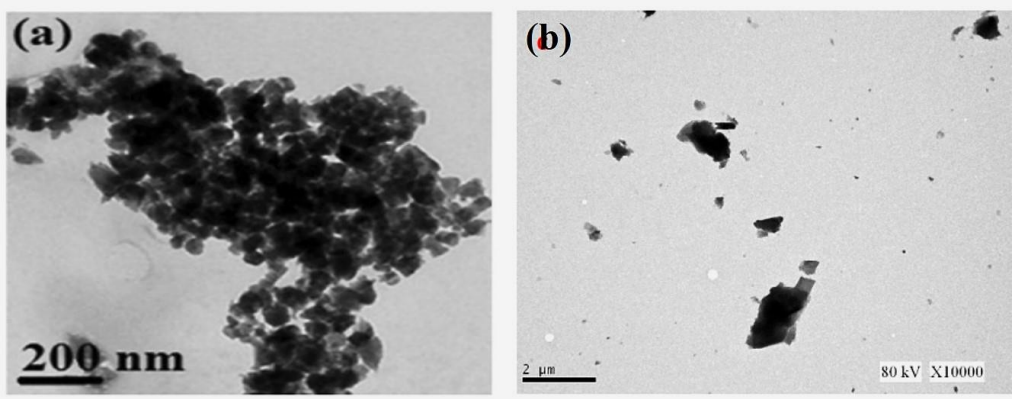

Figure 2.13: TEM images of *Carica papaya* leaves extract synthesized ZnO NPs by (a) Rathnasamy et al. (2017) and (b) Kwabena and Aquisman (2019)

On the other hand, the silver nanoparticles synthesized by two different groups of researchers using the same type of plant extract were also found to be similar in the particle size and shapes (Banala et al., 2015; Anbarasu et al., 2018). The rich amount of phytochemicals in the *Carica papaya* leaves made it a cost effective and environmentally friendly materials to be used in synthesizing CuO NPs by Sankar et al. (2014) for the purpose of degrading Coomassive brilliant blue R-250 dye while Turakia et al. (2020) applied it to inhibit the growth of bacteria on the surface of textiles. The abilities of semiconductor nanoparticles in antimicrobial applications were well studied in literature. The CuO NPs prepared by the leaves extract of

Tinospora cordifolia, *Psidium guajava*, *Abutilon indicum*, *Bauhinia tomentosa* and tea leaves were some of the examples used in inhibition of microorganisms' growth (Sutradhar et al., 2014; Udayabhanu et al., 2015; Ijaz et al., 2017; Sreeju et al., 2017; Sharmila et al., 2018;). The CuO NPs synthesis mediated by leaves extract of *Gundelia tournefortii* and *Solanum nigrum* plants also showed their effectiveness as a catalyst in synthesizing *N*-monosubstitued urea, reducing 4-nitrophenol and degrading methylene blue dye (Nasrollahzadeh et al., 2015a; Muthuvel et al., 2020).

Table 2.3: Various CuO NPs synthesized from different parts of plants

Part of plant used	Size (nm)	Shape	References
Flowers (*Anthemis nobilis*)	18.02–61.29	Irregular	Nasrollahzadeh et al., 2015b
Peel (*Cavendish banana*)	50–85	Spherical	Aminuzzaman et al., 2017
Leaves (*Carica papaya*)	< 100	Square and rectangle	Turakhia et al., 2015
Leaves (*Tinospora cordifolia*)	~ 6–8	Agglomerated spherical	Udayabhanu et al., 2015
Leaves (*Psidium guajava*)	19.19	Elongated spherical	Sreeju et al., 2017
Leaves & stems (*Gundelia tournefortii*)	- *	Spherical	Nasrollahzadeh et al., 2015a
Flowers & seeds (*Madhuca longifolia*)	30–120	Irregular and spherical	Das et al., 2018
Leaves (*Abutilon indicum*)	16.78	Agglomerated irregular and spherical	Ijaz et al., 2017

Seeds (*Caesalpinia bonducella*)	13.07	Rice-shaped	Sukumar et al., 2020

*'-' indicated not reported.

2.5.3 Copper oxide nanoparticles (CuO NPs)

The multifunctional transition metal oxide nanoparticles in variety of fields and areas were highly attractive than their bulk materials (Suresh et al., 2015). Metal or metal oxide nanomaterials exhibit notable functions as antimicrobial, biocidal or inhibitor for microorganisms in biological applications. The examples of metals studied for these purposes were gold, silver, zinc oxide, magnesium oxide, calcium oxide and titanium dioxide (Mageshwari and Sathyamoorthy, 2013; Sutradhar et al., 2014).

As compared to rare and precious metals like gold (Au), silver (Ag), palladium (Pd), platinum (Pt), ruthenium (Ru) and rhodium (Rh), copper (Cu) based nanoparticles were less expensive when applied as catalyst (Nasrollazadeh et al., 2015a; Ijaz et al., 2017). In general, copper oxide had two oxidation states which were copper (I) oxide or cuprous oxide (Cu_2O) and copper (II) oxide or cupric oxide (CuO). Both of them were non-toxic, naturally abundant and cheaper semiconductor. Cu_2O is cubic while CuO is monoclinic in structure with direct band gap energy of 2.1 and 1.2 eV, each (Barreca, D., 2007).

CuO is one of the very useful semiconductors due to its excellent optical, electrical, magnetic, catalytic and biological properties (Phang et al., 2021). In addition, CuO can withstand high temperature, mechanical strength, high conductance of heat and electricity, chemical and corrosion resistance (Sharmila et al., 2018; Hasan et al., 2020). Up to date, CuO NPs in various shapes and structures have been synthesized to meet variety of applications. Nanoscale CuO such as nanorods, nanosheets, flower-like, leaf-like, nanodendrites and nanowires were reported by previous researchers (Udayabhanu et al., 2015; Sreeju et al., 2017).

2.6 *Carica papaya*

Papaya is one of the most ordinary fruits distributed all over the world. *Carica papaya* Linn, also known as papaya, pawpaw (called by Australians), Fan mu gua, papye, Lapaya, lechosa (called by the Venezuelans) and etc. (Moy, 2003; Gunde and Amnerka, 2016). Papaya belongs to the family of *Caricacea* which almost can be found all over the world. Papaya is originated from tropical America then spread to the Philippines followed by Malacca and India until it can be found throughout the tropical and subtropical regions in the world (Moy, 2003). The papaya tree is a tall plant which can grow up to 5 – 10 m high without branch on the stem. The leaves of the papaya tree are spirally aligned to the trunk of the plant. In addition, the leaves of the papaya can be identified easily with the deeply palmately lobed shape. The size of the leaves can grow up to an average of 60 cm in diameter (Moy, 2003; Gunde and Amnerka, 2016).

According to Moy (2003), papaya tree can be categorized to male, female and hermaphrodite tree. The flowers consist of male and female parts on the same flowers are known as hermaphrodite. Monoecious is the plant where the flowers of male and female can be on the same plant while dioecious is with male and female parts on the separate plants (Moy, 2003). The papaya fruits of hermaphrodite are mostly cylindrical and pear-shaped while round fruits are found from the female tree (Moy, 2003). Papaya fruits are covered with thin skin which is green when unripe and yellow when ripe.

Papaya is a rich source of vitamins including β-carotene, vitamin B (thiamine, riboflavin, niacin and folate), vitamin C, vitamin E, minerals (Na, K, Fe, Ca), and fibre (Vij and Prashar, 2015). Papaya juice is consumed for the treatment of various diseases like constipation, dyspepsia, diabetes, cancer, heart stroke, blood pressure, etc. (Saeed et al., 2014). A huge amount of papaya is consumed across the world because of its high nutritional and medicinal values. Since papaya is a common nutritive food, the high consumption may result in generation of large amount of waste, for instance, peels and seeds that could be a significant source of pollution if they are not disposed of properly. Hence, value-adding to the biowaste is one of the methods to reduce waste generation and pollution to the environment.

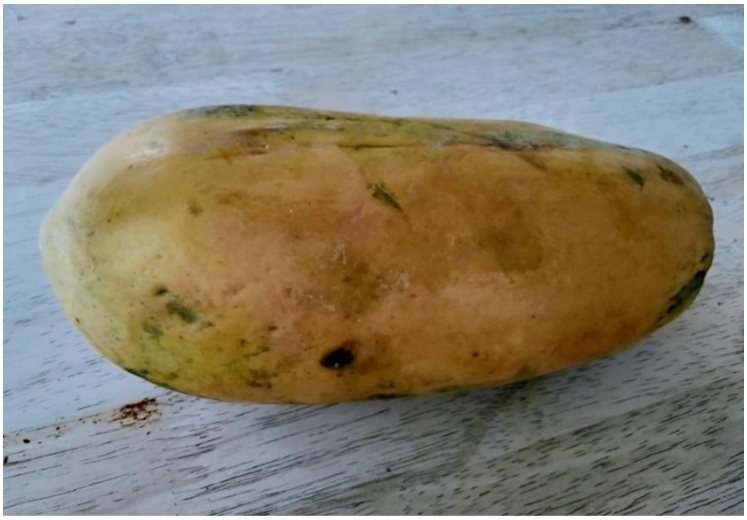

Figure 2.14: Papaya fruit purchased from local market

CHAPTER 3

RESEARCH METHODOLGY

3.1 Conventional filtration system set up

A simple and low cost filtration system was set up by using different ratio of fine sand, coarse sand and activated carbon in a 4.5 L plastic container. The filtration system was built by inserting the materials in the ascending order of coarse sand, activated carbon and fine sand following the ratio of 1:1:3 (Kamala et al., 2018). The flow rate of the POME in unit of mL/s was measured by collecting the filtrate in a 100 mL graduated measuring cylinder. The **Figure 3.1** below showed the filtration system set up for this project.

Figure 3.1: Conventional filtration system set-up

3.2 Synthesis of copper oxide nanoparticles (CuO NPs)

3.2.1 Materials

Carica papaya was used in this project and the papayas were purchased from the local market in Kampar, Perak. The papaya peel biowastes were collected after consuming the fruits. The salt precursor being used for CuO NPs synthesis was copper (II) nitrate trihydrate [$Cu(NO_3)_2.3H_2O$]. The copper salt purchased from Quality Reagent Chemical, QRëC, New Zealand was used as received. Deionised water was used for the entire experiment. All glasswares were washed with deionised water and dried in oven before used.

3.2.2 Papaya peel extract (PPE) preparation

The papaya peels collected freshly were washed with deionised water thoroughly to eliminate dust and organic contaminants stuck on it. Then, around 100 g of papaya peel was weighed and cut into small pieces before adding 150 mL of deionised water to it, in a 500 mL beaker. The mixture was boiled at 70 – 80 ^{o}C for a duration of 20 minutes. When heating was completed, a yellow coloured solution was formed. The yellow solution was allowed to cool to room temperature prior proceed to vacuum filtration. After underwent two times filtration, the filtrate was collected in a 250 mL beaker and readied for CuO NPs synthesis directly.

3.2.3 Synthesis of CuO NPs

About 40 mL of the filtered PPE was measured using a measuring cylinder and boiled at 70 – 80 ^{o}C in a 100 mL beaker. Then, about 1 g of copper (II) nitrate trihydrate was added into the hot PPE slowly. The yellow solution turned greenish-blue immediately when the salt precursor was added in. When the heating continued, the green colour of the solution was getting darker. After the solution was concentrated, a dark green paste was formed and it was transferred to a ceramic crucible to be heated in the furnace at 450 ^{o}C for 2 hours. When the calcination was completed, the black powder in the crucible was the CuO NPs that was targeted in this project. The black powder was ground in a mortar and pestle to obtain a fine CuO powder. A series of characterizations were needed to be carried out for the biosynthesized CuO NPs. The synthesis process of the CuO NPs was summarized and illustrated in **Figure 3.2**.

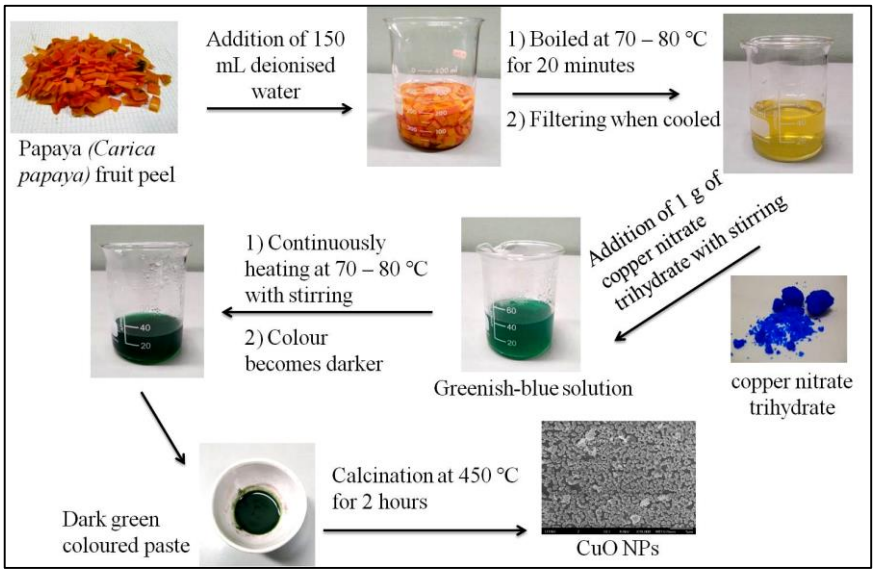

Figure 3.2: Synthesis pathway of biosynthesized CuO NPs (Phang et al., 2021)

3.3 Characterizations of CuO NPs

3.3.1 Ultraviolet-visible (UV-vis) Spectroscopy

The UV-vis absorption spectrum of the biosynthesized CuO NPs was obtained to determine the maximum absorption wavelength (λ_{max}). The nanoparticles synthesized were prepared in 0.1 wt% by dispersing in 10 mL deionised water. Then, the mixture solution was subjected to ultrasonication for 30 minutes using ultrasonic bath (Branson 5510 with mechanical timer, 220 V), to break down any aggregation of particles to ensure the nanoparticles were well dispersed in the solution. After 30 minutes, the solution was scanned from 200 – 800 nm in the Thermo Scientific Genesys 10S UV-Vis spectrophotometer. At the same time, the UV-vis absorption spectra of $Cu(NO_3)_2.3H_2O$ salt precursor, papaya peel extract and the intermediate solution after the mixture of both starting materials were also recorded.

The band gap energy (E_g) of the biosynthesized CuO NPs can be calculated by applying Tauc's plot equation:

$$\alpha h\nu = A(h\nu - E_g)^{n/2} \qquad \text{(Eq. 3.1)}$$

where, α is the absorption coefficient of the nanoparticles. The n represented the nature of the transition of the electron between valence and conduction band such that n = 1 for direct band gap while n = 4 for indirect band gap. Symbol A denoted as constant and $h\nu$ defined as the incident photon energy. A plot of

$(\alpha h\nu)^2$ versus $h\nu$ was constructed and the band gap energy for the biosynthesized CuO NPs was estimated through extrapolation of the straight line part to the x-axis.

3.3.2 Fourier Transform Infrared Spectroscopy Analysis (FT-IR)

The functional groups in the papaya peel, papaya peel extract (PPE) and the biosynthesized CuO NPs were by using FT-IR spectrophotometer (Perkin Elmer RX1). The papaya peel was minced then the mince papaya peel was frozen at -20 ^{o}C then subjected to freeze dryer for overnight. The same procedure applied to PPE, 5 mL of the extract was freeze-dried into dried solid in the freeze dryer overnight before analysis. Potassium bromide (KBr) pellet method was chosen for the pellet preparation for the analysis of functional groups. All the samples were scanned within the scanning range of 4000 – 400 cm^{-1} wavenumbers.

3.3.3 X-ray Diffraction (XRD) Analysis

The crystal phase of the CuO NPs synthesized was identified by using X-ray Diffractometer (XRD Shidmazu 6000). The CuO NPs was scanned from 10^{o} to 80^{o} in 2θ by X-Ray diffratometer with Cu Kα radiation (λ = 1.540600 Å, step size = 0.020 $^{o}s^{-1}$).

3.3.4 Scanning Electron Microscopy (SEM) with Energy Dispersive X-ray Analysis (EDX) and Transmission Electron Microscopy (TEM)

In order to understand the morphology and elemental composition of biosynthesized CuO NPs. The nanoparticles were characterized by the integration of EDX into SEM using Field Emission Scanning Electron Microscope (JEOL JSM-6710F). The nanoparticles were coated with gold before viewed under SEM.

The particle size and the surface of the particles in addition to the structure can be measured and observed as well using HRTEM (JEOL JEM-3010).

3.3.5 Raman Spectroscopy

Raman spectroscopy is the common analysis to be carried out to analyse the local atomic arrangements and vibrations of the materials in order to study the structural nature of the nanomaterials.

3.3.6 X-ray Photoelectron Spectroscopy (XPS) Analysis

The XPS survey scan of biosynthesized CuO NPs was conducted to identify the oxidation state of the copper and oxygen that were present in the nanoparticles. The nanoparticles were scanned using Perkin Elmer PHI5600 (ULVAC, PHI, Inc, Waltham, MA, USA).

3.4 Microalgae cultivation

The microalgae used in this project were *Chlorella vulgaris* (*C. vulgaris*) and *Chlamydomonas reinhardtii* (*C. reinhardtii*). The mother stock of these strains were cultured in 100 % modified Bold's Basal Medium (BBM) in 250 mL conical flask. The mother stocks were then transferred and subcultured in new flasks until the day of harvesting. The BBM and glasswares used in the microalgae cultivation were autoclaved to ensure free of foreign microbes. The microalgae were put in a rack with sunlight exposure. The ingredients of the BBM are shown in **Table 3.1**.

Table 3.1: Ingredients for the preparation of 100 % BBM

No.	Chemical	Stock solution	mL/L
1	KH_2PO_4	8.75 g / 500 mL	10
2	$CaCl_2.2H_2O$	1.25 g / 500 mL	10
3	$MgSO_4.7H_2O$	3.75 g / 500 mL	10
4	$NaNO_3$	12.5 g / 500 mL	10
5	K_2HPO_4	3.75 g / 500 mL	10
6	NaCl	1.25 g / 500 mL	10
7	$Na_2EDTA.2H_2O$	10 g/L	1
	KOH	6.2 g/L	
8	$FeSO_4.7H_2O$	4.98 g/L	1
	H_2SO_4 (concentrated)	1 mL/L	
9	*Trace metal solution	See below	1

10	H_3BO_3	5.75 g / 500 mL	0.7

*Trace metal solution:

Substance	g/Litre
H_3BO_3	2.86
$MnCl_2.4H2O$	1.81
$ZnSO_4.7H_2O$	0.222
$Na_2MoO_4.5H_2O$	0.390
$Co(NO_3)_2.6H_2O$	0.0494
$CuSO_4.5H_2O$	0.079

3.5 POME treatment

3.5.1 Physical treatment

The POME sample was collected directly from a local palm oil mill located in Selangor, Malaysia. During transportation, the POME was kept in a black, air-tight container to avoid light exposure. The collected POME was filtered through the conventional filtration system to remove extra solids in the POME. The filtrate was collected for further treatment and analysis.

3.5.2 Chemical treatment

The filtered POME collected was further treated with biosynthesized CuO NPs to remove the organic pollutants present in the POME. A 500 ppm of CuO NPs

solution was prepared by weighing 250 mg CuO NPs into 500 mL filtered POME. The mixture was then stirred in dark condition for 30 minutes before exposed to direct ultraviolet (UV) light. The mixture was allowed to undergo photodegradation under direct UV light for at least 4 hours before the water sample was collected for other analysis. The samples collected were centrifuged at 7000 rpm for 10 minutes to remove the nanoparticles prior to analysis. A blank was prepared by irradiating the POME samples under UV light without adding CuO NPs. Another set of POME sample was run in dark condition by adding the same amount of CuO NPs into the same volume of POME, acting as the negative control of the experiment.

3.6 Water analysis

3.6.1 pH, colour and conductivity

The pH of the POME samples was measured by Mettler Toledo^{TM} Benchtop pH meter. The colour of the POME samples was measured following Platinum-Cobalt (Pt/Co) method also known as APHA colour, at 455 nm using DR6000 UV-vis spectrophotometer (Hach, Germany). The conductivity of the samples was measured using Mettler Toledo^{TM} FiveEasy Plus^{TM} FP30 Benchtop conductivity meter.

3.6.2 Chemical oxygen demand (COD)

A 2 mL of the treated sample was measured and subjected into the COD-LR vial which was then digested at 150 ^{o}C for 2 h with COD digital reactor (Hach

DRB200). The COD digital reactor was pre-heated to 150 ºC before inserting the COD-LR vials. The digestion process was started after the temperature of the heating block reached 150 ºC. After the digestion process, the COD vials were cooled to room temperature. Then, the COD concentration of the samples were measured using DR6000 UV-vis spectrophotometer (Hach, Germany).

3.6.3 Biochemical oxygen demand (BOD)

The biochemical oxygen demand values of the POME samples were analysed according to the APHA 5210 B. 5-day BOD test procedure. The pH of the samples was adjusted to neutral using sulphuric acid or sodium hydroxide. Then the samples were prepared in different dilution factors and mixed well. After that, the samples were incubated at 20 $\pm$ 1 °C in a dark incubator to avoid algae growing in the bottles. The dissolved oxygen (DO) of the POME samples before and after 5 days of incubation were measured by DO meter.

3.6.4 Ammoniacal nitrogen analysis

In this project, the nitrogen content in the water samples were determined in ammonia form by using Nessler's method. This method had been reported by (Subramaniam, 2018) in leachate analysis. In order to measure the ammonia concentration of the treated POME, a calibration graph was needed for the calculation. Anhydrous ammonium chloride was used to prepare the standard solutions. About 1.9095 g of anhydrous ammonium chloride was weighed and dissolved into 500 mL volumetric flask. The Rochelle salt solution was prepared by weighing 50 g of potassium sodium tartrate and dissolving into a 100 mL

volumetric flask with distilled water. The Nessler's reagent was purchased from Merck and used as ready.

The standard solutions for calibration graph were prepared from the ammonium chloride intermediate standard stock solution (50 ppm). The dilution of the standard solutions was carried out as shown in table below, into 50 mL volumetric flask.

Table 3.2: Preparation of ammonia standard solutions for calibration

Concentration (ppm)	Volume of intermediate solution needed (mL)
0.1	0.10
0.2	0.20
0.5	0.50
1.0	1.00
2.0	2.00

All the standard solutions were added with 1 mL of Rochelle salt solution followed by 1 mL of Nessler's reagent. The absorbances of the solutions were scanned at 425 nm with UV-vis spectrophotometer. The ammonia content was evaluated from the standard calibration curve in the unit of parts-per-million (ppm). For the preparation of blank, the same amount and volume of reagents were added into 50 mL of distilled water.

3.6.5 Phosphate test

The phosphate test was carried out by using phosphomolybdenum method referring to Mahadevaiah et al (2007). A 0.387 M of ammonium molybdate solution was prepared by dissolving 1.7081 g of ammonium molybdate into a 250 mL of volumetric flask. The reducing agent reported by Mahadevaiah and co-workers (2007) was replaced with ascorbic acid in this experiment. A 2.839×10^{-3} M of ascorbic acid solution was prepared by dissolving 0.05 g of ascorbic acid in 100 mL of distilled water. A standard calibration curve was needed for the measurement of phosphate concentration. The standard stock solution was made by weighing and dissolving 0.1145 g of disodium hydrogen phosphate into 250 mL of volumetric flask. About 306.7 mg PO_4^{3-}/L had been prepared from this step. Then, an intermediate standard stock solution of 30.67 mg PO_4^{3-}/L was prepared by diluting 5 mL of the solution to 50 mL with distilled water. A diluted sulphuric acid (0.25 N) was prepared by diluting concentrated sulphuric acid with distilled water.

A series of standard solutions were prepared from the intermediate stock solution. The standard solutions for calibration were prepared as following in 10 mL volumetric flask.

Table 3.3: Preparation of phosphate standard solutions for calibration

Concentration (mg PO_4^{3-}/L)	Volume of intermediate solution needed (mL)
0.30	0.10

0.61	0.20
0.92	0.30
1.53	0.50
3.07	1.00
4.60	1.50
6.13	2.00
9.20	3.00

The concentration of phosphate was measured by formation of blue colour phosphomolybdate complex using spectrophotometric method. The maximum absorption wavelength (λ_{max}) of phosphomolybdate complex was determined by adding 0.5 mL of ammonium molybdate solution, 3 mL of sulphuric acid followed by 1 mL of ascorbic acid solution into the highest concentration of phosphate standard solution. The solution was scanned at the range of 600-900 nm to identify the maximum absorption wavelength (λ_{max}) of phosphomolybdate. The λ_{max} was identified to be at 715 nm in this study. After obtained the λ_{max}, the phosphate calibration and analysis were determined at the specific wavelength by adding the same amount of reagents into 10 mL of standard solutions and samples.

3.7 Microalgae growth

3.7.1 Cell counting

The growth of the microalgae was investigated by counting the number of cells using haemacytometer. The number of cells was counted daily from the starting

day (Day-0) to the end of fixed duration (Day-7). A binocular inverted microscope (Motic, AE31 Elite, United States) was used to view the cells. The number of cells was estimated by using the following equation:

$$\text{number of cells (cells/mL)} = \left(\frac{\text{Counted cells}}{4}\right) \times \text{dilution factor} \times 10^4 \quad \text{(Eq. 3.2)}$$

3.7.2 Chlorophyll and carotenoid extraction

Besides cell counting, the chlorophyll and carotenoid content of the microalgae cells can also be used as an indicator of the microalgae growth. About 10 mL of the samples were taken daily and centrifuged at 5000 rpm to obtain the cell pellet. After discarded the supernatant, 5 mL of pure methanol was added to the cell pellet and shaken to disperse well. The suspension was centrifuged again at 5000 rpm for 10 minutes to remove the cells. Then, the absorbance of the methanol extract was measured at the wavelength of 470, 652.4 and 665.2 nm. The absorbance recorded were substituted into the equations to calculate the amount of chlorophyll and carotenoid.

$$\text{Chlorophyll } a \text{ (μg/mL)} = 16.72\, A_{665.2} - 9.16\, A_{652.4} \quad \text{(Eq. 3.3)}$$

$$\text{Chlorophyll } b \text{ (μg/mL)} = 34.09\, A_{652.4} - 15.28\, A_{665.2} \quad \text{(Eq. 3.4)}$$

$$\text{Carotenoid (μg/mL)} = \frac{(1000A_{470} - 1.63\ \text{Chlorophyll a} - 104.96\ \text{Chlorophyll b})}{221} \quad \text{(Eq. 3.5)}$$

3.8 Phytotoxicity evaluation

3.8.1 Phytotoxicty of POME

The phytotoxicity of POME samples were determined using mung bean (*Vigna radiata* L.) seeds before and after every treatment stages. The mung bean seeds were rinsed with 0.5 % (w/v) of NaOCl solution for sterilization. After washing thoroughly with distilled water, ten healthy and uniform size seeds were selected and placed on the cotton that was spread evenly in the petri dishes for each treatment stage. The cottons were moistened with 5 mL of POME solutions (each treatment stages) and 5 mL of tape water for the control set at an interval of 12 hours for 7 days. After 7 days, the phytotoxicity of the POME samples were evaluated by measuring the radicle lengths using the following equation (Dugandžić et al., 2017):

$$\text{Phytotoxicity} = \frac{L_c - L_s}{L_c} \times 100\ \% \qquad \text{(Eq. 3.6)}$$

where L_c is the radicle length of control and L_s is the radicle length of samples.

3.8.2 Phytotoxicity of biosynthesized CuO NPs

The phytotoxicity of the biosynthesized CuO NPs were also evaluated to investigate the effect of CuO NPs on the growth of plants. The same procedure using mung bean seeds as indicator was applied to this study. In this case, the mung bean seeds were irrigated with different concentration of biosynthesized

CuO NPs dispersed in the distilled water. A series of CuO NPs solutions were prepared in the concentration of 50, 100, 250, 500 and 1000 ppm. Before irrigation, all CuO NPs solutions were put in water bath sonicator for 5 minutes to ensure even dispersion of nanoparticles. After 7 days, the phytotoxicity of biosynthesized CuO NPs was calculated according to Eq. 3.6. Besides, the phytotoxicity of the biosynthesized CuO NPs was compared with the commercial copper oxide. Another set of experiment was conducted by dispersing commercial copper oxide in the same concentration range for the irrigation of mung beans.

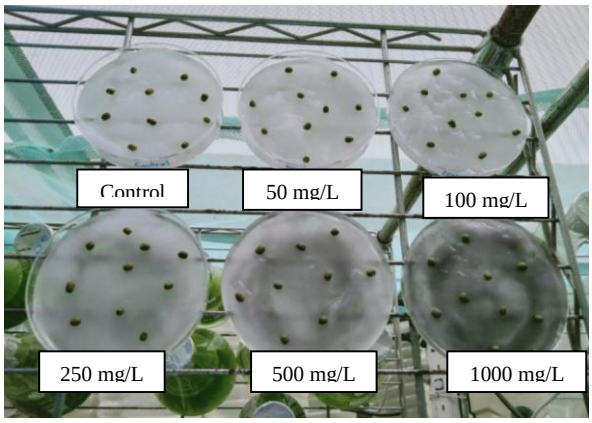

Figure 3.3: Cultivation of mung bean seeds with different concentrations of CuO NPs

3.9 Statistical Analysis

All the experiments in this study were carried out in triplicates. The data obtained were presented as the average of the experiment ± standard deviation (SD). One-way analysis of variance (ANOVA) was used to analysed the data statistically. At 95 % confidence level ($p < 0.05$), the data was analysed against the probability value (p value) using Microsoft Excel program.

CHAPTER 4

RESULTS AND DISCUSSION

4.1 Conventional filtration system

The basic components for the filtration system were course sand, fine sand and activated carbon. The total volume of the filtration system was about 4021 cm^3. The filtration system was constructed using coarse sand at the bottom level followed by activated carbon and fine sand on top in the ratio of 1:1:3. The volume of the coarse sand, activated carbon and fine sand were approximately 804, 804 and 2413 cm^3, respectively. The flow rate of the filtration setup was examined to be 4.22 ± 0.02 mL/s using the following equation.

$$\text{Flow rate} = \frac{100 \text{ mL}}{\text{Average time taken (s)}} \quad \text{(Eq. 4.1)}$$

Table 4.1: Flow rate of 100 mL POME when filtering through conventional filtration system

Sample	1st trial (mL/s)	2nd trial (mL/s)	3rd trial (mL/s)	Average (mL/s)
Untreated POME	4.26	4.19	4.22	4.22 ± 0.02

4.2 Instrumental analysis of CuO NPs

4.2.1 UV-visible (UV-vis) spectroscopy

The UV-vis absorption spectra of all the starting materials and processes were recorded to study the formation of CuO NPs. The UV-vis spectrum of the $Cu(NO_3)_2.3H_2O$ salt solution was obtained. Absorption peaks at 230 nm, 300 nm and weak absorption band at wavelength above 650 nm were observed as shown in **Figure 4.1**. The peak at 230 nm and broad absorption band in the visible light region corresponded to the $[Cu(H_2O)_6]^{2+}$ complex formed in the aqueous solution (Ong et al., 2015). The absorption peak at 230 nm could be also attributed to the d-d transition of Cu^{2+} ions (Ong et al., 2015; Siddiqi et al., 2020). The aqueous extract of the papaya peel showed absorption peaks at 265 nm and 330 nm as shown in the **Figure 4.1**.

The sequential formation of CuO NPs can be identified through the colour change of papaya peel extract from clear yellow to green colour solution after the addition of $Cu(NO_3)_2.3H_2O$ salt. The green colour intermediate solution exhibited a peak at 215 nm and a shoulder at 245 nm showing the characteristic peaks of the salt precursor and the papaya peel extract were shifted. The UV-vis spectrum of papaya peel extract was similar to the UV-vis absorption spectrum of papaya leaves extract reported by Anbarasu et al. (2018).

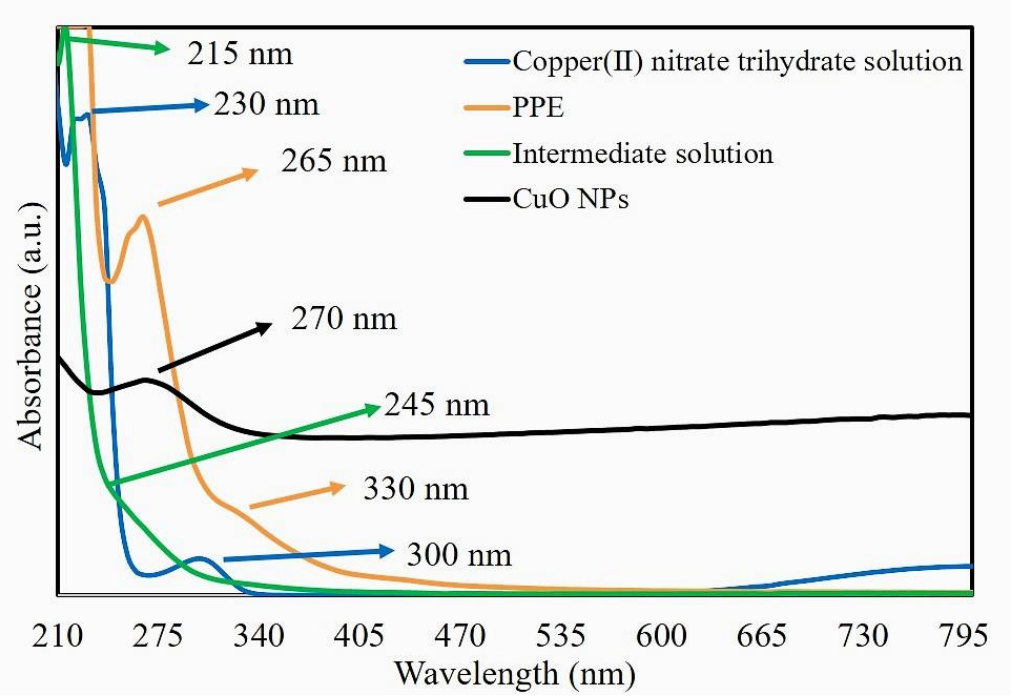

Figure 4.1: UV-vis absorption spectra of copper(II) nitrate trihydrate solution, papaya peel extract (PPE), intermediate solution and CuO NPs

Figure 4.2: Colour of the respective solutions taken for the UV-vis measurements

The UV-vis absorption of the biosynthesized CuO NPs was prepared in 0.1 wt % by dispersing in deionized water and scanned at room temperature. An absorption peak at 270 nm indicated a blue shift occurred when compared to the

value of 375 nm reported by Xu and co-workers (2008). The resonant oscillating of electrons at the conduction band triggered by the incident electromagnetic radiation which is known as surface plasmon resonance was the reason of absorption of CuO NPs at 270 nm (Suresh et al., 2015). The band gap energy (E_g) of the biosynthesized CuO NPs were calculated by Tauc's plot equation (Dhineshbabu et al., 2016):

$$\alpha h\nu = A(h\nu - E_g)^{n/2} \quad \text{(Eq. 4.2)}$$

where α is the absorption coefficient of the nanoparticles. The n is the nature of the transition of the electron between the valence and conduction band such that $n = 1$ for the direct bad gap while $n = 4$ for the indirect band gap (Radhakrishnan and Beena, 2014). Symbol A denotes as constant and $h\nu$ defines as the incident photon energy. A plot of $(\alpha h\nu)^2$ against $h\nu$ was plotted and the band gap energy for the biosynthesized CuO NPs was determined by extrapolation of the straight line part to the x-axis which was presented in the inset of Figure 4.3. The feature of the plot indicated that it had a direct transition due to the linear absorption at the end of the plot (Mokhtari et al., 2016). The E_g of the biosynthesized CuO NPs (3.3 eV) was found to be higher than the literature value (1.9–2.1 eV) could be due to quantum confinement effect which a reduction in particle size result in increase of band gap energy (Das et al., 2013).

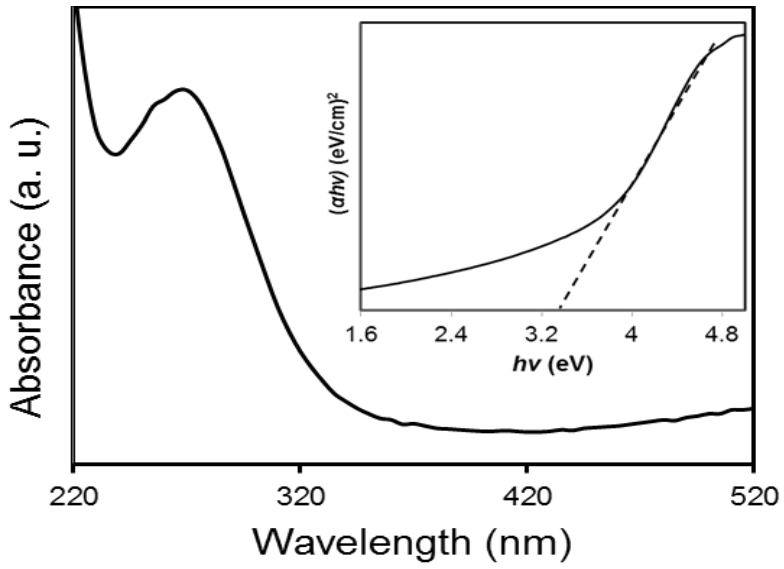

Figure 4.3: UV-vis absorption spectrum of biosynthesized CuO NPs. The inset represented the plot of the $(\alpha h\nu)^2$ against $h\nu$

4.2.2 Fourier-transform infrared spectroscopy (FTIR)

FTIR can be used to identify the functional groups involving during the CuO NPs formation. The results will be complementary to Raman spectroscopy and serve as a fingerprint of the chemical components present. The papaya peel extract (PPE) was scanned with FTIR to compare the functional groups with CuO NPs. From the FTIR spectra, a sharp and intense absorption pea at 532 cm^{-1} which was not shown in PPE indicating the stretching of Cu–O in CuO NPs. The bands at 1412 cm^{-1} for PPE, shifted band at 1384 cm^{-1} for CuO NPs and peaks at around 618 cm^{-1} showed the O–H bending of the phenolic group (Rahman A et al., 2010). Stretching of C–O was identified at 1076 cm^{-1} in the spectrum of PPE while at a shifted band of 1120 cm^{-1} for CuO NPs. The presence of primary amide groups can be differentiated from the absorption bands at 1636 cm^{-1} and 1647 cm^{-1} for PPE and CuO NPs, respectively proving that protein in the papaya peel acted as a capping and stabilizing agents in the

synthesis of CuO NPs (Aminuzzaman et al., 2018). The O–H stretching in both PPE and CuO NPs can be identified from the wavenumbers of 3400 cm^{-1} and 3368 cm^{-1}, respectively. The C–H stretching observed in PPE (2937 cm^{-1}) was not presence in CuO NPs. Other weak absorption bands were spotted at 1261, 921 and 778 cm^{-1} in PPE and 883 cm^{-1} in CuO NPs. The FTIR spectra proved that natural products such as phenolic compounds, flavanoids, catechin, etc. in papaya were the important components acting as bioreducing agents in CuO NPs synthesis (Mello et al., 2020).

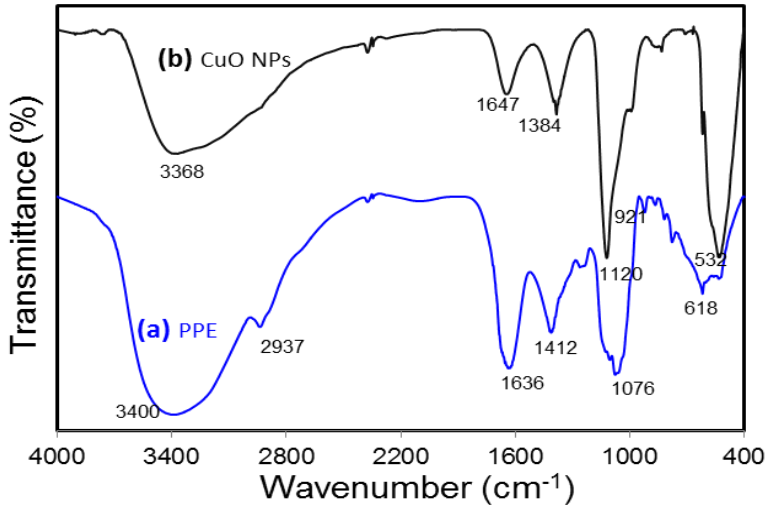

Figure 4.4: FTIR spectrum of (a) papaya peel extract (PPE) and (b) CuO NPs

4.2.3 X-ray diffraction analysis (XRD)

XRD was used to study the crystal phase and crystallinity of the biosynthesized CuO NPs. Figure 4.5 showed the XRD pattern of the CuO NPs. The observed diffraction peaks at 2θ = 32.51°, 32.53°, 38.75°, 46.26°, 48.78°, 53.50°, 58.34°, 61.57°, 66.28°, 68.04°, 72.46° and 75.00° were assigned to (110), (–111), (111),

(–112), (–202), (020), (202), (–113), (–311), (220), (311) and (004) lattice planes, respectively which were well-matched with International Centre for Diffraction Data (ICDD): Entry number-00-045-0937. The CuO NPs were monoclinic phase with lattice parameters a = 4.6853 Å, b = 3.4257 Å, c = 5.1303 Å and β = 99.549 Å. The CuO NPs synthesized were well-crystalline which was confirmed by the well-defined and high intensity diffraction reflection peaks. Debye-Scherrers's equation was applied to calculate the crystalline size (D) of the CuO NPs.

From the calculation, the biosynthesized CuO NPs was found to be 28.06 nm in size.

$$D = \frac{0.9\,\lambda}{\beta \cos\theta} \qquad \text{(Eq. 4.3)}$$

λ is the wavelength (CuKα)

β is the full-width half maximum (FWHM)

θ is the diffraction angle

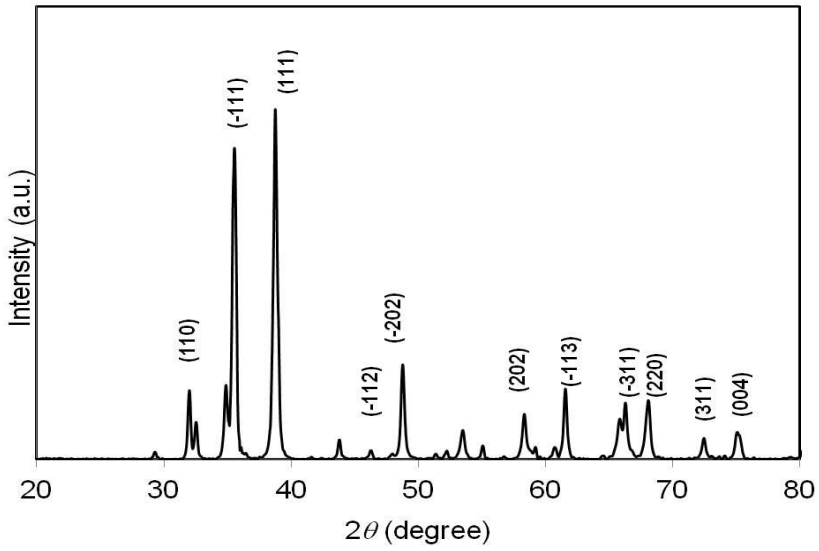

Figure 4.5: XRD spectrum of biosynthesized CuO NPs

4.2.4 Morphological studies

FESEM and TEM were used to study the morphology and size of the biosynthesized CuO NPs. According to the SEM images, the CuO NPs formed were almost agglomerated spherical in shape with a discrete rough appearance. The particles size measured from SEM was ranging from 85–140 nm.

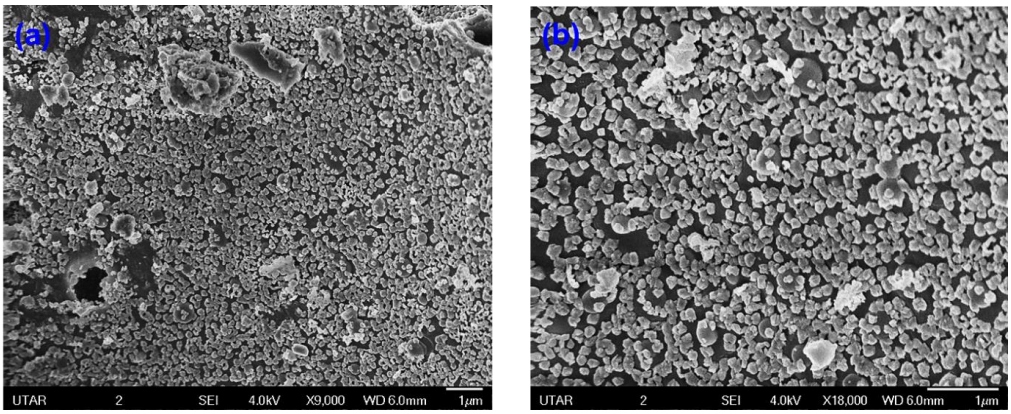

Figure 4.6: SEM images of biosynthesized CuO NPs with magnification of (a) ×9000 and (b) ×18000

The TEM images further confirmed that the CuO NPs were densely clumped as illustrated in **Figure 4.7** with the diameter of 277–500 nm. During the preparation step before TEM analysis, ultrapure water was used to disperse the nanoparticles that will result in agglomeration of the CuO NPs (Lalau et al., 2015; Son et al., 2015).

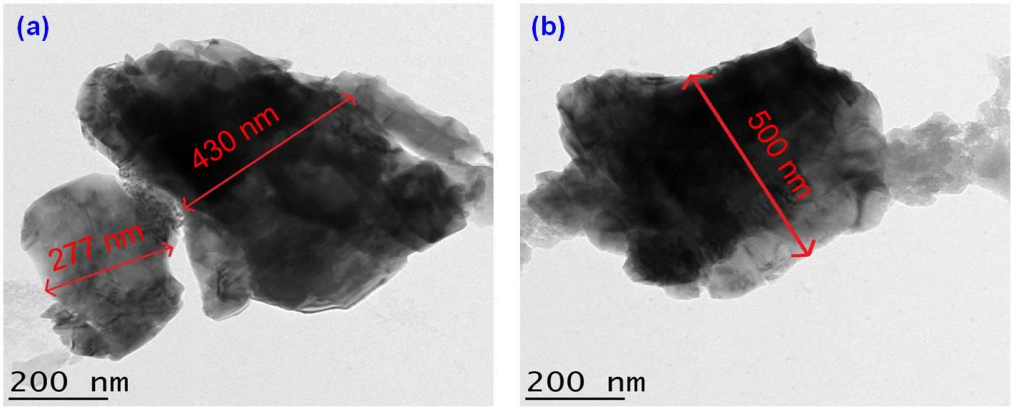

Figure 4.7: Different particles measured by using TEM

4.2.5 Raman spectroscopy

Raman spectroscopy is the common analysis used to study the structural nature of the nanomaterials (Rashad et al., 2013). There were three one-phonon modes observed at 289, 323 and 623 cm^{-1} in **Figure 4.8**. According to Reddy (2017), the Raman shift at 289 cm^{-1} can be assigned to the A_g mode of vibration while 323 and 623 cm^{-1} were B_g mode of vibration. The wavenumbers detected in this study were closely matched to the monoclinic CuO nanomaterials reported in the literature (282, 330 and 616cm^{-1}) (Barrreca, 2007).

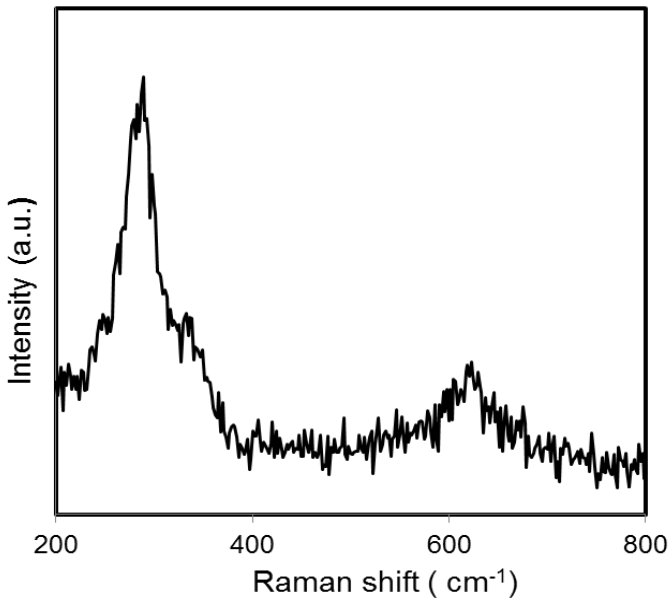

Figure 4.8: Raman spectrum of biosynthesized CuO NPs

4.2.6 Chemical composition of CuO NPs

Other than physical properties of the CuO NPs, the chemical composition of the CuO NPs was also determined with XPS and EDX. In the XPS spectrum, the Cu 2*p* core level showed two peaks at 931.77 and 951.65 eV which were identified as the Cu $2p_{3/2}$ and Cu $2p_{1/2}$, respectively (Barreca, 2007). There were two peaks located at 941.40 and 961.40 eV higher in binding energy than the main spin-orbit components that correspond to the shake-up satellites of Cu^{2+} peaks (Reddy, 2017).

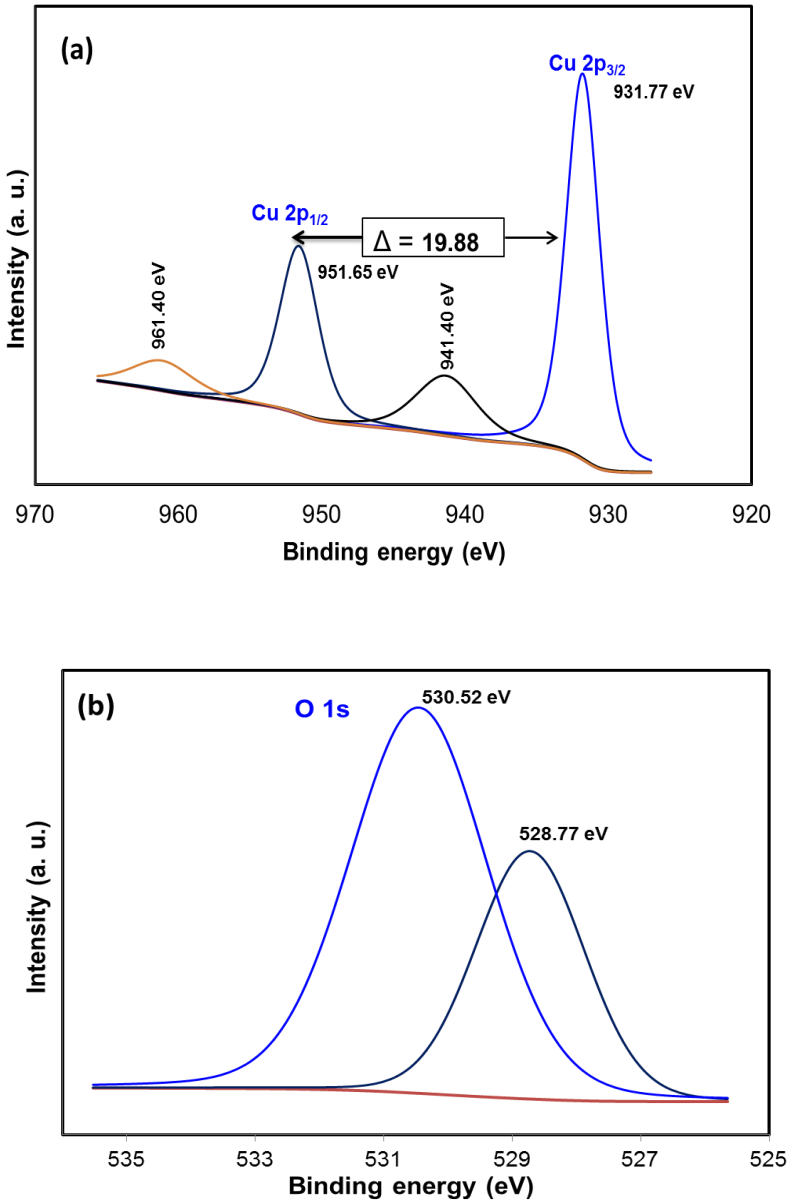

Figure 4.9: XPS spectra of CuO NPs (a) Cu 2*p* (b) O 1*s*

Figure 4.9(b) showed the O 1*s* XPS spectra of the sample and according to the O 1*s* peaks, the O^{2-} in CuO NPs was assigned to the lower energy peak at 528.77 eV while the higher peak at 530.52 eV indicated the O that adsorbed on the surface of the CuO NPs (Barreca, D., 2007; Padil and Černík, 2013). Hence, the XPS measurements excluded the presence of Cu_2O and $Cu(OH)_2$ impurities

in the biosynthesized CuO NPs as there would be no satellite peaks observed in Cu $2p_{3/2}$ and Cu $2p_{1/2}$ of Cu^{2+} (Tamuly et al., 2014; Zheng et al., 2016). The existence of satellite peaks proved the presence of fingerprint of the d^9 Cu^{2+} species that caused by the relaxation phenomenon of the strong configuration interaction in the final state (Barreca, 2007).

To further confirm the formation of CuO, EDX analysis was carried out as illustrated in **Figure 4.10**. The outcome indicated the presence of strong signals of Cu and O elements in the sample which further revealed the good quality and purity of the biosynthesized CuO NPs.

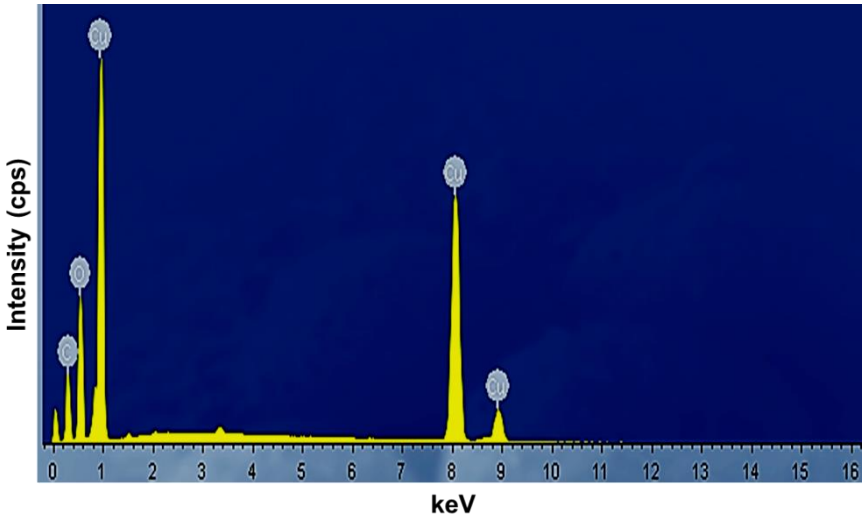

Figure 4.10: EDX spectrum of biosynthesized CuO NPs

4.3 Photodegradation of POME using CuO NPs

The papaya peel biosynthesized CuO NPs was used as a heterogeneous photocatalyst in degradation of the POME. A blank analysis was also run by exposing the POME sample under direct UV irradiation without adding CuO

NPs to prove the function of CuO NPs as a photocatalyst in degrading POME. In **Figure 4.11**, the degradation of POME under different conditions were tested.

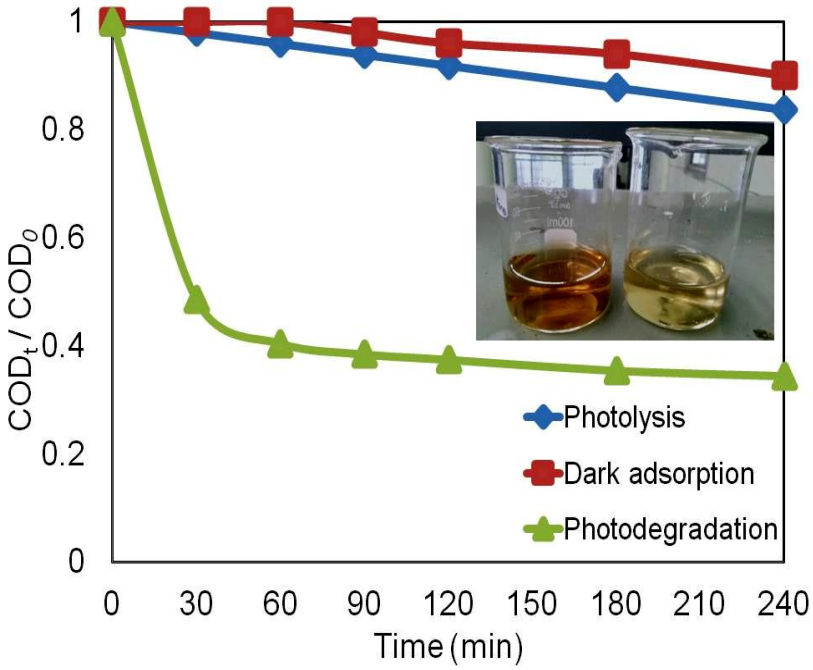

Figure 4.11: Photocatalytic performance of CuO NPs on POME at different conditions. The inset showed the POME before and after photodegradation

From the figure, the POME loaded with CuO NPs in dark condition showed about 10 % reduction in COD after 4 hours. The reduction in COD was mostly caused by the adsorption of organic matters like carbohydrates, amino acids, lignin, phenolic, etc. within the POME on the surface of CuO NPs. Besides, the POME irradiated by UV lamp without the presence of CuO NPs showed about 17 % of COD reduction. On the other hand, after 4 hours of UV light irradiation, the COD content in the POME had been reduced by 66 %. From the graph plotted, there was no significant drop of COD after 3 hours of UV irradiation, hence, the photodegradation should have reached its optimum

reaction time at 3 hours. As shown in the inset of **Figure 4.11**, the dark-brown colour of POME became pale yellow after the UV irradiation proved that photodegradation of POME occurred. The possible organic matters degraded by CuO NPs photocatalyst in the POME were soluble proteins and carbohydrates (Kuppusamy et al., 2017).

CuO NPs is a semiconductor capable of generating electron-hole pairs (e^-/h^+) after absorbing the photon energy ($h\nu$) upon the irradiation of UV light, creating holes in the valance band due to the transition of excited electrons from the valence band to conduction band. Hydroxyl radical ($OH^\bullet$) which was responsible for the mineralization of organic compounds in POME formed subsequently from the reaction of oxygen and water molecules in the POME with the electron-hole pairs. The oxygen (O_2) reacted with the excited electrons (e^-) and dissociated hydrogen ions (H^+) from water molecules to form hydrogen peroxide (H_2O_2). The hydrogen peroxide generated will be further reduced to hydroxyl radicals and hydroxide ions under the UV irradiation. The hydroxyl radicals were involved in degrading the organic matters in POME into simpler molecules including water, carbon dioxide and methane gas (Kuppusamy et al., 2017). A similar mechanism using CuO nanomaterials for the photodegradation of organic pollutants in aqueous media had been proposed before and a summary of the mechanism was illustrated in **Figure 4.12**.

$$\text{CuO NPs} + h\nu \text{ (UV light)} \rightarrow \text{CuO NPs } (e^- + h^+) \qquad \text{(Eq. 4.4)}$$

$$2\,e^- + O_2 + 2H^+ \rightarrow H_2O_2 \qquad \text{(Eq. 4.5)}$$

$$e^- + H_2O_2 \rightarrow OH^\bullet + OH^- \quad \text{(Eq. 4.6)}$$

$$OH^\bullet + \text{POME} \rightarrow \text{intermediates} \rightarrow H_2O + CO_2 + CH_4 \quad \text{(Eq. 4.7)}$$

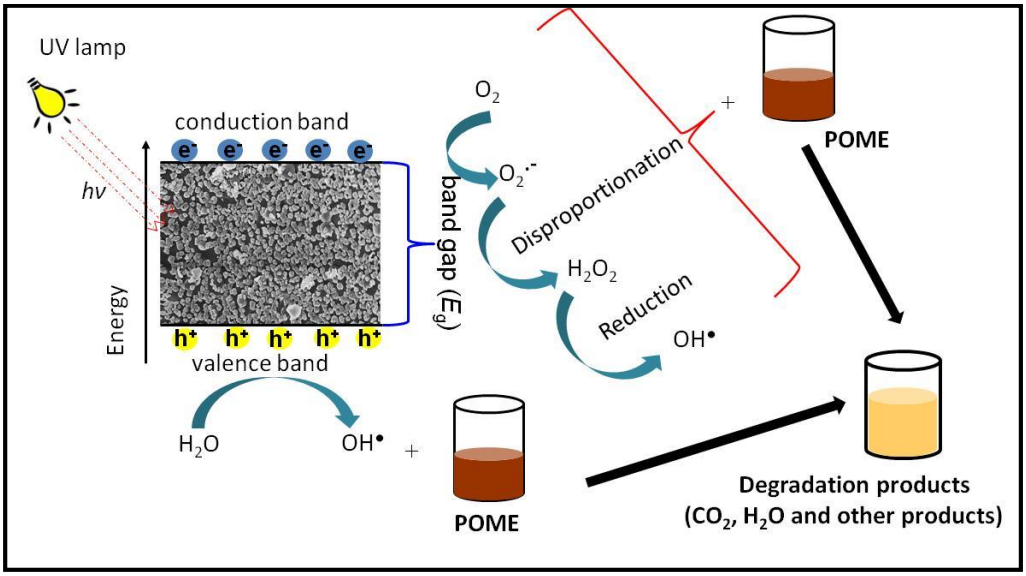

Figure 4.12: Mechanism of POME photomineralization using biosynthesized CuO NPs

4.4 Microalgae treatment

After degrading the POME with UV irradiation, the photo-treated POME was subjected for biological treatment which was microalgae cultivation. The photodegradation process can only break down the organic pollutants in the POME into simpler molecules but it cannot remove the inorganic pollutants like trace metals and nutrients (phosphorus and ammonia). Hence, microalgae can be used as the water polisher to remove the remaining organic and inorganic pollutants in the POME as nutrients to grow in the end enhancing the water quality. Two type of microalgae were investigated in this project which were

Chlorella vulgaris and *Chlamydomonas reinhardtii*. The cultivations of microalgae were held for one week (7 days) prior the water quality analysis.

4.4.1 Cell counting of *Chlorella vulgaris*

The number of *Chlorella vulgaris* (*C. vulgaris*) cells were counted with the aid of the inverted microscope using haemacytometer. A set of control was run by using BBM as the media while the sample was the photo-treated POME. The cell counting was started on the day that the *C. vulgaris* were injected to the samples and ended after one week (Day-7).

From the graph plotted in **Figure 4.13**, the number of cells in the control were decreasing gradually along time. There was no lag phase observed from the *C. vulgaris* cultured in BBM. The growth of *C. vulgaris* was stable until 6th day before decrease of number of cells on 7th day. On the other hand, a lag phase was observed on the first two days of the *C. vulgaris* cultured in photo-treated POME. Although the photo-treated POME was clear and pale yellow in colour it was not as clear as the synthetic BBM. The light penetration might be blocked by the suspended solids that will restrain microalgae growth. In addition, one of the main reason was that the microalgae needed time to accommodate to the new environment (Khalid et al., 2019). The *C. vulgaris* experienced an exponential growth from second day to the fourth day after adapted to the POME environment. The increase of *C. vulgaris* cells was due to the nutrients and carbonaceous materials in the POME. The microalgae entered stationary phase on 6th days onward after the exponential growth. The decrease in number

of cells was due to the increase in pH of the samples caused by the growth and photosynthetic activities of *Chlorella* sp. that will eventually lead to cell inhibition (Guckert and Cooksey, 1990; Chavan et al., 2014).

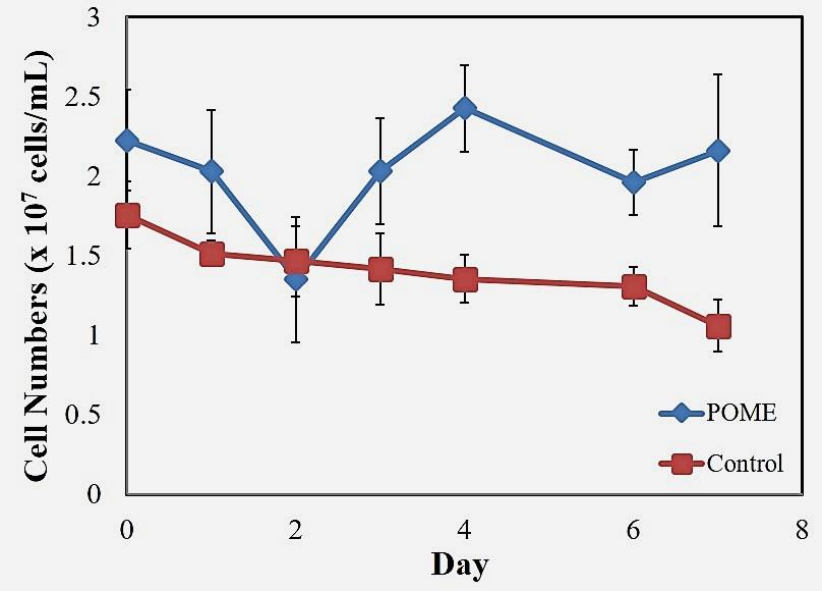

Figure 4.13: Comparison of the growth of *Chlorella vulgaris* in photo-treated POME and BBM media (control)

4.4.2 Cell counting of *Chlamydomonas reinhardtii*

According to **Figure 4.14**, the *Chlamydomonas reinhardtii* (*C. reinhardtii*) cultivated in BBM were increasing throughout the experiment. There was no lag phase shown by *C. reinhardtii*. BBM was a culture medium prescribed with known chemical composition providing the necessary nutrients for microalgae growth. Furthermore, the *C. reinhardtii* cells can grow rapidly in BBM because the culture medium was free from suspended solids and clear hence provide better light penetration for photosynthesis (Khalid et al., 2019).

C. reinhardtii experienced lag phase as *C. vulgaris* when cultivated in the photo-treated POME. The lag phase was caused by the acclimatization of the *C. reinhardtii* to the different environment in the first two days. After that, an exponential growth was observed by the *C. reinhardtii* in day-3 before it reached a stationary phase later. After day-6, the number of *C. reinhardtii* started to drop which can be related to the depletion of nutrients (phosphorus and nitrogen) in the photo-treated POME.

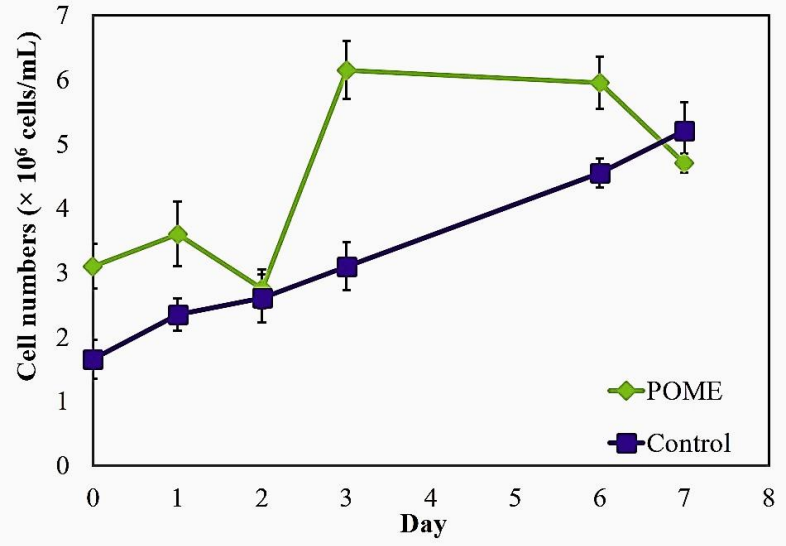

Figure 4.14: Comparison of the growth of *Chlamydomonas reinhardtii* in photo-treated POME and BBM media (control)

4.4.3 Chlorophyll and carotenoid extraction

Microalgae are autotrophs and plant-like organisms that harvest light energy and convert it into sugars through photosynthesis process. There are three main categories of algae which are Chlorophyceae (green algae), Phaeophyceae

(brown algae) and Rhodophyceae (red algae). The *C. vulgaris* and *C. reinhardtii* in this project belong to Chlorophyceae due to the presence of green pigment chlorophyll *a* (*chl a*) and *b* (*chl b*) in their chloroplasts. *Chl a* is the main pigment for photosynthesis while *Chl b* is an accessory pigment that responsible for the broadening of spectrum absorption of the organisms (Martin, 2019). Both chlorophylls have almost the same structure by differing in the third carbon's position (C-3) where *chl a* is bonded with a methyl group ($–CH_3$) while *chl b* is connected to an aldehyde group (–CHO) as shown in Figure 4.14 (Xu et al., 2001).

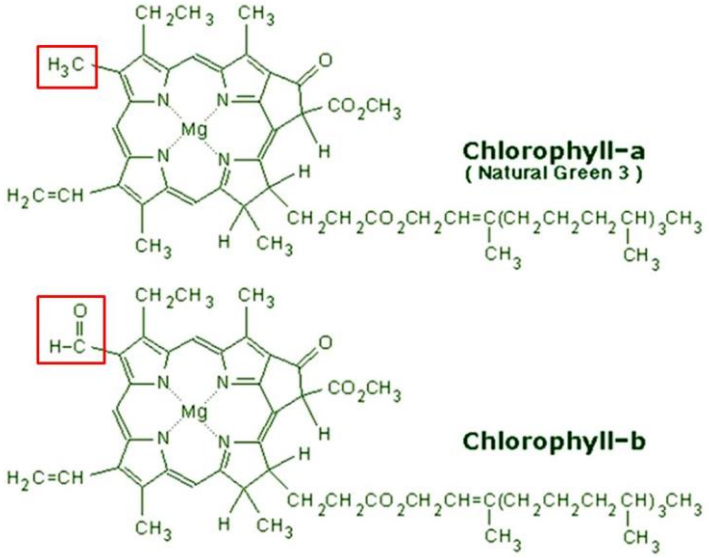

Figure 4.15: Difference in structure of chlorophyll *a* and *b* (Phu, 2014).

Microalgae are organisms capable of converting solar energy into various profitable commercial metabolites including carbohydrates, proteins, lipids, vitamins and carotenoids that can be processed into food and feed, health supplements, pharmaceutical and nutraceutical products (Henríquez, V. et al., 2016). Similar to chlorophyll *b*, carotenoids are accessory pigments present in

the chloroplasts functioning in harvesting light and protecting the photosynthetic apparatus. The yield of carotenoids will increase when microalgae undergo stress condition, for instance, high salinity, high temperature, nutrient deficiency, or high light intensity. Reactive oxygen species (ROS) such as hydrogen peroxide (H_2O_2), superoxide anions (O_2^-), peroxyl radicals (ROO^-), lipid hydroperoxides (ROOH), and hydroxyl radicals (^-OH) will be formed inside the cells as the cellular reaction towards stress condition (Sun et al., 2018). In low light condition, the carotenoids in microalgae cells will assist in light harvesting and pass the energy to chlorophyll. The conjugated double bonds in carotenoids are the main part responsible in absorbing photons ranging from 400–550 nm. When there is excess light, the antioxidant properties of carotenoids will play an important role in protecting the photosynthetic apparatus by receiving excess energy from chlorophyll and dissipate it (Henríquez et al., 2016; Novoveská et al., 2019).

From the results obtained in *C. vulgaris* cultivation (**Figure 4.16**), the *chl a* in the control set was observed to be higher than the *chl b* throughout the duration of study. The results showed that *C. vulgaris* can grow in the BBM without affected by culture medium as *chl a* is the major pigment involving in photosynthesis. On the other hand, the *chl a* of the *C. vulgaris* in the photo-treated POME was low on Day-0. The *chl a* increased from Day-0 to Day-6 as cultivation continued. The *C. vulgaris* had a higher amount of *chl b* which can be related to the lag phase as illustrated in the cell numbers in previous section. The high amount of *chl b* indicated the *C. vulgaris* adapting to the photo-treated POME medium. After adapting to the environment, the *chl a* started to increase

while *chl b* was dropped on Day-2. However, the *chl b* concentration was increasing afterwards due to adaption to the darker colour of POME medium and increasing saturation of microalgae cells which will inhibit penetration of light (Martin, 2019).

In the cultivation of *C. vulgaris*, the carotenoids in the control set was accumulated similar to the growing trend of chlorophyll. The production of carotenoids was reduced initially and started to increase from second day of cultivation onwards. The increase of carotenoids content in BBM medium can be caused by the higher light penetration efficiency resulting from the clear-colourless medium. An excess light environment may induce the microalgae cells to generate more radicals that will damage the cells, thus, carotenoids in the cells can function as radical scavengers to protect the cells. On the last day of cultivation, there was a slightly drop in the carotenoids content. The increasing cell's abundance will inhibit the light penetration which inducing the decrease in *chl a* and increase in *chl b.* At this stage, the carotenoids in the microalgae cells can play the role as accessory pigment in light harvesting. However, the carotenoids in the *C. vulgaris* cells of photo-treated POME samples was detected only on Day-2 to Day-6. The growth of *chl a* throughout the cultivation period indicated a nutrient rich and suitable environment for the growth of *C. vulgaris* in the photo-treated POME. The carotenoids were increasing gradually from the second day until the sixth-day of cultivation. There were no carotenoids detected on the last day of cultivation, mainly due to the cell abundance and limited light penetration in the POME medium. *Chl b* was the dominant photosynthetic chlorophyll on this day.

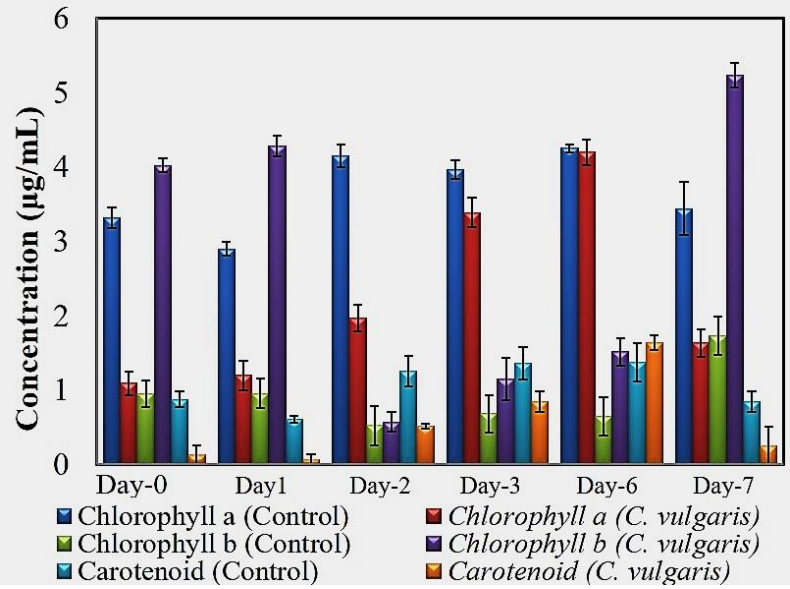

Figure 4.16: Chlorophyll *a*, chlorophyll *b* and carotenoid content of *C. vulgaris* over cultivation period in photo-treated POME

According to **Figure 4.17**, *chl a* in the control set of *C. reinhardtii* was the dominant photosynthetic apparatus from the beginning to the end of cultivation period. A slightly drop in the chlorophyll content was observed in the control set but the chlorophyll was increasing in the following days. The *chl b* was growing in the trend corresponding to *chl a*. The dominating *chl a* was due to the clear BBM medium with better light penetration. The carotenoids in the *C. reinhardtii* was increasing as the cultivation period carried on. Under other conditions, the chlorophylls and carotenoids content in the *C. reinhardtii* were growing in the trend similar to that of the control set. *Chl a* was the dominant chlorophyll throughout the cultivation period unless on the last day, *chl b* was the dominating chlorophyll in response to the POME environment.

The carotenoids were increasing gradually then decrease when the experiment going to end.

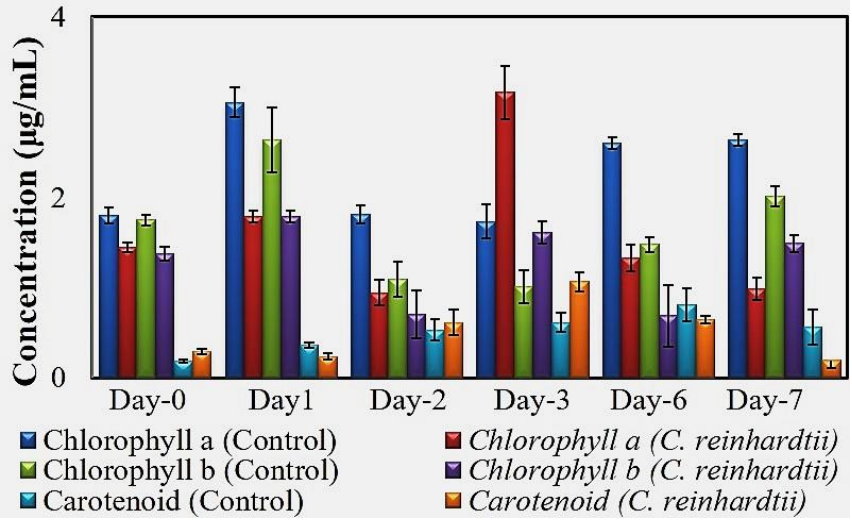

Figure 4.17: Chlorophyll *a*, chlorophyll *b* and carotenoid content of *C. reinhardtii* over cultivation period in photo-treated POME

4.5 Water quality analysis

4.5.1 pH

The pH of the POME before and after every treatment stages were measured using pH meter. The untreated POME was slightly basic having a pH 9.52. After filtration, there was not much changes in the pH as the filtration only remove insoluble solid content in the POME. Then, the filtered POME was treated with CuO NPs photocatalyst under UV irradiation. After photodegradation, there was also slightly drop in the pH which the POME was remained basic (pH 9.42). The photo-treated POME was used as the culture medium for microalgae in the biological treatment. The basicity of the POME increased after the microalgae treatment. The pH of the POME treated with *C. vulgaris* was 11.12 while the POME treated with *C. reinhardtii* was pH 12.35. The increase in pH of the

POME was due to the growth and photosynthetic activities of microalgae (Guckert and Cooksey, 1990).

4.5.2 Chemical oxygen demand (COD) and biochemical oxygen demand (BOD)

The COD and BOD of the water sample were the common parameters tested in industrial effluent. Based on the results obtained, every treatment stages showed a trend of decreasing in COD and BOD concentrations. The reduction in COD and BOD after filtration was due to the removal of insoluble solids and larger particles in the POME. After that, the filtered POME was undergone photodegradation using UV lamp to break down the organic pollutants in the POME into simpler molecules, thus further reduce the COD and BOD content. At the last treatment stage, microalgae were employed to remove the remaining nutrients in the water. Surprisingly, the COD and BOD content of the treated POME were not dropped, but was increased instead.

There were few possible reasons contributing to the increase of COD and BOD values. First of all, the old microalgae in the POME will be worn out and decomposed by the microorganisms in the POME. Furthermore, microalgae will liberate organic matters after carbon dioxide fixation (Lee et al., 2019). Apart from that, there were also other microorganisms present in the POME medium. In this complex environment, the microalgae will excrete metabolites such as kawaguchipeptin, 12-epi-hapalindole E, calothrixine, etc. to inhibit bacterial activities. In addition, under nutrients depletion, algal metabolites will

be secreted as a response to environment changes (Lee et al., 2016). The COD and BOD of the POME indicating that there were significant differences between every treatment stages from filtration to photodegradation followed by water polishing by the microalgae (Appendix A and B).

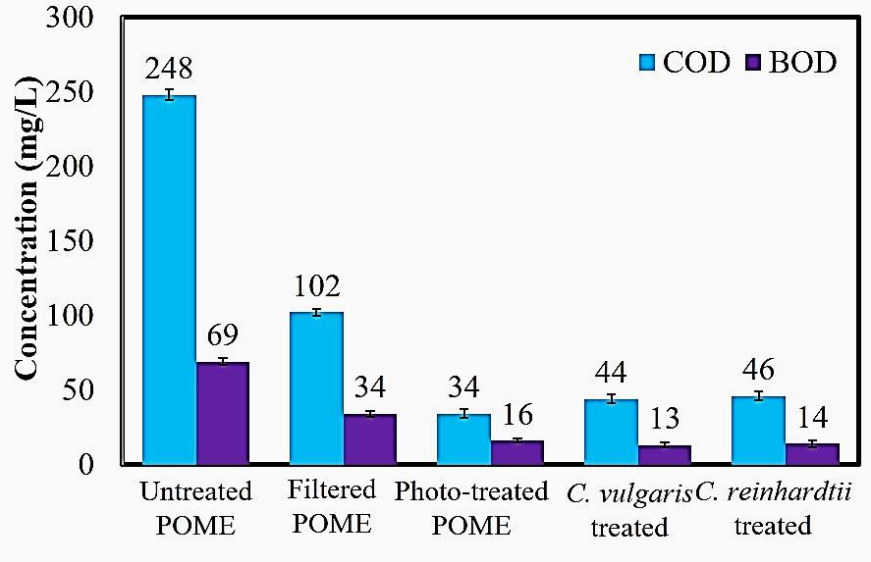

Figure 4.18: Comparison of COD and BOD after every treatment stages

4.5.3 Nutrients composition

Other than carbon-based pollutants, the excess nutrients in the wastewater could be harmful to the surrounding aquatic organisms. Eutrophication is the most common phenomenon caused by nutrients overload in water bodies. The organisms in water will die from suffocating as the degradation of dead algae in the water will use up the oxygen in the water and blocking sunlight from reaching the bottom of the water bodies. The main contributors to this incident are nitrogen and phosphorus elements. Nitrogen is needed for the microalgae to

synthesis amino acids which are the building blocks for other nitrogenated metabolites. The nitrogen can be available in nitrite, nitrate and ammonia form. The phosphorus usually referred to the soluble phosphate which has a higher bioavailability to microalgae for the aim of producing adenosine triphosphate (ATP), nucleic acids ad phospholipids (Pascoal et al., 2021).

The phosphorus content in the POME samples were determined in phosphate, PO_4^{3-} form. From the results obtained, there were no significant drop in PO_4^{3-} concentration after the filtration and photodegradation treatment. However, the PO_4^{3-} content in the POME samples were almost fully removed by both *C. vulgaris* and *C. reinhardtii* microalgae. *C. vulgaris* was able to remove 100 % of the PO_4^{3-} while *C. reinhardtii* removed 90.8 % of the PO_4^{3-} in the POME wastewater.

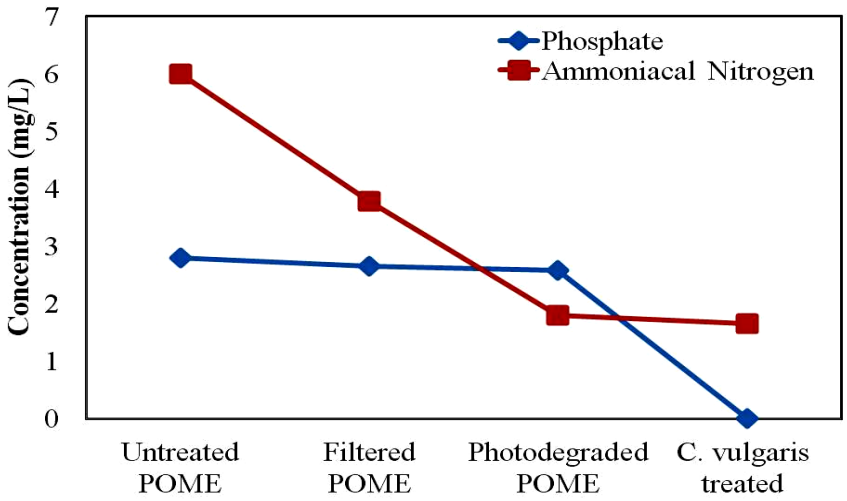

Figure 4.19: Nutrients removal at every treatment stages and by *C. vulgaris* microalgae

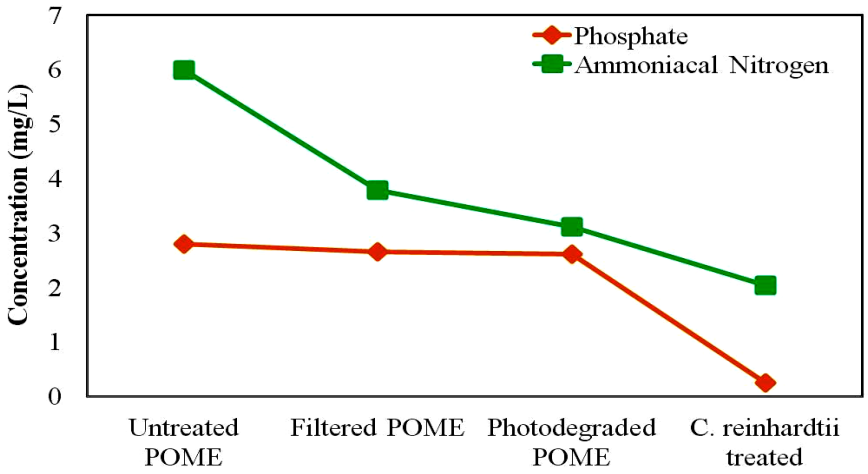

Figure 4.20: Nutrients removal at every treatment stages and by *C. vulgaris* microalgae

Another nutrient that may harm the environment when in excess is nitrogen. In this project, the nitrogen content in the POME was assessed in the ammoniacal nitrogen form (NH_3–N). The amount of ammonia was reduced 36.8 % after the filtration. According to the results, there was about 17.7 % of reduction in ammonia after photodegradation process. The results verified that semiconductor photocatalyst can also be a potential agent for oxidative degradation of pollutants (He et al., 2018). He and co-workers (2018) stated that nitrogen gas (N_2), nitrite (NO_2^--N) and nitrate (NO_3^--N) were the possible by-products of the photodegradation which N_2 was the major by-products. Then, the remaining ammonia was utilized by microalgae as nutrients for growth resultantly reduce 46.93 % of ammonia by *C. vulgaris* and 34.41 % by *C. reinhardtii*. The low removal of nitrogen can be due to the non-optimal N/P ratio in the treated POME for the cultivation of microalgae in the conical flasks compared with bulk cultivation using bioreactor (Kong et al., 2010). The total phosphorus and nitrogen removal by the treatment system developed in this

project were 100 % and 72 % for *C. vulgaris*, 91 % and 66 % for *C. reinhardtii*, respectively.

4.5.4 Colour and conductivity

The conductivity of the POME at every treatment stages were measured. From the graph, the conventional filtration system had reduced 53 % of conductivity in the POME. The drastically drop of conductivity was due to the removal of solids in the wastewater. There was slightly increase in conductivity after photodegradation process. This phenomenon can be explained by the breaking down of organic pollutants into other smaller organic acid (Andayani and Bagyo, 2011). Then, the conductivity continued to reduce after the microalgae treatment.

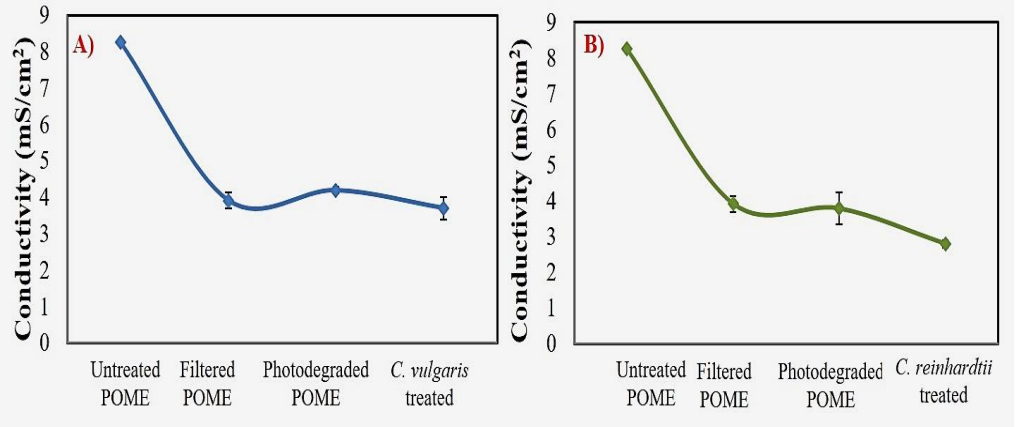

Figure 4.21: Conductivity of POME after every treatment

The colour intensity of the treated POME was also measured to study the treatment efficiency of the integrated system. The colour (Pt/Co) of the

POME was reduced 61.2 % after passing through the conventional filtration system. Then, in order to study the photodegradation performance of CuO NPs the filtered POME was diluted to about 100 ppm COD for the easier light penetration. The diluted POME had a colour intensity of 1464 Pt/Co. After the photodegradation, the colour of the POME was reduced average of 67.3 %. Then, the photodegraded POME was used as the culture medium for *C. vulgaris* and *C. reinhardtii*, respectively. After 7 days of cultivation, the colour of the POME was further reduced by 50.8 % and 28.2 %, each. In literature, *Chlorella sp*. was able remove 53 % of colour of undiluted filtered POME in 16 days of cultivation (Tan et al., 2018). The colour of the POME after treatment of every stages were reduced significantly ($p < 0.5$) (Appendix D).

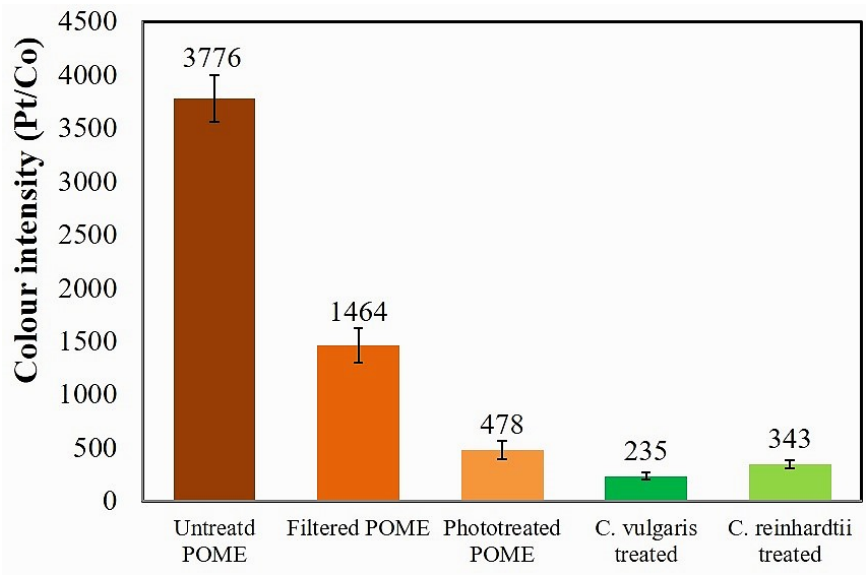

Figure 4.22: Colour intensity of POME after each treatment stages

4.6 Phytotoxicity Evaluation

4.6.1 Phytotoxicity test on treated POME

In order to avoid contamination of aquatic system, phytotoxicity test using mung bean seeds was performed to evaluate the impact of treated POME to the water environment.

Figure 4.23: Photographs showing mung bean (*Vigna radiate* L.) seed germination in sample: 1. control, 2. untreated POME, 3. before photodegradation, 4. after photodegradation

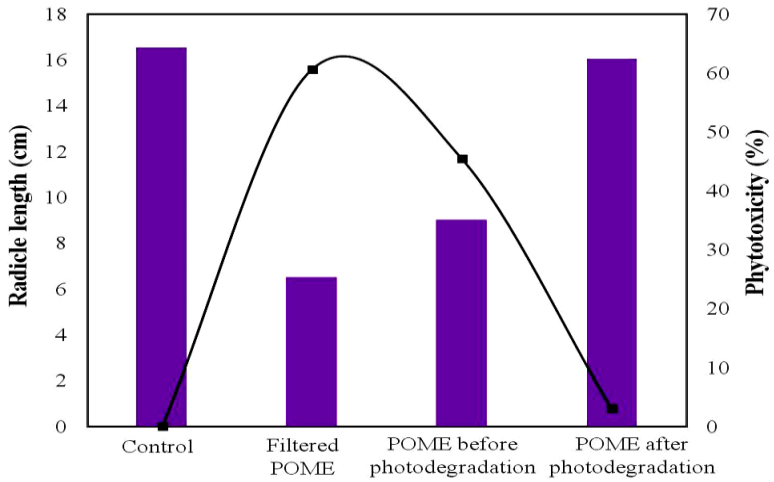

Figure 4.24: Phytotoxicity of POME before and after photodegradation using biosynthesized CuO NPs

According to **Figure 4.23**, the germination of mung bean seeds were strongly inhibited by the untreated POME with the initial phytotoxicity of 61 %. After filtration which was the POME before photodegradation, the phytotoxicity was just reduced slightly to 45 %. After undergone UV irradiation, the phytotoxicity of the treated POME was surprisingly dropped to 3 %. The average radicle lengths were found to be 6.5 cm and 9.0 cm for the untreated POME and POME before photodegradation, respectively. The radicle length of the mung bean seeds in POME after photodegradation (16.0 cm) had grown as well as tap water (16.5 cm). Thus, the biosynthesized CuO NPs possessed good photocatalytic activity and also able to reduce phytotoxicity of industrial effluent.

4.6.2 Phytotoxicity of biosynthesized CuO NPs

The phtotoxicity of biosynthesized CuO NPs to green plants were compared with commercial CuO NPs. In this project, mung bean was used as the representative of green plants. According to **Figure 4.24**, the growth of mung bean was inhibited as the concentration of CuO NPs increased. At low concentration of 50 and 100 mg/L, there were no significant toxicity observed. When the concentration of biosynthesized CuO NPs increased to 250 mg/L and above, the toxicity of the CuO NPs to mung beans were increased undoubtedly.

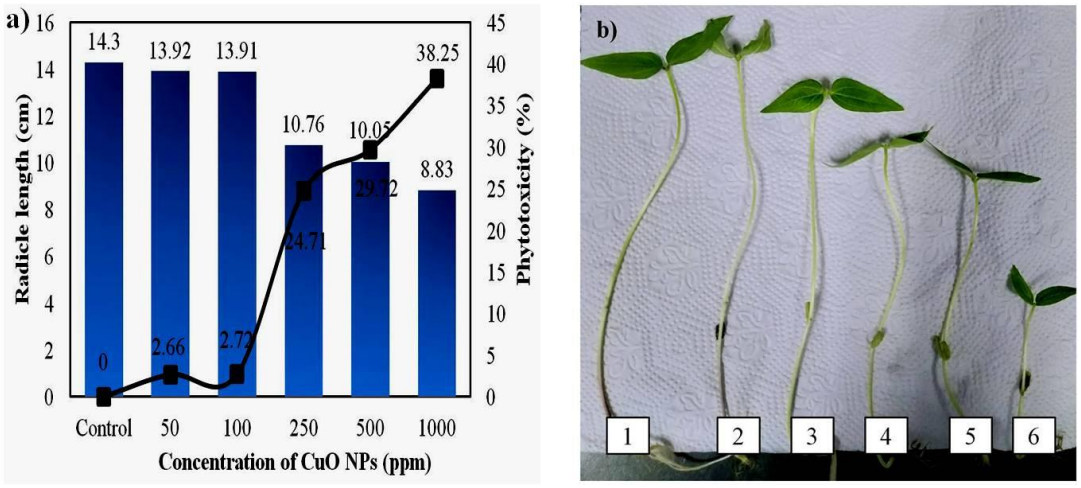

Figure 4.25: a) Phytotoxicity of biosynthesized CuO NPs on mung bean seeds and b) Photographs of mung bean plants treated with 1. control, 2. 50 mg/L, 3. 100 mg/L, 4. 250 mg/L, 5. 500 mg/L and 6. 1000 mg/L CuO NPs

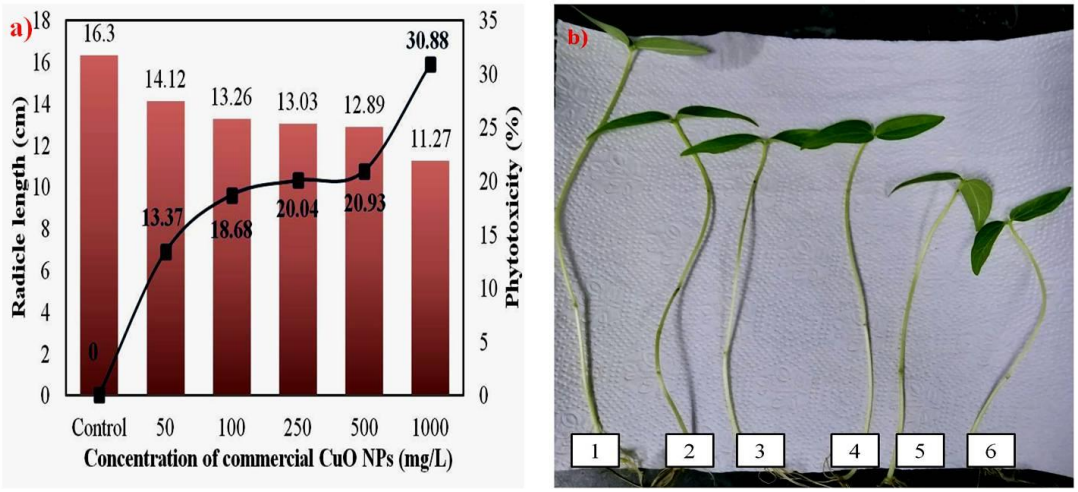

Figure 4.26: a) Phytotoxicity of commercial CuO NPs on mung bean seeds and b) Photographs of mung bean plants treated with 1. control, 2. 50 mg/L, 3. 100 mg/L, 4. 250 mg/L, 5. 500 mg/L and 6. 1000 mg/L CuO NPs

On the other hand, the commercial CuO NPs showed an average of higher toxicity compared to biosynthesized CuO NPs. As shown in **Figure 4.25** a), the commercial CuO NPs showed a higher toxicity even at low concentration

of 50 mg/L. The higher the concentration the stronger the inhibition to the growth of radicle.

The difference in the toxicity effect of the biosynthesized and commercial CuO NPs can be due to the capping agent on the surface of biosynthesized CuO NPs. According to Barrios et al. (2016), the cerium metal content in the tomato plants treated with citric acid coated cerium oxide nanoparticles were found to be lesser than the plants treated with uncoated cerium oxide nanoparticles. The capping agent on the nanoparticles will alter the zeta potential of the particles, hence, affect the adsorption of the nanoparticles to the surface of the roots of the plants. In the biosynthesized CuO NPs, the FTIR and EDX spectra confirmed the presence of plant materials from papaya peels o the CuO NPs. When the nanoparticles entered the plants, the nanoparticles will induce oxidative stress in the plants and enhance reactive oxidative species (ROS) production as a result interfere the metabolism of the plants (Rastogi et al., 2017).

CHAPTER 5

CONCLUSION

5.1 Conclusions

An integrated wastewater treatment system model was developed in this project. Copper oxide nanoparticles (CuO NPs) functioning as photocatalyst in degrading POME was successfully synthesized from papaya peel biowaste. The biosynthesized CuO NPs characterized with various instruments revealed that the particles size was ranging from 85 – 140 nm in agglomerated spherical shape with a direct band gap energy of 3.3 eV. The synthesis pathway also proved the phytochemicals in papaya peel acting as bioreducing and stabilizing agent during the nanoparticles formation. It was found that the low phytotoxicity CuO NPs were an effective photocatalyst as it was able to remove 66 % of the organic pollutants in the POME.

The integrated system was effective enough in eliminating the pollutants such as COD, BOD, colour, phosphate, ammoniacal nitrogen and conductivity in the POME. The microalgae chosen in this project were effective water polishers. The utilization of *C. vulgaris* and *C. reinhardtii* at the last stage of POME treatment allowed them to remove more than 90 % of phosphate and other remaining nutrients in the POME. However, the POME treatment using *Chlorella vulgaris* was more effective compared to *Chlamydomonas reinhardtii*.

5.2 Limitations of study

Overall, the research was conducted smoothly without many obstructions. In the middle of the research, the collection of POME sample from the local palm oil mill was restricted because of the pandemic of COVID-19. The progress of the research was affected when the Malaysian government announced the Movement Control Order (MCO) that all research work must be halted in the period. In the same time, the microalgae stock cultures were wasted and needed to be cultivated again during the lockdown period. In addition, the resources were limited as some of the instruments for the analyses that were not in the campus might need to be carried out outside of campus. The pandemic of COVID-19 had affected the transportation of the samples.

5.3 Recommendations for future studies

In future, it is recommended to collect POME samples from different palm oil mill at different seasons to compare the water quality and applicability of the treatment system to the POME. The use of doped nanoparticles or nanocomposite materials as photocatalyst may improve the efficiency of nanoparticles in mineralizing the organic pollutants in POME. Up to date, there is still limited study on degrading POME using doped nanoparticles. By using doping method, the nanomaterials may possess the abilities of both or more metals used in the synthesis process. Therefore, the defect present in the nanoparticles can be overcome by introducing other metals such as nickel (Ni), cerium (Ce), zinc (Zn) and etc. In addition, some metal composite for example

Zn doped CuO might have a broader absorption of light spectrum which can increase the photocatalytic performance.

Besides, microalgae other than *C. vulgaris* and *C. reinhardtii* can be examined for their effectiveness in removing nutrients. The combination of both species can also be studied in polishing the treated POME. The lipid content in the harvested microalgae can be evaluated to identify the potential of the species in converting the pollutants in POME into useful biodiesel.

LIST OF REFERENCES

Abdelbasir, S.M. and Shaln, A.E., 2019. An overview of nanomaterials for industrial wastewater treatment. *Korean Journal of Chemical Engineering*, 36 (8), pp. 1209 – 1225.

Aboud, N.A.A., Alkayat, W.M.S. and Hussain, D.H., 2020. Simple chemical synthesis of zinc oxide and copper oxide nanoparticles for biological protection. *Systematic Reviews in Pharmacy*, 11 (6), pp. 1188 – 1195.

Ahmadi, N., Nadoushan, M.A., Abolhasani, M.H. and Hosseini, A., 2021. Investigating the efficiency of biological treatment process of oil pollutants using mix of *Scenedesmus obliquus* and *Chlamydomonas reinhardtii* algae: A case study. *AIMS Environmental Science*, 8 (3), pp. 221 – 237.

Ahmed, M.F., Mokhtar, M.B. and Alam, L., 2020. Factors influencing people's willingness to participate in sustainable water resources management in Malaysia. *Journal of Hydrology: Regional Studies*, 31, 100737, pp. 1 – 20.

Alhaji, M.H. et al., 2016. Photocatalytic treatment technology for palm oil mill effluent (POME) – A review. *Process Safety and Environmental Protection*, 102, pp. 673 – 686.

Alhaji, M.H. et al., 2017. Modeling and optimization of photocatalytic treatment of pre-treated palm oil mill effluent (POME) in a UV/TiO_2 system using response surface methodology (RSM). *Cogent Engineering*, 4, 1382980, pp. 1 – 17.

Alqadi, M.A., Taib, S.M., Din, M.F.M. and Kamyab, H., 2017. Effect of photoperiod on the growth of *Chlamydomonas incerta* and pollutant removal. *Malaysian Journal of Civil Engineering*, 29 (1), pp. 69 – 78.

Aminuzzaman, M. et al., 2020. Biosynthesis of NiO nanoparticles using soursop (*Annona muricata* L.) fruit peel green waste and their photocatalytic performance on crystal violet dye. *Journal of Cluster Science*, 32, pp. 949 – 958.

Aminuzzaman, M., Kei, L.M. and Liang, W.H., 2017. Green synthesis of copper oxide (CuO) nanoparticles using banana peel extract and their photocatalytic activities. *AIP Conference Proceedings*, 1828, 020016, pp. 1 – 5.

Aminuzzaman, M, Ying, L.P., Goh, W.S. and Watanabe, A., 2018. Green synthesis of zinc oxide nanoparticles using aqueous extract of *Garcinia mangostana* fruit pericarp and their photocatalytic activity. *Bulletin of Materials Science*, 41, 50, pp. 1 – 10.

Anbarasu, A., Karnan, P., Deepa, N. and Usha, R., 2018. *Carica papaya* mediated green synthesized silver nanoparticles. *International Journal of Current Pharmaceutical Research*, 10 (3), pp. 15 – 20.

Andayani, W. and Bagyo, A.N.M., 2011. TiO2 beads for photocatalytic degradation of humic acid in peat water. *Indonesian Journal of Chemistry*, 11 (3), pp. 253 – 257.

Azadi, S., Karimi-Jashni, A., Javadpour, S. and Mahmoudian-Boroujerd, L., 2020. Photocatalytic landfill leachate treatment using P-type TiO_2 nanoparticles under visible light irradiation. *Environment, Development and Sustainability*, 23 (4), pp. 6047 – 6065.

Azam, A., Ahmed, A.S., Oves, M., Khan, M.S. and Memic, A., 2012. Size-dependent antimicrobial properties of CuO nanoparticles against Gram-positive and –negative bacterial strains. *International Journal of Nanomedicine*, 7(9), pp. 3527 – 3535.

Azmi, N.S. and Yunos, K.F.M., 2014. Wastewater treatment of palm oil mill effluent (POME) by ultrafiltration separation technique coupled with adsorption treatment as pre-treatment. *Agriculture and Agricultural Science Procedia*, 2, pp. 257 – 264.

Banala, R.R., Nagati, V.B. and Karnati, P.R., 2015. Green synthesis and characterization of *Carica papaya* leaf extract coated with silver nanoparticles through X-ray diffraction, electron microscopy and evaluation of bactericidal properties. *Saudi Journal of Biological Sciences*, 22, pp. 637 – 644.

Barreca, D., 2007. CVD Cu_2O and CuO nanosystems characterized by XPS. *Surface Science Spectra*, 14 (1), pp. 41 – 51.

Barrios, A.C. et al., 2016. Effects of uncoated and citric acid coated cerium oxide nanoparticles, bulk cerium oxide, cerium acetate, and citric acid on tomato plants. *Science of the Total Environment*, 563 – 564, pp. 956 – 964.

Bello, M.M. and Raman, A.A.A., 2017. Trend and current practices of palm oil mill effluent polishing: Application of advanced oxidation processes and their future perspectives. *Journal of Environmental Management*, 198, pp. 170 – 182.

Bokare, A.D. and Choi, W., 2014. Review of iron-free Fenton-like systems for activating H_2O_2 in advanced oxidation processes. *Journal of Hazardous Materials*, 275, pp. 121 – 135.

Brandt, M.J., Johnson, K.M., Elphinston, A.J. and Ratnayaka, D.D., 2017. Water filtration. *Twort's Water Supply*, 7th ed. Butterworth-Heinemann: Elsevier Ltd, pp. 367 – 406.

Chai, H.Y., Lam, S.M. and Sin, J.C., 2019. Green synthesis of ZnO using *Hibiscus rosa-sinensis* leaves extracts and evaluation of their photocatalytic activities. *AIP Conference Proceedings*, 2157, 020042, pp. 1 – 6.

Charles, A. and Cheng, C.K., 2019. Photocatalytic treatment of palm oil mill effluent by visible light-active calcium ferrite: Effects of catalyst preparation technique. *Journal of Environmental Management*, 234, pp. 404 – 411.

Chavan, K.J. et al., Environmental factors influencing algal biodiesel production. *Environmental Engineering Science*, 31 (11), pp. 602 – 611.

Cheah, W.Y., Show, P.L., Juan, J.C., Chang, J.S. and Ling, T.C., 2018. Microalgae cultivation in palm oil mill effluent (POME) for lipid productions and pollutants removal. *Energy Conversion and Management*, 174, pp. 430 – 438.

Cheah, W.Y. et al., 2020, Enhancing microalga *Chlorella sorokiniana* CY-1 biomass and lipid production in palm oil mill effluent (POME) using novel-designed photobioreactor. *Bioengineered*, 11 (1), pp. 61 – 69.

Cheng, C.K., Derahman, M.R. and Khan, M.R., 2015. Evaluation of the photocatalytic degradation of pre-treated palm oil mill effluent (POME) over Pt-loaded titania. *Journal of Environmental Chemical Engineering*, 3 (1), pp. 261 – 270.

Cheng, Y.W., Chang, Y.S., Ng, K.H., Wu, T.Y. and Cheng, C.K., 2017. Photocatalytic restoration of liquid effluent from oil palm agroindustry in Malaysia using tungsten oxides catalyst. *Journal of Cleaner Production*, 162, pp. 205 – 219.

Coronado-Reyes, J.A., Salazar-Torres, J.A., Juárez-Campos, B. and González-Hernández, J.C., 2020. *Chlorella vulgaris*, a microalgae important to be used in biotechnology: a review. *Food Science & Technology*, pp. 1 – 11.

Das, D., Nath, B.C., Phukon, P., kalita, A. and Dolui, S.K., 2013. Synthesis of ZnO nanoparticles and evaluation of antioxidant and cytotoxic activity. *Colloids and Surfaces B: Biointerfaces*, 111, pp. 556 – 560.

Das, P., Ghosh, S., Ghosh, R., Dam, S. and Baskey, M., 2018. *Madhuca longifolia* plant mediated green synthesis of cupric oxide nanoparticles: A promising environmentally sustainable material for waste water treatment and efficient antibacterial agent. *Journal of Photochemistry & Photobiology, B: Biology*, 189, pp. 66 – 73.

Dashti, A.F., Aziz, H.A., Ibrahim, A.H. and Zahed, M.A., 2020. Suspended solid removal of palm oil mill effluent using horizontal roughing filter and calcinated limestone. *Water, Air, & Soil Pollution*, 231 (393), pp. 1 – 15.

Dhineshbabu, N.R., Rajendran, V., Nithyavathy, N. and Vetumperumal, R., 2016. Study of structural and optical properties of cupric oxide nanoparticles. *Applied Nanoscience*, 6, pp. 933 – 939.

Ding, G.T. et al., 2020. Phycoremediation of palm oil mill effluent (POME) and CO_2 fixation by locally isolated microalgae: *Chlorella sorokiana* UKM2, *Coelastrella* sp. UKM4 and *Chlorella pyrenoidosa* UKM7. *Journal of Water Process Engineering*, 35, 101202, pp. 1 – 7.

Dugandžić, A.M., et al., 2017. Effect of inorganic ions, photosensitisers and scavengers on the photocatalytic degradation of nicosulfuron. *Journal of Photochemistry and Photobiology A: Chemistry*, *336*, pp. 146 – 155.

Elystia, S., Muria, R.S. and Anggraini, L., 2019. Removal of COD and total nitrogen from palm oil mill effluent in flat-photobioreactor using immobilised microalgae *Chlorella* sp. *Food Research*, 3 (2), pp. 126 – 130.

Feng, T., Feng, G. S., Yan, L. and Pan, J. H., 2014. One-dimensional nanostructured TiO_2 for photocatalytic degradation of organic pollutants in wastewater. *International Journal of Photoenergy*, 2014, 563879, pp. 1 – 14.

Gan, Y.X., Jayatissa, A.H., Yu, Z., Chen, X. and Li, M., 2020. Hydrothermal synthesis of nanomaterials. *Journal of Nanomaterials*, 2020, 8917013, pp. 1 – 3.

Gaya, U.I. and Abdullah, A.H., 2008. Heterogeneous photocatalytic degradation of organic contaminants over titanium dioxide: A review of fundamentals, progress and problem. *Journal of Photochemistry and Photobiology C: Photochemistrys Reviews*, 9, pp. 1 – 12.

Goi, C.L., 2020. The river water quality before and during the Movement Control Order (MCO) in Malaysia. *Case Studies in Chemical and Environmental Engineering*, 2, 100027, pp. 1 – 7.

Gong, X. et al., 2015. Photocatalytic degradation of high ammonia concentration wastewater by TiO_2. *Future Cites & Environment*, 1, 12, pp. 1 – 12.

Guckert, J.B. and Cooksey, K.E., 1990. Triglyceride accumulation and fatty acid profile changes in *Chlorella* (Chlorophyta) during high pH-induced cell cycle inhibition. *Journal of Phycology*, 26, pp. 72 – 79.

Gunde, M.C. and Amnerka, N.D., Nutritional, medicinal and pharmacological properties of papaya (*Carica papaya* linn.): A review. *Journal of Innovations in Pharmaceuticals and Biological Sciences*, 3 (1), pp. 162 – 169.

Halim, F.T.A. et al., 2016. Sustainable microalgae-based palm oil mill effluent treatment process with simultaneous biomass production. *The Canadian journal of Chemical Engineering*, 94 (10), pp. 1848 – 1854.

Hasan, I., Shekhar, C., Sharfan, I.I.B., Khan, R.A. and Alsalme, A., 2020. Ecofriendly green synthesis of the ZnO-doped CuO@Alg bionanocomposite for efficient oxidative degradation of *p*-nitrophenol. *ACS Omega*, 5, pp. 32011 – 32022.

Hasanpoor, M., Aliofkhazraei, M. and Delavari, H., 2015. Microwave-assisted synthesis of zinc oxide nanoparticles. *Procedia Materials Science*, 11, pp. 320 – 325.

Hassan, K.H. and Mahdi, E.R., 2016. Synthesis and characterization of copper, iron oxide nanoparticles used to remove lead from aquous solution. *Asian Journal of Applied Sciences*, 4 (3), pp. 730 – 738.

Hazman, N.A.S. et al., 2018. Integrated palm oil mill effluent treatment and CO_2 sequestration by microalgae. *Sains Malaysiana*, 47 (7), pp. 1455 – 1464.

He, S. et al., 2017. Bioremediation of wastewater by iron oxide-biochar nanocomposites loaded with photosynthetic bacteria. *Frontiers in Microbiology*, 8, 823, pp. 1 – 10.

He, S. et al., 2018. High efficient visible-light photocatalytic performance of Cu/ZnO/rGO nanocomposite for decomposing of aqueous ammonia and treatment of domestic wastewater. *Frontiers in Chemistry*, 6, 219, pp. 1 – 13.

Henríquez, V., Escobar, C., Galarza, J. and Gimpel, J., 2016. Carotenoids in microalgae. In: Stange C. (eds). *Carotenoids in Nature*, Subcellular Biochemistry, 79. Springer, Cham, pp. 219 – 237.

Ibrahim, R.I., Wong, Z.H. and Mohammad, A.W., 2015. Optimization and performance evaluation for nutrient removal from palm oil mill effluent wastewater using microalgae. *IOP Conference Series: Materials Science and Engineering*, 78, 012006, pp. 1 – 7.

Ijaz, F., Shahid, S., Khan, S.A., Ahmad, W. and Zaman, S., 2017. Green synthesis of copper oxide nanoparticles using *Abutilon indicum* leaf extract: Antimicrobial, antioxidant and photocatalytic dye degradation activities. *Tropical Journal of Pharmaceutical Research*, 16 (4), pp. 743 – 753.

Jasney, N.F., Ahmad, A.L. and Ismail, S., 2014. Ultrafiltration membrane for POME treatment: Comparison physical & chemical cleaning process. *Jurnal Teknologi*, 69 (4), pp. 77 – 83.

Jiang, W. et al., 2015. Silver oxide as superb and stable photocatalyst under visible and near-infrared light irradiation and its photocatalytic mechanism. *Industrial & Engineering Chemistry Research*, 54, pp. 832 – 841.

Kamala, S.S., Tey, L.H. and Sim, Y.L., 2018. Combined chemical, physical and biological treatment using *Chlorella vulgaris* sp. on landfill leachate. *AIP Conference Proceedings*, 2026, 020006, pp. 1 – 10.

Kamyab, H. et al., 2015. Efficiency of microalgae *Chlamydomonas* on the removal of pollutants from palm oil mill effluent (POME). *Energy Procedia*, 75, pp. 2400 – 2408.

Kanakaraju, D. et al., 2017. Performance of solar photocatalysis and photo-Fenton degradation of palm oil mill effluent. *Malaysian Journal of Analytical Sciences*, 21 (5), pp. 996 – 1007.

Khalid, A.A.H., Yaakob, Z., Abdullah, S.R.S. and Takriff, M.S., 2019. Assessing the feasibility of microalgae cultivation in agricultural wastewater: The nutrient characteristics. *Environmental Technology & Innovation*, 15, 100402, pp. 1 – 10.

Khedr, T.M., El-Sheikh, S.M., Ismail, A.A., Kowalska, E. and Bahnemann, D.W., 2019. Photodegradation of microcystin-LR using visible light-activated C/N-co-modified mesoporous TiO_2 photocatalyst. *Materials*, 12, 1027, pp. 1 – 18.

Kokila, T., Ramesh, P.S. and Geetha, D., 2016. Biosynthesis of AgNPs using *Carica Papaya* peel extract and evaluation of its antioxidant and antimicrobial activities. *Ecotoxicology and Environmental Safety*, 134, pp. 467 – 473.

Kong, Q.X., Li, L., Martinez, B., Chen, P. and Ruan, R., 2010. Culture of microalgae *Chlamydomonas reinhardtii* in wastewater for biomass feedstock production. *Applied Biochemistry and Biotechnology*, 160, pp. 9 – 18.

Kuppusamy, P. et al., 2017. Treating of palm oil mill effluent using *Commelina nudiflora* mediated copper nanoparticles as a novel bio-control agent. *Journal of Cleaner Production*, 141, pp. 1023 – 1029.

Kwabena, D.E. and Aquisman, A.E., 2019. Morphology of green synthesized ZnO nanoparticles using low temperature hydrothermal technique from aqueous *Carica papaya* extract. *Nanosciecne and Nanotechnology*, 9 (1), pp. 29 – 36.

Lalau, C.M. et al., 2014. Toxicology effects of copper oxide nanoparticles on the growth rate, photosynthetic pigment content, and cell morphology of the duckweed *Landoltia punctata*. *Protoplasma*, 252 (1), pp. 221 – 229.

Lee, J., Lee, J., Shukla, S.K., Park, J. and Lee, T.K., 2016. Effect of algal inoculation on COD and nitrogen removal, and indigenous bacterial dynamics in municipal wastewater. *Journal of Microbiology and Biotechnology*, 26 (5), pp. 900 – 908.

Lee, S.A., Lee, N., Oh, H.M. and Ahn, C.Y., 2019. Enhanced and balanced microalgal wastewater treatment (COD, N, and P) by interval inoculation of activated sludge. *Journal of Microbiology and Biotechnology*, 29 (9), pp. 1434 – 1443.

Lin, C.K., Bashir, M.J.K., Amr, S.S.A. and Sim, L.C., 2016. Post-treatment of palm oil mill effluent (POME) using combined persulphate with hydrogen peroxide ($S_2O_8^{2-}/H_2O_2$) oxidation. *Water Science & Technology*, 74 (11), pp. 2675 – 2682.

Mageshwari, K. and Sathyamoorthy, R., 2013. Flower-shaped CuO nanostructures: synthesis, characterization and antimicrobial activity. *Journal of Materials Science and Technology*, 29 (10), pp. 909 – 914.

Mahadevaiah et al., 2007. A simple spectrophotometric determination of phosphate in sugarcane juices, water and detergent samples. *E-Journal of Chemistry*, 4 (4), pp. 467 – 473.

Malaysian Palm Oil Council (MPOC), 2020a, *Palm Oil Industry – A Learning Experience* [Online]. Available at: http://mpoc.my/palm-oil-industry-a-learning-experience/ [Accessed: 30 December 2020].

Malaysian Palm Oil Council (MPOC), 2020b, *The Oil Palm Tree* [Online]. Available at: http://mpoc.my/the-oil-palm-tree/ [Accessed: 24 December 2020].

Malaysian Palm Oil Council (MPOC), 2020c, *Palm Oil And The Environment* [Online]. Available at: https://mpoc.org.my/palm-oil-and-the-environment/ [Accessed: 30 December 2020].

Martin, L., 2019, *What are the roles of chlorophyll A & B?* [Online]. Available at: https://sciencing.com/what-are-the-roles-of-chlorophyll-a-b-12526386.html [Accessed: 2 July 2021].

Maurya, A., Singh, M.K. and Kumar, S., 2020. Biofiltration technique for removal of waterborne pathogens. *Waterborne Pathogens*, Butterworth-Heinemann: Elsevier Ltd, pp. 123 – 141.

Mello, V.S., Faria, E.A., Alves, S.M. and Scandian, C., 2020. Enhancing CuO nanolubricant performance using dispersing agents. *Tribology International*, 150, 106338, pp. 1 – 9.

Mokhtari, A. et al., 2016. Fabrication and characterization of $Cu(OH)_2$/CuO nanowires as the novel sensitivity enhancer of luminol-H_2O_2 chemiluminescence system: Determination of cysteine in human plasma. *RSC Advances*, 6 (7), pp. 5320 – 5329.

Momin, M.A., Pervin, R., Uddin, M.J., Khan, G.M.A. and Islam, M., 2010. One step synthesis and optical evaluation of copper oxide (CuO) nanoparticles. *Journal of the Bangladesh Electronics*, 10 (1-2), pp. 57 – 63.

Moon, M., et al., 2013. Mixotrophic growth with acetate or volatile fatty acids maximizes growth and lipid production in *Chlamydomonas reinhardtii*. *Algal Research*, 2, pp. 352 – 357.

Moy, J.H., 2003. Papayas. *Encyclopedia of Food Sciences and Nutrition (Second Edition)*, 2003, pp. 4345 – 4351.

Muthuvel, A., Jothibas, M. and Manoharan, C., 2020. Synthesis of copper oxide nanoparticles by chemical and biogenic methods: photocatalytic degradation and in vitro antioxidant activity. *Nanotechnology for Environmental Engineering*, 5, 14, pp. 1 – 19.

Naseem, T. and Durrani, T., 2021. The role of some important metal oxide nanoparticles for wastewater and antibacterial applications: A review. *Environmental Chemistry and Ecotoxicology*, 3, pp. 59 – 75.

Nasrollahzadeh, M., Maham, M. and Sajadi, S.M., 2015a. Green synthesis of CuO nanoparticles by aqueous extract of *Gundelia tournefortii* and evaluation of their catalytic activity for the synthesis of *N*-monosubstituted ureas and

reduction of 4-nitrophenol. *Journal of Colloid and Interface Science*, 455, pp. 245 – 253.

Nasrollahzadeh, M., Sajadi, S.M. and Rostami-Vartooni, A., 2015b. Green synthesis of CuO nanoparticles by aqueous extract of *Anthemis nobilis* flowers and their catalytic activity for the A^3 coupling reaction. *Journal of Colloid and Interface Science*, 459, pp. 183 – 188.

Neena, D. et al., 2018. Enhanced visible light photodegradation activity of RhB/MB from aqueous solution using nanosized novel Fe-Cd co-modified ZnO. *Scientific Reports*, 8, 10691, pp. 1 – 12.

Ng, K.H. and Cheng, C.K., 2016. Photo-polishing of POME into CH_4-lean biogas over the UV-responsive ZnO photocatalyst. *Chemical Engineering Journal*, 300, pp. 127 – 138.

Novoveská, L. et al., 2019. Microalgal carotenoids: A review of production, current markets, regulations, and future direction. *Marine Drugs*, 17, 640, pp. 1 – 21.

Ong, H.R. et al., 2015. Facile synthesis of copper nanoparticles in glycerol at room temperature: Formation mechanism. *RSC Advances*, 5 (31), pp. 24544 – 24549.

Ooi, P.K., Ng, S.S., Abdullah, M.J., Hassan, H.A. and Hassan, Z., 2013. Effects of oxygen percentage on the growth of copper oxide thin films by reactive radio frequency sputtering. *Materials Chemistry and Physics*, 140, pp. 243 – 248.

Padil, V.V.T. and Čerńik, M., 2013. Green synthesis of copper oxide nanoparticles using gum karaya as a biotemplate and their antibacterial application. *International Journal of Nanomedicine*, 8, pp. 889 – 898.

Pahl-Wost, C., 2002. Towards sustainability in the water sector – The importance of human actors and processes of social learning. *Aquatic Sciences*, 64, pp. 391 – 411.

Pascoal, P.V. et al., 2021. Biochemical and phylogenetic characterization of the wastewater tolerant *Chlamydomonas biconvexa* Embrapa | LBA40 strain cultivated in palm oil mill effluent. *PLoS One*, 16 (4), e0249089, pp. 1 – 21.

Phang, Y.K. et al., 2021. Green synthesis and characterization of CuO nanoparticles derived from papaya peel extract for the photocatalytic degradation of palm oil mill effluent (POME). *Sustainability*, 13 (2), 796, pp. 1 – 15.

Phu, S.T.P., 2014, Research on the correlation between chlorophyll-a and organic matter BOD, COD, phosphorus, and total nitrogen in stagnant lake basins. In: Kaneko N. et al. (eds), *Sustainable Living with Environment Risks*. Springer, Tokyo, pp. 177 – 191.

Poh, P.E., Yong, W.J. and Chong, M.F., 2010. Palm oil mill effluent (POME) characteristics in high crop season and the applicability of high-rate anaerobic bioreactors for the treatment of POME. *Industrial & Engineering Chemistry Research*, 49 (22), pp. 11732 – 11740.

Prakash, S. et al., 2018. Green synthesis of copper oxide nanoparticles and its effective applications in Biginelli reaction, BTB photodegradation and antibacterial activity. *Advanced Powder Technology*, 29 (12), pp. 3315 – 3326.

Putri, E.V., Din, M.F.M., Ahmed, Z., Jamaluddin, H. and Chelliapan, S., 2011. Investigation of microalgae for high lipid content using pal oil mill effluent (Pome) as carbon source. *2011 International Conference on Environment and Industrial Innovation (IPCBEE)*, 12, pp. 85 – 89.

Qiu, G. et al., 2012. Facile microwave-assisted hydrothermal synthesis of CuO nanomaterials and their catalytic and electrochemical properties. *The Journal of Physical Chemistry*, 112, pp. 468 – 477.

Radhakrishnan, A.A. and Beena, B.B., 2014. Structural and optical absorption analysis of CuO nanoparticles. *Indian Journal of Advances in Chemical Science*, 2 (2), pp. 158 – 161.

Rahman, A., Ismail, A., Jumbianti, D., Magdalena, S. and Sudrajat, H., 2009. Synthesis of copper oxide nano particles by using *Phormidium cyanobacterium*. *Indonesian Journal of Chemistry*, 9 (3), pp. 355 – 360.

Rashad, M., Rüsing, M., Berth, G., Lischka, K. and Pawlis, A., 2013. CuO and Co_3O_4 nanoparticles: Synthesis, characterizations, and Raman spectroscopy. *Journal of Nanomaterials*, 2013, 714853, pp. 1 – 6.

Rastogi, A. et al., 2017. Impact of metal and metal oxide nanoparticles on plant: a critical review. *Frontiers in Chemistry*, 5, 78, pp. 1 – 16.

Rathnasamy, R., Thangasamy,P., Thangamuthu, R., Sampath, S. and Alagan, V., 2017. Green synthesis of ZnO nanoparticles using *Carica papaya* leaf extracts for photocatalytic and photovoltaic applications. *Journal of Materials Science: Materials in Electronics*, 28, pp. 10374 – 10381.

Reddy, K.R., 2017. Green synthesis, morphological and optical studies of CuO nanoparticles. *Journal of Molecular Structure*, 1150, pp. 553 – 557.

Ru, I.T.K., Sung, Y.Y., Jusoh, M., Wahid, M.E.A. and Nagappan, T., 2020. *Chlorella vulgaris*: a perspective on its potential for combining high biomass with high value bioproducts. *Applied Phycology*, 1 (1), pp. 2 – 11.

Saeed, F. et al., 2014. Nutritional and phyto-therapeutic potential of papaya (*Carica papaya* Linn.): an overview. *International Journal of Food Properties*, 17, pp. 1637 – 1653.

Sankar, R. et al., 2014. Green synthesis of colloidal copper oxide nanoparticles using *Carica papaya* and its application in photocatalytic dye degradation. *Spectrochimica Acta Part A: Molecular and Biomolecular Spectroscopy*, 121, pp. 746 – 750.

Saravanakumar, K. et al., 2019. Biosynthesis and characterization of copper oxide nanoparticles from indigenous fungi and its effect of photothermolysis on human lung carcinoma. *Journal of Photochemistry & Photobiology, B: Biology*, 190, pp. 103 – 109.

Sayuti, S.C. and Azoddein, A.A.M., 2015. Treatment of palm oil mill effluent (POME) by using electrocoagulation as an alternative method. *Malaysian Journal of Analytical Sciences*, 19 (4), pp. 663 – 668.

Selmani, N., Mirghani, M.E.S. and Alam, M.Z., 2013. Study the growth of microalgae in palm oil mill effluent waste water. *IOP Conference Series: Earth and Environmental Science*, 16, 012006, pp. 1 – 4.

Sharmila, G. et al., 2018. Biogenic synthesis of CuO nanoparticles using *Bauhinia tomentosa* leaves extract: Characterization and its antibacterial application. *Journal of Molecular Structure*, 1165, pp. 288 – 292.

Siddiqi, K.S. et al., 2020. Green synthesis, characterization, antibacterial and photocatalytic activity of black cupric oxide nanoparticles. *Agriculture & Food Security*, 9, 17, pp. 1 – 15.

Siddiqui, V.S., Ansari, A., Chauhan, R. and Siddiqi, W.A., 2021. Green synthesis of copper oxide (CuO) nanoparticles by *Punica granatum* peel extract. *Materials Today: Proceedings*, 36 (3), pp. 751 – 755.

Singaravelan, R. and Alwar, S.B.S., 2015. Electrochemical synthesis, characterisation and phytogenic properties of silver nanoparticles. *Applied Nanoscience*, 5, pp. 983 – 991.

Singh, J. et al., 2018. 'Green' synthesis of metals and their oxide nanoparticles: applications for environmental remediation. *Journal of Nanobiotechnology*, 16, 84, pp. 1 – 24.

Singh, P.K., Kumar, P., Hussain, M., Das, A.K. and Nayak, G.C., 2016. Synthesis and characterization of CuO nanoparticles using strong base electrolyte through electrochemical discharge process. *Bulletin of Materials Science*, 39 (2), pp. 469 – 478.

Soleimaninanadegani, M. and Manshad, S., 2014. Enhancement of biodegradation of palm oil mill effluents by local isolated microorganisms. *International Scholarly Research Notices*, 2014, 727049, pp. 1 – 9.

Son, J., Vavra, J. and Forbes, V.E., 2015. Effects of water quality parameters on agglomeration and dissolution of copper oxide nanoparticles (CuO-NPs) using a central composite circumscribed design. *Science of the Total Environment*, 521-522, pp. 183 – 190.

Sreeju, N., Rufus, A. and Philip, D., 2017. Studies on catalytic degradation of organic pollutants and anti-bacterial property using biosynthesized CuO nanostructures. *Journal of Molecular Liquids*, 242, pp. 690 – 700.

Subramaniam, S.K., 2018. *Treatment of mature landfill leachate using combined coagulation, filtration and microalgae processes*. MSc Thesis, Universiti Tunku Abdul Rahman, Malaysia.

Sukumar, S., Rudrasenan, A. and Nambiar, D.P., 2020. Green-synthesized rice-shaped copper oxide nanoparticles using *Caesalpinia bonducella* seed extract and their applications. *ACS Omega*, 5 (2), pp. 1040 – 1051.

Suleiman, M., Mousa, M. and Hussein, A.I.A., 2015. Wastewater disinfection by synthesized copper oxide nanoparticles stabilized with surfactant. *Journal of Materials and Environmental Science*, 6 (7), pp. 1924 – 1937.

Sun, X.M., Ren, L.J., Zhao, Q.Y., Ji, X.J. and Huang, H., 2018. Microalgae for the production of lipid and carotenoids: a review with focus on stress regulation and adaptation. *Biotechnology for Biofuels*, 11, 272, pp. 1 – 16.

Suresh, D. et al., 2015. *Chironji* mediated facile green synthesis of ZnO nanoparticles and their photoluminescence, photodegradative, antimicrobial and antioxidant. *Materials Science in Semiconductor Processing*, 40, pp. 759 – 765.

Sutradhar, P., Saha, M. and Maiti, D., 2014. Microwave synthesis of copper oxide nanoparticles using tea leaf and coffee powder extracts and its antibacterial activity. *Journal of Nanostructure in Chemistry*, 4, 86, pp. 1 – 6.

Tamuly, C., Saikia, I., Hazarika, M. and Das, M.R., 2014. Bio-derived CuO nanocatalyst for oxidation of aldehyde: a greener approach. *RSC Advances*, 4 (40), pp. 20636 – 20640.

Tan, K.A., Morad, N., Norli, I., Lalung, J. and Omar, W.M.W., 2018. Post-treatment of palm oil mill effluent (POME) using freshwater green microalgae. *Malaysian Journal of Microbiology*, 14 (2), pp. 145 – 151.

Trang, N.T.H., Dung, P.D., Ngoc, L.S., Van, P.T.H. and Thang, P.Q., 2018. Green synthesis of copper nanoparticles using Mandarin (*Citrus reticulata*) peel extract and antifungal study. *Asian Journal of Biotechnology and Bioresource*, 3 (3), pp. 1 – 9.

Turakhia, B., Divakara, M.B., Santosh, M.S. and Shah, S., 2020. Green synthesis of copper oxide nanoparticles: a promising approach in the development of antibacterial textiles. *Journal of Coatings Technology and Research*, 17, pp. 531 – 540.

Udaiyappan, A.F.M., Hasan, H.A., Takriff, M.S. and Abdullah, S.R.S., 2017. A review of the potentials, challenges and current status of microalgae biomass applications in industrial wastewater treatment. *Journal of Water Process Engineering*, 20, pp. 8 – 21.

Udayabhanu et al., 2015. *Tinospora cordifolia* mediated facile green synthesis of cupric oxide nanoparticles and their photocatalytic, antioxidant and antibacterial properties. *Materials Science in Semiconductor Processing*, 33, pp. 81 – 88.

Verma, S., Daverey, A. and Sharma, A., 2017. Slow sand filtration for water and wastewater treatment - A review. *Environmental Technology Reviews*, 6 (1), pp. 47 – 58.

Vij, T. and Prashar, Y., 2015. A review on medicinal properties of *Carica papaya* Linn. *Asian Pacific Journal of Tropical Disease*, 5 (1), pp. 1 – 6.

Wirth, R. et al., 2020. *Chlorella vulgaris* and its phycosphere in wastewater: Microalgae-bacteria interactions during nutrient removal. *Frontiers in Bioengineering and Biotechnology*, 8, 557572, pp. 1 – 15.

Wong, K.A., Lam, S.M. and Sin, J.C., 2019. Wet chemically synthesized ZnO structures for photodegradation of pre-treated palm oil mill effluent and antibacterial activity. *Ceramics International*, 45, pp. 1868 – 1880.

Xu, H., Vavilin, D. and Vermaas, W., 2001. Chlorophyll *b* can serve as the major pigment in functional photosystem II complexes of cyanobacteria. *Proceedings of the National Academy of Sciences*, 98 (24), pp. 14168 – 14173.

Xu, X., Zhang, M., Feng, J. and Zhang, M., 2008. Shape-controlled synthesis of single-crystalline cupric oxide by microwave heating using an ionic liquid. *Materials Letter*, 62, pp. 2787 – 2790.

Yacob, S., Hassan, M.A., Shirai, Y., Wakisaka, M. and Subash, S., 2006. Baseline study of methane emission from anaerobic ponds of palm oil mill effluent treatment. *Science of the Total Environment*, 366, pp. 187 – 196.

Ye, J. et al., 2019. Photocatalytic simultaneous removal of nitrite and ammonia via a Zinc ferrite/activated carbon hybrid catalyst under UV/visible irradiation. *ACS Omega*, 4. pp. 6411 – 6420.

Zainal, N.H., Jalani, N.F., Mamat, R. and Astimar, A.A., 2017. A review on the development of palm oil mill effluent (POME) final discharge polishing treatments. *Journal of Oil Palm Research*, 29 (4), pp. 528 – 540.

Zainuri, N.Z. et al., 2018. Reusability performance of zinc oxide nanoparticles for photocatalytic degradation of POME. *E3S Web of Conferences*, 34, 02013, pp. 1 – 9.

Zhang, J.G., Zhang, F., Thakur, K., Hu, F. and Wei, Z.J., 2017. Valorization of spent *Escherichia coli* media using green microalgae *Chlamydomonas reinhardtii* and feedstock production. *Frontiers in Microbiology*, 8, 1026, pp. 1 – 9.

Zheng, Y. et al., 2016. Growth of the Cu_2O nanoparticle on reduced graphene sheets with high photocatalytic activity for degradation of Rhodamine B. *Fullerenes, Nanotubes and Carbon Nanostructures*, 24 (2), pp. 149 – 153.

Zou, X., Fan, H., Tian, Y., Zhang, M. and Yan, X., 2015. Chemical bath deposition of Cu_2O quantum dots onto ZnO nanorod arrays for application in photovoltaic devices. *RSC Advances*, 5 (30), pp. 23401 – 23409.

APPENDICES

Appendix A

Table A.1: Single factor ANOVA analysis of COD against every treatment stages.

SUMMARY

Groups	*Count*	*Sum*	*Average*	*Variance*
Untreated POME	3	744	248	19
Filtered POME	3	306	102	9
Photo-treated POME	3	102	34	13
C. vulgaris treated	3	132	44	13
C. reinhardtii treated	3	138	46	13

ANOVA

Source of Variation	*SS*	*df*	*MS*	*F*	*P-value*	*F crit*
Between Groups	96542.4	4	24135.6	1801.164	3.07E-14	3.47805
Within Groups	134	10	13.4			
Total	96676.4	14				
Total	78344.92	11				

APPENDIX B

Table B.1: Single factor ANOVA analysis of BOD against every treatment stages.

SUMMARY

Groups	*Count*	*Sum*	*Average*	*Variance*
Untreated POME	3	207	69	7
Filtered POME	3	102	34	7
Photo-treated POME	3	48	16	3
C. vulgaris treated	3	39	13	4
C. reinhardtii treated	3	42	14	7

ANOVA

Source of Variation	*SS*	*df*	*MS*	*F*	*P-value*	*F crit*
Between Groups	6824.4	4	1706.1	304.6607	2.13E-10	3.47805
Within Groups	56	10	5.6			
Total	6880.4	14				

APPENDIX C

Table C.1: Single Factor ANOVA analysis of conductivity against every treatment stages

SUMMARY

Groups	*Count*	*Sum*	*Average*	*Variance*
Untreated POME	3	24.75	8.25	0.0036
Filtered POME	3	11.73	3.91	0.0775
Photodegraded POME	3	12.57	4.19	0.0133
C. vulgaris treated	3	11.1	3.70	0.1407
C. reinhardtii treated	3	8.37	2.79	0.0196

ANOVA

Source of Variation	*SS*	*df*	*MS*	*F*	*P-value*	*F crit*
Between Groups	54.14304	4	13.53576	265.7197	4.19E-10	3.47805
Within Groups	0.5094	10	0.05094			
Total	54.65244	14				

APPENDIX D

Table D.1: Single Factor ANOVA analysis of colour against every treatment stages

SUMMARY

Groups	*Count*	*Sum*	*Average*	*Variance*
Untreatd POME	3	11328	3776	71743
Filtered POME	3	4392	1464	39325
Phototreated POME	3	1434	478	11911
C. vulgaris treated	3	705	235	1849
C. reinhardtii treated	3	1029	343	2199

ANOVA

Source of Variation	*SS*	*df*	*MS*	*F*	*P-value*	*F crit*
Between Groups	26624720	4	6656180	261.9986	4.49E-10	3.47805
Within Groups	254054	10	25405.4			
Total	26878774	14				

APPENDIX E

Publication 1

sustainability

MDPI

Article

Green Synthesis and Characterization of CuO Nanoparticles Derived from Papaya Peel Extract for the Photocatalytic Degradation of Palm Oil Mill Effluent (POME)

You-Kang Phang [1], Mohammod Aminuzzaman [1,*], Md. Akhtaruzzaman [2,*], Ghulam Muhammad [3], Sayaka Ogawa [4], Akira Watanabe [4] and Lai-Hock Tey [1,*]

[1] Department of Chemical Science, Faculty of Science, Universiti Tunku Abdul Rahman (UTAR), Kampar Campus, Jalan Universiti, Kampar 31900, Malaysia; youkang06@hotmail.com
[2] Solar Energy Research Institute (SERI), Universiti Kebangsaan Malaysia (UKM), Bangi 43600, Malaysia
[3] Department of Computer Engineering, College of Computer and Information Sciences, King Saud University, Riyadh 11543, Saudi Arabia; ghulam@ksu.edu.sa
[4] Institute of Multidisciplinary Research for Advanced Materials (IMRAM), Tohoku University, Sendai 980-8577, Japan; s.ogawa@tagen.tohoku.ac.jp (S.O.); akira.watanabe.c6@tohoku.ac.jp (A.W.)
* Correspondence: mohammoda@utar.edu.my (M.A.); akhtar@ukm.edu.my (M.A.); teylh@utar.edu.my (L.-H.T.)

Abstract: In recent years, the green chemistry based-approach for the synthesis of nanoparticles has shown tremendous promise as an alternative to the costly and environmentally unfriendly chemically synthesized nanoparticles. In this study, copper oxide nanoparticles (CuO NPs) were synthesized through a green approach using the water extract of papaya (*Carica papaya* L.) peel biowaste as reducing as well as stabilizing agents, and copper (II) nitrate trihydrate salt as a precursor. The structural properties, crystallinity, purity, morphology, and the chemical composition of as-synthesized CuO NPs were analyzed using different analytical methods. The analytical results revealed that the synthesized CuO was observed as spherical-like in particles with measured sizes ranging from 85–140 nm and has monoclinic crystalline phase with good purity. The Fourier transform infrared (FTIR) spectroscopic results confirmed the formation of the Cu-O bond through the involvement of the potential functional groups of biomolecules in papaya peel extract. Regarding photocatalytic activity, the green-synthesized CuO NPs were employed as a photocatalyst for the degradation of palm oil mill effluent (POME) beneath the ultraviolet (UV) light and results showed 66% degradation of the POME was achieved after 3 h exposure to UV irradiation. The phytotoxicity experiment using mung bean (*Vigna radiata* L.) seed also showed a reduction of toxicity after photodegradation.

Keywords: CuO nanoparticles; green synthesis; palm oil mill effluent (POME); papaya peel; biowaste; photocatalyst

check for updates

Citation: Phang, Y.-K.; Aminuzzaman, M.; Akhtaruzzaman, M.; Muhammad, G.; Ogawa, S.; Watanabe, A.; Tey, L.-H. Green Synthesis and Characterization of CuO Nanoparticles Derived from Papaya Peel Extract for the Photocatalytic Degradation of Palm Oil Mill Effluent (POME). *Sustainability* **2021**, *13*, 796. https://doi.org/10.3390/su13020796

Received: 7 December 2020
Accepted: 30 December 2020
Published: 15 January 2021

Publisher's Note: MDPI stays neutral with regard to jurisdictional claims in published maps and institutional affiliations.

Copyright: © 2021 by the authors. Licensee MDPI, Basel, Switzerland. This article is an open access article distributed under the terms and conditions of the Creative Commons Attribution (CC BY) license (https://creativecommons.org/licenses/by/4.0/).

1. Introduction

Due to the high demand for economical, nutritional, and edible vegetable oil, the palm oil industry has become one of the fast-growing industries in the world. Malaysia has become the second largest palm oil producer in the world after Indonesia since 2006 and the palm oil industry is vigorously contributing to this country's economy. Nevertheless, the palm oil industry is generating a large amount of brownish colloidal liquid waste known as palm oil mill effluent (POME) and previous research studies suggest that 0.5–0.75 tons of POME is generated for every tonnage of fresh fruit bunch processed [1]. POME is typically acidic (pH 4.5–5) with 95–96% water, 4–5% total solids including 2–4% suspended solids, as well as 0.6–0.7% of oil and grease [2]. Moreover, POME also contains organic matters such as lignin (4700 ppm), phenolics (5800 ppm), pectin (3400 ppm), and amino acids [3]. Consequently, POME can cause a severely destructive impact on the environment if discharged directly to water sources owing to its high chemical oxygen

APPENDIX F

Publication 2

4th International Symposium on Green and Sustainable Technology (ISGST 2021) IOP Publishing
IOP Conf. Series: Earth and Environmental Science **945** (2021) 012077 doi:10.1088/1755-1315/945/1/012077

Investigation of the growth of *Chlorella vulgaris* and *Chlamydomonas reinhardtii* cultivated in pre-treated palm oil mill effluent (POME) as the culture medium

Y K Phang[1], L-H Tey[1*], M Aminuzzaman[1,2], M Akhtaruzzaman[3], A Watanabe[4]

[1] Department of Chemical Science, Faculty of Science, Universiti Tunku Abdul Rahman (UTAR), Jalan Universiti, Bandar Barat, 31900 Kampar, Perak, Malaysia

[2] Centre for Photonics and Advanced Materials Research (CPAMR), Universiti Tunku Abdul Rahman (UTAR), Jalan Sungai Long, Bandar Sungai Long, 43000 Kajang, Selangor, Malaysia

[3] Solar Energy Research Institute (SERI), Universiti Kebangsaan Malaysia (UKM), 43600 Bangi, Selangor, Malaysia

[4] Institute of Multidisciplinary Research for Advanced Materials (IMRAM), Tohoku University, Sendai 980-8577, Japan

Corresponding author's email: teylh@utar.edu.my

Abstract. The application of microalgae in wastewater treatment has attracted the attention of researchers since a few decades ago. Palm oil industry is one of the lucrative main exporting industry in Malaysia which has drawn the attention of researchers in mitigating the polluting impacts caused by the palm oil mill effluent (POME) released from the oil palm processing. In this study, the growth of the green algae *Chlorella vulgaris* and *Chlamydomonas reinhardtii* in the pre-treated POME was studied for 7 continuous days. The number of microalgae cells, chlorophylls and carotenoids contents were monitored throughout the cultivation period. The potential of both strains of microalgae as the water polisher for post-treatment of POME was investigated as well. The findings revealed that both microalgae showed lag phase at the beginning of cultivation and grew exponentially later. When monitoring the chlorophyll content, chlorophyll *a* and chlorophyll *b* played a role in photosynthesis when the microalgae detected environmental changes. The carotenoids in the microalgae acted as the accessory pigments which assisted in light harvesting under poor light condition and as the antioxidant protecting the cells when there was excess light. *C. vulgaris* was able to remove 98.1 % of phosphate and 53.1 % of ammoniacal nitrogen while *C. reinhardtii* removed 90.1 % and 37.3 %, respectively. This study indicated that two microalgae species have a high potential to be integrated in the post-treatment for POME.

Content from this work may be used under the terms of the Creative Commons Attribution 3.0 licence. Any further distribution of this work must maintain attribution to the author(s) and the title of the work, journal citation and DOI.
Published under licence by IOP Publishing Ltd

APPENDIX G

Publication 3

Journal of Cluster Science
https://doi.org/10.1007/s10876-020-01859-8

ORIGINAL PAPER

Biosynthesis of NiO Nanoparticles Using Soursop (*Annona muricata* L.) Fruit Peel Green Waste and Their Photocatalytic Performance on Crystal Violet Dye

Mohammod Aminuzzaman[1] · Chan-Yong Chong[1] · Wee-Sheng Goh[1] · You-Kang Phang[1] · Tey Lai-Hock[1] · Swee-Yong Chee[1] · Md. Akhtaruzzaman[2] · Sayaka Ogawa[3] · Akira Watanabe[3]

Received: 1 June 2020
© Springer Science+Business Media, LLC, part of Springer Nature 2020

Abstract
A simple, inexpensive, and eco-friendly route has been demonstrated for synthesizing spherical NiO nanoparticles (NiO NPs) with a size range between 20 and 90 nm using aqueous extract of soursop (*Annona muricata* L.) fruit peel green waste which plays the role of reducing and stabilizing agent during the synthesis. The formation, morphology, structure and other physicochemical properties of the resulting NiO NPs were characterized by various experimental techniques such as X-ray diffraction (XRD), energy dispersive X-ray (EDX) analysis, Raman spectroscopy, X-ray photoelectron spectroscopy (XPS), ultraviolet–visible (UV–vis) spectroscopy, Fourier transform infrared (FT-IR) spectroscopy, field emission scanning electron microscopy (FESEM) and transmission electron microscopy (TEM). The photocatalytic performance of the prepared NiO NPs was assessed toward the photodegradation of crystal violet (CV) dye as a model pollutant under sunlight illumination. The measurement of chemical oxygen demand (COD) values verified the degree mineralization of CV dye. The results show that nearly 99.0% of CV pollutant was photodegraded at 105 min of illumination, making it a promising candidate for wastewater treatment.

Keywords Green synthesis · NiO nanoparticles · Green waste · Photocatalyst · Photodegradation

Introduction

Pollution of water resources by anthropogenic pollutants such as organic dyes, pigments, heavy metals, herbicides, and antibiotics is a growing environmental disquietude. Among various water pollutants, organic dyes cause a significant threat for all living beings, ranging from aquatic species to human beings even at low concentrations [1]. Moreover, many of the organic dyes along with their products are carcinogenic and mutagenic in nature responsible for number sorts of cancers for human beings [2–4]. Consequently, it is a matter of great concern to treat these dyes before releasing into water resources. In the recent past, various physico-chemical methods have been developed to eliminate these toxic organic dyes from industry effluent/wastewater to decrease their environmental impact. These methods include biological methods (aerobic and anaerobic processes) [5], adsorption [6–8], chemical oxidation [9], ion exchange [10], coagulation–flocculation [11–13], photocatalytic degradation [14, 15], electrochemical processes [16], membrane filtration [17],

Electronic supplementary material The online version of this article (https://doi.org/10.1007/s10876-020-01859-8) contains supplementary material, which is available to authorized users.

✉ Mohammod Aminuzzaman
mohammoda@utar.edu.my

[1] Department of Chemical Science, Faculty of Science, Universiti Tunku Abdul Rahman (UTAR), Perak Campus, Jalan Universiti, Bnadar Barat, 31900 Kampar, Perak D. R., Malaysia

[2] Solar Energy Research Institute (SERI), Universiti Kebangsaan Malaysia (UKM), 43600 Bangi, Selangor, Malaysia

[3] Institute of Multidisciplinary Research for Advanced Materials (IMRAM), Tohoku University, Katahira 2-1-1, Aoba-ku, Sendai 980-8577, Japan

Published online: 17 August 2020